SiGe HBT Parameter Extraction Using Mextram 505.00

by

Anni Zhang

A thesis submitted to the Graduate Faculty of
Auburn University
in partial fulfillment of the
requirements for the Degree of
Master of Science

Auburn, Alabama
May 5, 2018

Keywords: Mextram 505.00, Parameter Extraction, Temperature Scaling

Approved by

Guofu Niu, Professor of Electrical and Computer Engineering
Fa Foster Dai, Professor of Electrical and Computer Engineering
Bogdan Wilamowski, Professor of Electrical and Computer Engineering

Abstract

Applications of SiGe HBT need a robust model which can accurately describe the performance of SiGe HBT at various temperatures. Circuit simulation requires accurate transistor model and reliable parameters.

This work presents SiGe HBT parameter extraction using the latest version of Mextram (Most EXquisite TRAnsistor Model) 505.00. A first generation SiGe HBT with 50 GHz cutoff frequency is used to show the extraction procedure using ADS simulator and extraction software IC-CAP.

Low current model parameters are first extracted at reference temperature, including capacitance parameters, Early effect parameters, avalanche parameters, saturation currents, from low current $I-V$ or $C-V$ characteristics, where self-heating is negligible. Temperature scaling parameters of these low current model parameters are then determined by fitting low current $I-V$ at all temperatures. Next, high current model parameters at reference temperature are extracted, including series resistances, self-heating thermal resistance, epi-layer model parameters, avalanche current dependence. Simultaneous fitting of high current characteristics at all temperatures is used to determine or refine temperature scaling parameters for high current parameters. Following this strategy, the extraction results show that simulated curves are well correlated with measured data.

Acknowledgments

First, I would like to express my sincere appreciation to my advisor Dr. Guofu Niu for his patient guidance and never-ending support throughout my research. Without his help, this thesis would not have been possible. I would like to thank my committee members, Dr. Fa Foster Dai and Dr. Bogdan Wilamowski, for their brilliant comments and suggestions and precious time.

I would also like to express my deep gratitude for my group members for their assistance and accompany through the years in Auburn.

Finally, I am grateful for my family and my boyfriend for their love, continuous encouragement and support.

Table of Contents

List of Figures

List of Tables

Chapter 1

Introduction

1.1 SiGe HBT Characteristics

The first transistor was invented by W. Shockley, J. Bardeen and W. Brattain in 1947. Since then, the technology of bipolar junction transistors (BJTs) has been growing rapidly. The silicon-germanium heterojunction bipolar transistor (SiGe HBT) is the first practical bandgap engineering device realized in silicon, and it further improves the performance of bipolar transistors. SiGe HBT device inherits the structure from the advanced Si BJT [1] as shown in Figure 1.1 [2].

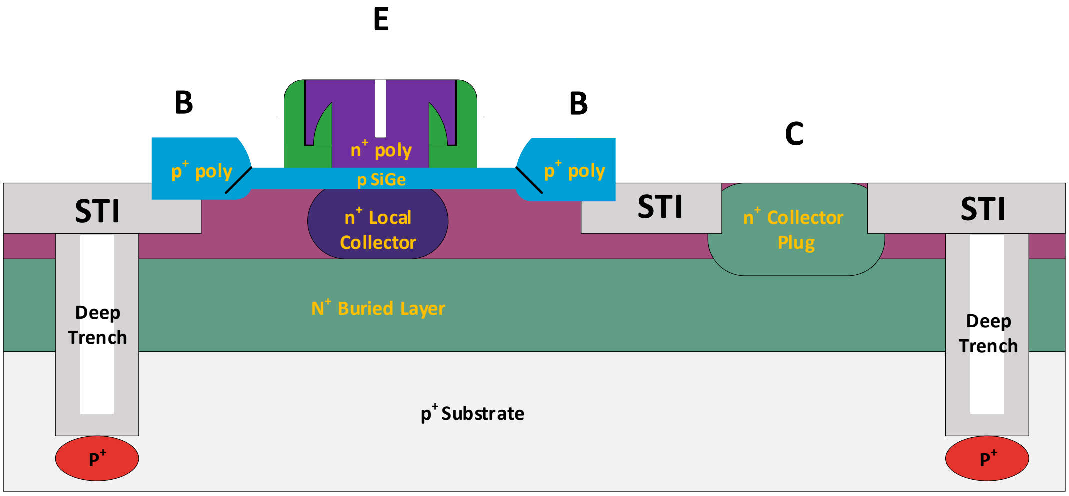

Figure 1.1: Advanced SiGe HBT cross-section

The device has the following features:

- N^+ poly-emitter contact
- P^+ poly-base contact
- N^+ local collector implant
- Buried N^+ sub-collector
- Deep trench isolation

SiGe HBT is typically formed by adding Ge during the base region's growth. The fundamental principle of SiGe HBT is illustrated by the band diagram shown in Figure 1.2. It shows the difference of the base energy band diagrams between Si BJT and SiGe HBT at identical forward bias. Here we only consider an ideal, graded base SiGe HBT with constant doping in each region. The Ge content increases linearly from zero concentration at emitter-base (EB) junction to some maximum concentration near collector-base (CB) junction, and then rapidly decreases to zero [3]. The figure also shows that SiGe base has a smaller bandgap than that of Si. Actually, SiGe alloys can produce an energy bandgap reduction of approximate 7.5 meV for each 1 percent of Ge introduced [4].

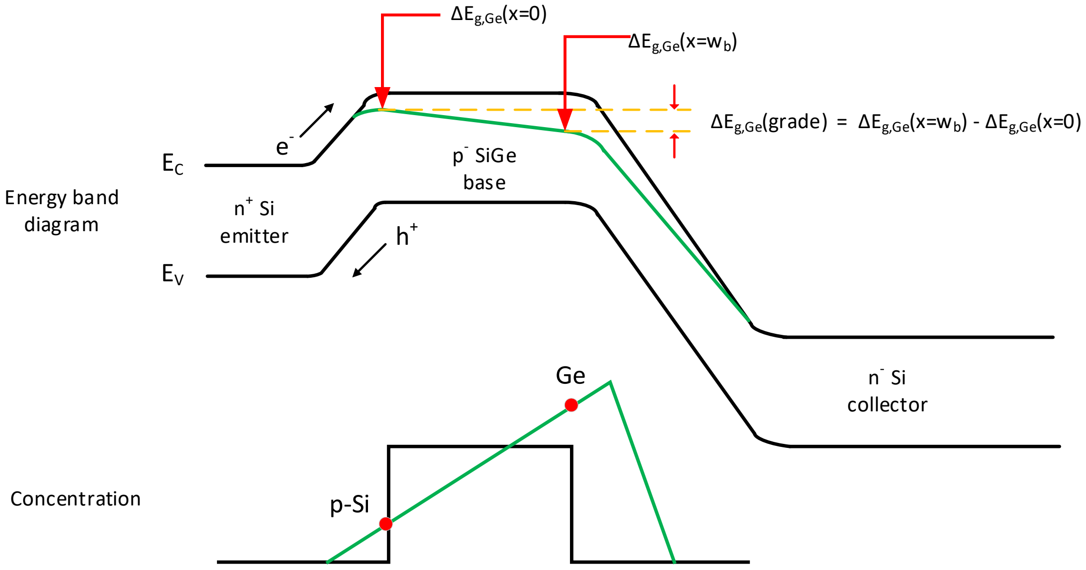

Figure 1.2: Energy band diagrams for a Si BJT and a graded-base SiGe HBT biased in forward mode

The energy band diagram also shows that Ge-profile is graded. Referred to the base bandgap of Si, the bandgap difference at EB junction is $\Delta E_{g,Ge}(x = 0)$, the bandgap difference at CB junction is $\Delta E_{g,Ge}(x = W_b)$. Hence a Ge-induced bandgap grading over the neutral base is obtained as $\Delta E_{g,Ge}(grade)$ = $\Delta E_{g,Ge}(x = W_b)$ - $\Delta E_{g,Ge}(x = 0)$. Bandgap grading improves the performance of a transistor in many aspects. For instance, it causes a reduction of base transit time, which gives a higher f_T. It also increases the electron injection in the base so that the current gain β is increased. Furthermore, SiGe HBT has a higher base doping, which reduces the base resistance [5].

1.2 Mextram fundamentals

Compact models are physics-based models that use a set of equations and parameters to describe transistor electrical characteristics. These models must be sufficiently simple to be incorporated in circuit simulators and are sufficiently accurate to make the outcome of the simulators useful to circuit designers [6]. Mextram (Most EXquisite TRAnsistor Model) is a vertical bipolar transistor compact model which is widely used these days, it possesses many features that the well-known Ebers-Moll model and Gummel-Poon model lack [7]. Mextram has been developed for more than three decades. The first Mextram was introduced by Philips Electronics in 1985 as level 501. Then several following updates level 502, 503 and 504 were released respectively in 1987, 1994 and 2000. The current version is level 505.00, which has been released by Auburn University in 2017 [8]. Mextram is a world standard transistor model. The latest Mextram model contains descriptions for the following effects [8]:

- Bias-dependent Early effect
- Low-level non-ideal base currents
- High-injection effects
- Ohmic resistance of the epilayer
- Velocity saturation effects on the resistance of the epilayer
- Hard and quasi-saturation (including Kirk effect)

- Weak avalanche in the collector-base junction (optionally including snap-back behaviour)
- Zener-tunneling current in the emitter-base junction
- Charge storage effects
- Split base-collector and base-emitter depletion capacitance
- Substrate effects and parasitic PNP
- Explicit modelling of inactive regions
- Current crowding and conductivity modulation of the base resistance
- First order approximation of distributed high frequency effects in the intrinsic base (high-frequency current crowding and excess phase-shift)
- Recombination in the base (meant for SiGe transistors)
- Early effect in the case of a graded bandgap (meant for SiGe transistors)
- Temperature scaling
- Self-heating
- Thermal noise, shot noise and $1/f$-noise

Figure 1.3 shows the full Mextram 505.00 equivalent circuit of a NPN transistor [8]. Currents and charges placed on a drawing of transistor cross section are used to show their physical origins. The figure also shows the different regions of the transistor. An additional circuit for self-heating is shown in Figure 1.3 as well. The same model can be used for PNP transistors by switching setting flags.

The circuit has some external nodes and internal nodes. The external nodes are used to connect the transistor with the rest of the world. These external nodes are the collector node C, the base node B, the emitter node E, and the substrate node S. Mextram 505.00 has 7 internal nodes. B_2, C_2 and E_1 are intrinsic NPN terminals. B_1 is an internal node for base resistance related parasitic effects. C_1, C_3 and C_4 are internal nodes for collector resistance related parasitic effects. C_3 and C_4 are for distributive buried layer resistance effects and turned off by default [8].

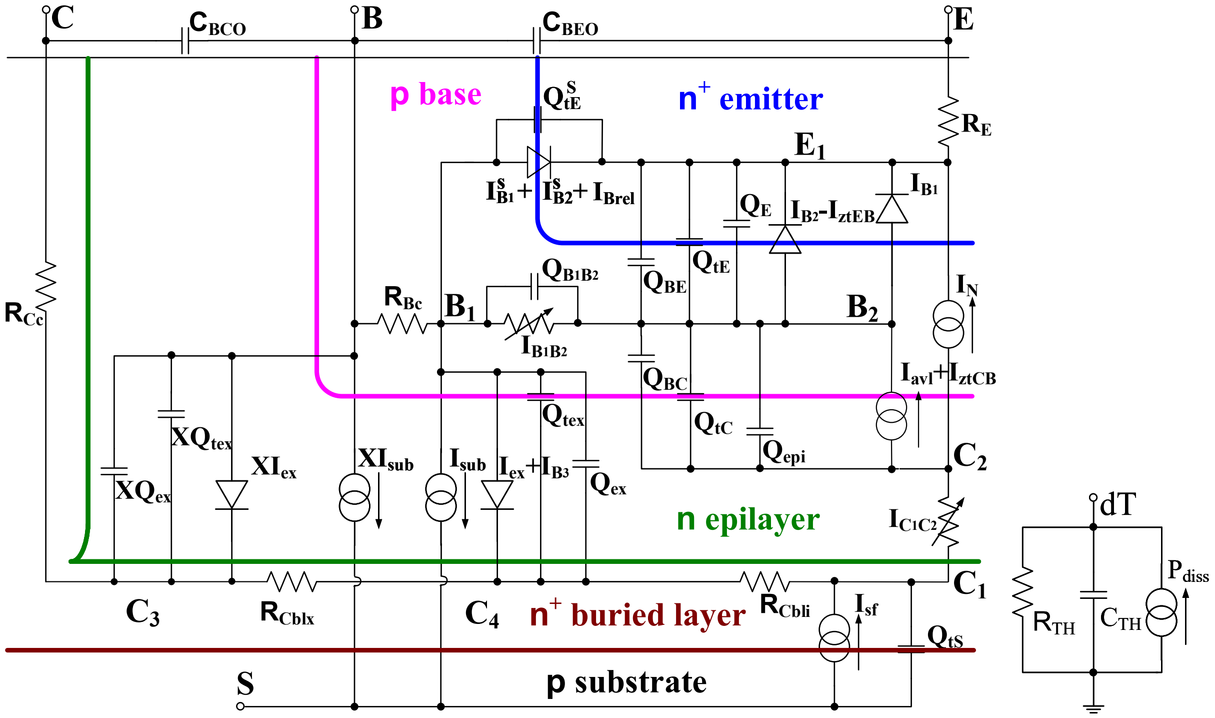

Figure 1.3: The full Mextram equivalent circuit for the vertical NPN transistor

Figure 1.4 shows the same equivalent circuit, but with only the DC components. Instead of overlaying the components on a physical cross section, we use a counterclockwise placement of standard counterclockwise placement of the collector, base, emitter and substrate terminals, which is more familiar to circuit designers. Figure 1.4 shows the DC equivalent circuit of Mextram 505.00 while Figure 1.5 shows the AC equivalent circuit including charges. First we look at Figure 1.4.

Now we introduce the elements in the DC equivalent circuit starting with the resistances. R_{Cblx} and R_{Cbli} are resistances of buried layer. Node E_1 is connected to node E via the emitter resistor R_E. The base node B is connected to the internal node B_2 via a constant base resistor R_{Bc} and a variable resistor R_{Bv}. The node B_1 is between these two resistors. R_{Bv} describes DC current crowding under the emitter, so it is represented by a controlled current source I_{B1B2}. Since the epilayer is lightly doped, it has its own resistance also represented by a controlled current source I_{C1C2}.

Then we introduce the currents. I_N, I_{avl}, I_{ztCB}, I_{B1}, I_{B2} and I_{ztEB} are placed between the intrinsic nodes B_2, C_2 and E_1 to model the intrinsic NPN transistor. I_{ex}, I_{B3} and I_{sub} are used

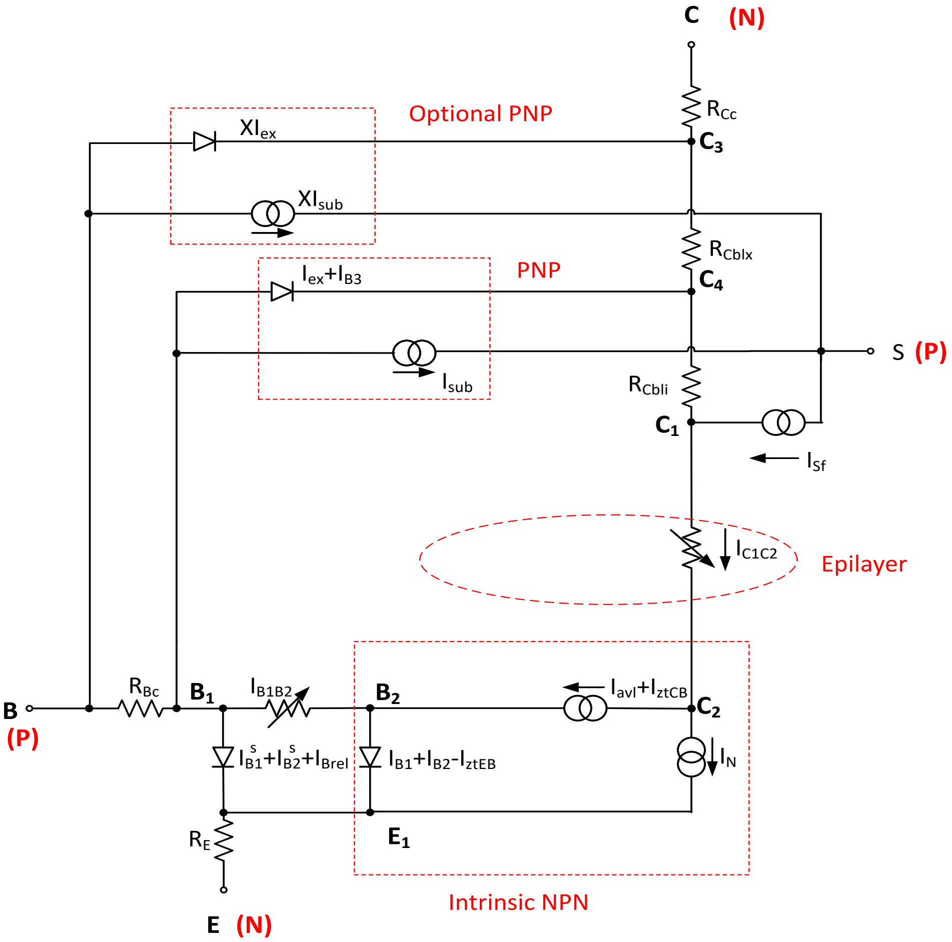

Figure 1.4: DC equivalent circuit for NPN transistor

to model the parasitic PNP transistor. The currents of parasitic PNP transistor can be further partitioned as XI_{ex} and XI_{sub}. I^S_{B1},I^S_{B2} and I_{Brel} are used to describe the base-emitter sidewall parasitics. I_{sf} is the substrate failure current used to warn the designer that the substrate is at a wrong potential. The summaries of these resistances and currents are given in Table 1.1 and 1.2.

Next we discuss the charges present in Mextram 505.00 shown in Figure 1.5, which is obtained by adding AC elements to Figure 1.4. The charges are represented in the circuit by capacitances.

C_{BEO} and C_{BCO} are the overlap capacitances used to shown the constant capacitances between base and emitter or base and collector, due to for instance overlapping metal layers. There are five charges in the intrinsic transistor, which are Q_{t_E}, Q_{BE}, Q_E, Q_{t_C}, and

Currents	
R_E	Constant emitter resistance
R_{Bc}	Constant base resistance
R_{Cc}	Collector Constant resistance
$Rcblx$	Extrinsic collector buried layer resistance
$Rcbli$	Intrinsic collector buried layer resistance

Table 1.1: The resistances of the equivalent circuit given in Figure 1.4.

Currents	
I_N	Main current
I_{avl}	Avalanche current
I_{ztCB}	Collector-base junction tunneling current
I_{B_1}	Ideal forward base current
I_{B_2}	Non-ideal forward base current
I_{ztEB}	Emitter-base junction tunneling current
I_{ex}	Extrinsic reverse base current
I_{B_3}	Non-ideal reverse base current
I_{sub}	Substrate current
XI_{ex}	Extrinsic reverse base current
XI_{sub}	Substrate current
$I_{B_1}^S$	Ideal side-wall base current
$I_{B_2}^S$	Non-ideal side-wall base current
I_{Brel}	Side-wall base current for reliability modeling
I_{Sf}	Substrate failure current
$I_{C_1C_2}$	Epilayer current
$I_{B_1B_2}$	Pinched-base current

Table 1.2: The currents of the equivalent circuit given in Figure 1.4.

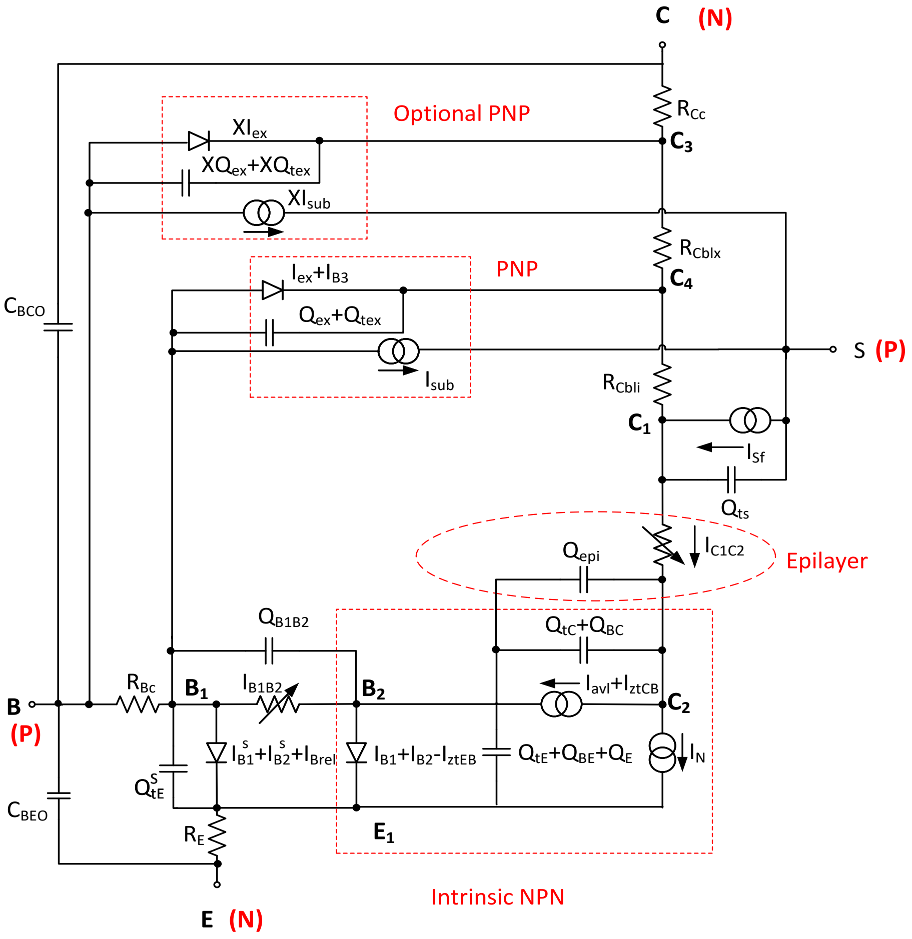

Figure 1.5: AC equivalent circuit for NPN transistor

Q_{BC}. $Q_{t_E}$and Q_{t_C} are almost ideal depletion charges resulting from the base-emitter and base-collector pn-junctions. Q_{BE} and Q_{BC} are referred to as junction diffusion charges. Q_{BE} is related to forward operation and Q_{BC} is related to reverse operation. Q_E is emitter neutral charge. The charge Q_{epi}, which is placed in the epilayer region in Figure 1.5, describes the epilayer diffusion charge. $Q^S_{t_E}$ is the depletion charge of the base-emitter sidewall. Q_{t_S} is the depletion charge of the collector-substrate junction. Q_{ex} and Q_{tex} are the diffusion charge and depletion charge of extrinsic base-collector. XQ_{ex} and XQ_{tex} can be further partitioned from Q_{ex} and Q_{tex}. $Q_{B_1B_2}$ is placed parallel to $I_{B_1B_2}$, used to model the charge due to AC-current crowding in the pinched base. Table 1.3 gives the summary of charges.

Charges	
Q_{BEO}	Base-emitter overlap charge
Q_{BCO}	Base-collector overlap charge
Q_E	Emitter charge or emitter neutral charge
Q_{t_E}	Base-emitter depletion charge
$Q_{t_E}^S$	Sidewall base-emitter depletion charge
Q_{BE}	Base-emitter diffusion charge
Q_{BC}	Base-collector diffusion charge
Q_{t_C}	Base-collector depletion charge
Q_{epi}	Epilayer diffusion charge
$Q_{B_1B_2}$	AC current crowding charge
Q_{tex}	Extrinsic base-collector depletion charge
XQ_{tex}	Extrinsic base-collector depletion charge
Q_{ex}	Extrinsic base-collector diffusion charge
XQ_{ex}	Extrinsic base-collector diffusion charge
Q_{t_S}	Collector-substrate depletion charge

Table 1.3: The charges of the equivalent circuit given in Fig. 1.5.

1.3 Overview of parameters

Mextram 505.00 contains 121 parameters when considering substrate and self-heating. The parameters can be classified into several groups such as general parameters like the level and the model flag, current parameters of the basic model and avalanche model, parameters of resistances and epilayer, the parameters of the depletion capacitances and the transit times. The noise and temperature scaling parameters are also included. Table 1.4 gives all the parameters of Mextram 505.00 [8]. The parameters denoted with a '*' in the description are not used in the DC model.

Table 1.4: Parameters of Mextram 505.00

#	**symbol**	**name**	**units**	**description**
1	DTA	dta	°C	Difference between local ambient and global ambient temperatures
2	MULT	mult	—	Multiplication factor
3	VERSION	version	—	Model level
4	TYPE	type	—	Flag for NPN (1) or PNP (-1) transistor type
5	T_{ref}	tref	°C	Reference temperature. Default is 25°C
6	EXMOD	exmod	—	Flag for extended modeling of the reverse current gain
7	EXPHI	exphi	—	*Flag for distributed high-frequency effects in transient
8	EXAVL	exavl	—	Flag for extended modeling of avalanche currents
9	EXSUB	exsub	—	Flag for extended modeling of substrate currents
10	I_s	is	A	CE saturation current
11	N_{FF}	nff	—	Non-ideality factor of forward main current
12	N_{FR}	nfr	—	Non-ideality factor of reverse main current

#	symbol	name	units	description
13	$\mathsf{I_k}$	ik	A	CE high injection knee current
14	$\mathsf{V_{er}}$	ver	V	Reverse Early voltage
15	$\mathsf{V_{ef}}$	vef	V	Forward Early voltage
16	$\mathsf{I_{BI}}$	ibi	A	Saturation current of ideal base current
17	$\mathsf{N_{BI}}$	nbi	—	Non-ideality factor of ideal base current
18	$\mathsf{I^S_{BI}}$	ibis	A	Saturation current of ideal side wall base current
19	$\mathsf{N^S_{BI}}$	nbis	—	Non-ideality factor of ideal side wall base current
20	$\mathsf{I_{Bf}}$	ibf	A	Saturation current of non-ideal forward base current
21	$\mathsf{m_{Lf}}$	mlf	—	Non-ideality factor of non-ideal forward base current
22	$\mathsf{I^S_{Bf}}$	ibfs	A	Saturation current of non-ideal side wall forward base current
23	$\mathsf{m^S_{Lf}}$	mlfs	—	Non-ideality factor of non-ideal side wall forward base current
24	$\mathsf{I_{BX}}$	ibx	A	Saturation current of extrinsic reverse base current
25	$\mathsf{I_{kBX}}$	ikbx	A	Extrinsic CE high injection knee current
26	$\mathsf{I_{Br}}$	ibr	A	Saturation current of non-ideal reverse base current
27	$\mathsf{m_{Lr}}$	mlr	V	Non-ideality factor of non-ideal reverse base current
28	$\mathsf{X_{ext}}$	xext	—	Part of I_{ex}, Q_{tex}, Q_{ex} and I_{sub} that depends on V_{BC_3} instead of $V_{B_1C_4}$
29	$\mathsf{I_{zEB}}$	izeb	A	Pre-factor of EB Zener tunneling current

#	symbol	name	units	description
30	N_{zEB}	nzeb	—	Coefficient of EB Zener tunneling current
31	I_{zCB}	izcb	A	Pre-factor of CB Zener tunneling current
32	N_{zCB}	nzcb	—	Coefficient of CB Zener tunneling current
33	SWAVL	swavl	—	Switch of avalanche factor G_{EM} model
34	A_{avl}	aavl	—	Ionization rate coefficient A of G_{EM} when swavl $= 1$
35	C_{avl}	cavl	—	Exponent in G_{EM} model when swavl $= 1$
36	I_{TOavl}	itoavl	—	Current temperature parameter of avalanche when swavl $= 1$
37	B_{avl}	bavl	—	Ionization rate coefficient B of G_{EM} when swavl $= 1$
38	$V_{d_{C}avl}$	vdcavl	—	CB diffusion voltage dedicated for G_{EM} model when swavl $= 1$
39	W_{avl}	wavl	m	Epilayer thickness used in weak-avalanche model
40	V_{avl}	vavl	V	Voltage determining curvature of avalanche current
41	S_{fH}	sfh	—	Current spreading factor of avalanche model (when EXAVL $= 1$)
42	R_{E}	re	Ω	Emitter resistance
43	R_{Bc}	rbc	Ω	Constant part of base resistance
44	R_{Bv}	rbv	Ω	Zero-bias value of variable part of the base resistance
45	R_{Cc}	rcc	Ω	Constant part of collector resistance
46	R_{cblx}	rcblx	Ω	Resistance of Collector Buried Layer: extrinsic part

#	symbol	name	units	description
47	R_{cbli}	rcbli	Ω	Resistance of Collector Buried Layer: Intrinsic part
48	R_{Cv}	rcv	Ω	Resistance of un-modulated epilayer
49	SCR_{Cv}	scrcv	Ω	Space charge resistance of epilayer
50	I_{hc}	ihc	A	Critical current for velocity saturation in the epilayer
51	a_{x_i}	axi	—	Smoothness parameter for onset of quasi-saturation
52	V_{d_C}	vdc	V	CB diffusion voltage
53	C_{j_E}	cje	F	*Zero-bias EB depletion capacitance
54	V_{d_E}	vde	V	EB diffusion voltage
55	p_E	pe	—	EB grading coefficient
56	XC_{j_E}	xcje	—	*Sidewall fraction of the EB depletion capacitance
57	C_{BEO}	cbeo	F	*EB overlap capacitance
58	C_{j_C}	cjc	F	*Zero-bias CB depletion capacitance
59	V_{d_Cctc}	vdcctc	V	CB diffusion voltage of depletion capacitance
60	p_C	pc	—	CB grading coefficient
61	SWVCHC	swvchc	—	Switch of V_{ch} for CB depletion capacitance
62	SWVJUNC	swvjunc	—	Switch of V_{junc} for CB depletion capacitance
63	X_p	xp	—	Constant part of C_{j_C}
64	m_C	mc	—	Coefficient for current modulation of CB depletion capacitance
65	XC_{j_C}	xcjc	—	*Fraction of CB depletion capacitance under the emitter
66	C_{BCO}	cbco	F	*CB overlap capacitance
67	m_τ	mtau	—	*Non-ideality factor of emitter stored charge

#	symbol	name	units	description
68	τ_E	taue	s	*Minimum transit time of stored emitter charge
69	τ_B	taub	s	*Transit time of stored base charge
70	τ_epi	tepi	s	*Transit time of stored epilayer charge
71	τ_R	taur	s	*Transit time of reverse extrinsic stored base charge
72	$\mathsf{dE_g}$	deg	eV	Bandgap difference over the base
73	$\mathsf{X_{rec}}$	xrec	—	Pre-factor of recombination part of I_{B_1}
74	$\mathsf{X_{Q_B}}$	xqb	—	Emitter-fraction of base diffusion charge
75	$\mathsf{K_E}$	ke	—	*Fraction of Q_E in excess phase shift
76	$\mathsf{A_{Q_{B0}}}$	aqbo	—	Temperature coefficient of zero-bias base charge
77	$\mathsf{A_E}$	ae	—	Temperature coefficient of resistivity of emitter
78	$\mathsf{A_B}$	ab	—	Temperature coefficient of resistivity of base
79	$\mathsf{A_{epi}}$	aepi	—	Temperature coefficient of resistivity of epilayer
80	$\mathsf{A_{ex}}$	aex	—	Temperature coefficient of resistivity of extrinsic base
81	$\mathsf{A_C}$	ac	—	Temperature coefficient of resistivity of collector contact
82	$\mathsf{A_{CX}}$	acx	—	Temperature coefficient of extrinsic reverse base current
83	$\mathsf{A_{cbl}}$	acbl	—	Temperature coefficient of resistivity of collector buried layer
84	$\mathsf{V_{g_B}}$	vgb	V	Band-gap voltage of base
85	$\mathsf{V_{g_C}}$	vgc	V	Band-gap voltage of collector
86	$\mathsf{V_{g_E}}$	vge	V	Band-gap voltage of emitter
87	$\mathsf{V_{g_{CX}}}$	vgcx	V	Band-gap voltage of extrinsic collector

#	symbol	name	units	description
88	$\mathsf{V_{g_j}}$	vgj	V	Band-gap voltage recombination EB junction
89	$\mathsf{V_{gzEB}}$	vgzeb	V	Band-gap voltage at T_{ref} for EB tunneling
90	$\mathsf{A_{VgEB}}$	avgeb	V/K	Temperature coefficient of band-gap voltage for EB tunneling
91	$\mathsf{T_{VgEB}}$	tvgeb	K	Temperature coefficient of band-gap voltage for EB tunneling
92	$\mathsf{V_{gzCB}}$	vgzcb	V	Band-gap voltage at T_{ref} for CB tunneling
93	$\mathsf{A_{VgCB}}$	avgcb	V/K	Temperature coefficient of band-gap voltage for CB tunneling
94	$\mathsf{T_{VgCB}}$	tvgcb	K	Temperature coefficient of band-gap voltage for CB tunneling
95	$\mathsf{dV_{g\tau_E}}$	dvgte	V	*Band-gap voltage difference of emitter stored charge
96	$\mathsf{dA_{I_s}}$	dais	—	Fine tuning of temperature dependence of C-E saturation current
97	$\mathsf{t_{NFF}}$	tnff	/K	Temperature coefficient of N_{FF}
98	$\mathsf{t_{NFR}}$	tnfr	/K	Temperature coefficient of N_{FR}
99	$\mathsf{T_{Bavl}}$	tbavl	—	Temperature scaling parameter of B_{avl} when swavl $= 1$
100	$\mathsf{A_f}$	af	—	*Exponent of Flicker-noise of ideal base current
101	$\mathsf{A_{fN}}$	afn	—	*Exponent of Flicker-noise of non-ideal base current
102	$\mathsf{K_f}$	kf	—	*Flicker-noise coefficient of ideal base current
103	$\mathsf{K_{fN}}$	kfn	—	*Flicker-noise coefficient of non-ideal base current
104	$\mathsf{K_{avl}}$	kavl	—	*Switch for white noise contribution due to avalanche

#	symbol	name	units	description
105	K_C	kc	—	*Switch for RF correlation noise model selection
106	F_{taun}	ftaun	—	*Fraction of noise transit time to total transit time
107	I_{Ss}	iss	A	Saturation current of parasitic BCS transistor main current
108	I_{CSs}	icss	A	CS junction ideal saturation current
109	I_{ks}	iks	A	Knee current for BCS transistor main current
110	C_{jS}	cjs	F	*Zero-bias CS depletion capacitance
111	V_{dS}	vds	V	*CS diffusion voltage
112	p_S	ps	—	*CS grading coefficient
113	V_{gS}	vgs	V	Band-gap voltage of the substrate
114	A_S	as	—	Temperature coefcient of the mobility related to the substrate currents
115	A_{sub}	asub	—	Temperature coefficient for mobility of minorities in the substrate
116	R_{th}	rth	°C/W	Thermal resistance
117	C_{th}	cth	J/°C	*Thermal capacitance
118	A_{th}	ath	—	Temperature coefficient of thermal resistance
119	N_{FIBrel}	nfibrel	—	Non-ideality factor of base current for reliability simulation
120	I_{SIBrel}	isibrel	—	Saturation current of base current for reliability simulation
121	G_{min}	gmin	—	Minimum conductance

Some features of the model are optional and can be switched on or off by setting flags, which includes: a) The extended modeling of reverse behavior; b) The distributed high-frequency effects; c) The increase of the avalanche current when the current density in the epilayer exceeds the doping level; d) The increase of intrinsic base current noise with frequency and its correlation with intrinsic collector current noise; e) Additional noises from impact ionization; f) Avalanche multiplication. Compared to Mextram 504.12, Mextram 505.00 has some changes and new features listed below [8]:

- A model of CB junction tunneling current I_{ztCB} is added.
- Non-ideality factors $\mathsf{N_{FF}}$ and $\mathsf{N_{FR}}$ in forward and reverse transport current I_N, are added respectively. They are temperature dependent factors.
- Diffusion charge and diffusion capacitance expressions are modified accordingly to maintain the same transit time.
- Non-ideality factors $\mathsf{N_{BI}}$ and $\mathsf{N_{BI}^S}$ in ideal base current I_{B_1} and $I_{B_1}^S$, are added respectively.
- $I_{B_2}^S$, side-wall non-ideal base current, is added.
- I_{Brel}, side-wall base current for reliability modeling, is added.
- All base current components have their own saturation current and non-ideality factors where needed. Current gains (β_f, β_{ri}) are no longer used.
- Non-ideal reverse base current is now formulated the same way as forward non-ideal base current.
- 1/f noise of all ideal base currents is now calculated from $\mathsf{K_f}$ and $\mathsf{A_f}$, and placed between B_2 and E_1. 1/f noise of all non-ideal base currents is now calculated from $\mathsf{K_{fN}}$ and $\mathsf{A_{fN}}$, and placed between B_1 and E_1.
- Avalanche current I_{avl} is calculating in I_N as initiating current, and I_{avl} limits are also modulated accordingly.
- A new avalanche factor (G_{EM}) model is added and used as default.

- SWAVL, a switch parameter for avalanche factor, is added.

  SWAVL = 0, no avalanche current. SWAVL = 1 (default), the new avalanche factor model. SWAVL = 2, Mextram 504 avalanche model. EXAVL is meaningful only when SWAVL=2.

- $V_{d_C ctcT}$, diffusion voltage dedicated for CB depletion capacitance, is added.

- SWVJUNC, switch for V_{junc} calculation, is added. SWVJUNC = 0 (default), 1, and 2 (504).

  SWVJUNC=0: V_{junc}=$V_{B_2C_2}$. SWVJUNC=1: V_{junc}=$V_{B_2C_1}$.

  SWVJUNC=2: V_{junc}=$V_{B_2C_1}$+V_{xi0}.

- SWVCHC, switch for transition voltage width V_{ch} in CB capacitance-voltage curve smoothing, is added. SWVCHC=0 (default) and 1 (504).

  SWVCHC=0: V_{ch} = 0.1 V_{d_CT}.

  SWVCHC=1: V_{ch} = V_{d_CT} $\left(0.1 + 2\,\frac{I_{C_1C_2}}{I_{C_1C_2}+I_{qs}}\right)$.

- I_{ex} is now corrected to describe extrinsic BC junction current as hole injection into collector (in 504, it was described as electron injection current from collector to extrinsic base - which is not the case for real devices)

- I_{KS} means true substrate current's knee.

- Default value of EXSUB is 1 instead of 0.

- Range of I_{CS_S} is changed from (-inf, inf) to [0.0, inf).

- p_0^* and p_W are clipped to avoid convergence problems at high V_{CB}.

- X_{ext} coding is improved to allow X_{ext} = 0.

To be more flexible we introduce in Mextram 505 new saturation current and knee current parameters by removing all current gain parameters. The following conversion betweeen

Mextram 504 and 505 can be employed to keep the same number of these parameters;

$$\mathsf{I_{BI}} = \frac{\mathsf{I_s}}{\beta_f{}^{(504)}}$$

$$\mathsf{I_{BX}} = \frac{\mathsf{I_s}}{\beta_{ri}{}^{(504)}}$$

$$\mathsf{I_{kBX}} = \frac{\mathsf{I_k}}{\beta_{ri}{}^{(504)}}$$

Substrate knee current parameter in Mextram 505 uses same name but different meaning as that in Mextram 504:

$$\mathsf{I_{ks}}^{(505)} = \mathsf{I_{ks}}^{(504)} \cdot \frac{\mathsf{I_{Ss}}}{\mathsf{I_s}}$$

The new parameters of Mextram 505.00 are given in Table 1.5. Note that the parameters denoted with a '*' are not used in the DC model.

Table 1.5: New parameters of Mextram 505.00 compared to 504.12.

#	**symbol**	**name**	**units**	**description**
1	$\mathsf{N_{FF}}$	nff	—	Non-ideality factor of forward main current
2	$\mathsf{N_{FR}}$	nfr	—	Non-ideality factor of reverse main current
3	$\mathsf{I_{BI}}$	ibi	A	Saturation current of ideal base current
4	$\mathsf{N_{BI}}$	nbi	—	Non-ideality factor of ideal base current
5	$\mathsf{I^S_{BI}}$	ibis	A	Saturation current of ideal side wall base current
6	$\mathsf{N^S_{BI}}$	nbis	—	Non-ideality factor of ideal side wall base current
7	$\mathsf{I^S_{Bf}}$	ibfs	A	Saturation current of non-ideal side wall forward base current
8	$\mathsf{m^S_{Lf}}$	mlfs	—	Non-ideality factor of non-ideal side wall forward base current

#	**symbol**	**name**	**units**	**description**
9	$\mathsf{I_{BX}}$	ibx	A	Saturation current of extrinsic reverse base current
10	$\mathsf{I_{kBX}}$	ikbx	A	Extrinsic CE high injection knee current
11	$\mathsf{m_{Lr}}$	mlr	V	Non-ideality factor of non-ideal reverse base current
12	$\mathsf{I_{zCB}}$	izcb	A	Pre-factor of CB Zener tunneling current
13	$\mathsf{N_{zCB}}$	nzcb	—	Coefficient of CB Zener tunneling current
14	SWAVL	swavl	—	Switch of avalanche factor G_{EM} model
15	$\mathsf{A_{avl}}$	aavl	—	Ionization rate coefficient A of G_{EM} when swavl $= 1$
16	$\mathsf{C_{avl}}$	cavl	—	Exponent in G_{EM} model when swavl $= 1$
17	$\mathsf{I_{TOavl}}$	itoavl	—	Current temperature parameter of avalanche when swavl $= 1$
18	$\mathsf{B_{avl}}$	bavl	—	Ionization rate coefficient B of G_{EM} when swavl $= 1$
19	$\mathsf{V_{d_{C}avl}}$	vdcavl	—	CB diffusion voltage dedicated for G_{EM} model when swavl $= 1$
20	$\mathsf{V_{d_{C}ctc}}$	vdcctc	V	CB diffusion voltage of depletion capacitance
21	SWVCHC	swvchc	—	Switch of V_{ch} for CB depletion capacitance
22	SWVJUNC	swvjunc	—	Switch of V_{junc} for CB depletion capacitance
23	$\mathsf{K_{E}}$	ke	—	*Fraction of Q_E in excess phase shift
24	$\mathsf{A_{CX}}$	acx	—	Temperature coefficient of extrinsic reverse base current
25	$\mathsf{V_{g_{E}}}$	vge	V	Band-gap voltage of emitter
26	$\mathsf{V_{gcx}}$	vgcx	V	Band-gap voltage of extrinsic collector
27	$\mathsf{T_{VgCB}}$	tvgcb	K	Temperature coefficient of band-gap voltage for CB tunneling

#	symbol	name	units	description
28	$\mathsf{V}_{\mathsf{gzCB}}$	vgzcb	V	Band-gap voltage at T_{ref} for CB tunneling
29	$\mathsf{A}_{\mathsf{VgCB}}$	avgcb	V/K	Temperature coefficient of band-gap voltage for CB tunneling
30	$\mathsf{t}_{\mathsf{NFF}}$	tnff	/K	Temperature coefficient of N_{FF}
31	$\mathsf{t}_{\mathsf{NFR}}$	tnfr	/K	Temperature coefficient of N_{FR}
32	$\mathsf{T}_{\mathsf{Bavl}}$	tbavl	—	Temperature scaling parameter of B_{avl} when swavl $= 1$
33	A_{fN}	afn	—	*Exponent of Flicker-noise of non-ideal base current
34	$\mathsf{N}_{\mathsf{FIBrel}}$	nfibrel	—	Non-ideality factor of base current for reliability simulation
35	$\mathsf{I}_{\mathsf{SIBrel}}$	isibrel	—	Saturation current of base current for reliability simulation

1.4 Modeling tools of parameter extraction

Nowadays Mextram is one of the most prevalent bipolar transistor models, which can be used for the simulation of Si and SiGe bipolar transistors for both analog and digital circuit design. The accuracy of circuit simulation depends on the mathematical description of physical phenomena and the model parameters used. In this work, the parameters are extracted by using the analysis program ICCAP with simulator ADS.

Parameter extraction is a crucial part of model development, this process mathematically minimizes the difference between measured and simulated data. Mextram model equations are implemented in Verilog-A language, which is a language that is commonly used by most simulators to describe the analog behavior of devices. The SiGe HBT used in this thesis utilizes

Filename	Description
bjt505t.va	Fully defines Mextram model including the module and ports then loads the following files to calculate
frontdef.inc	Assigns values to model constants and defines limiting functions
parameters.inc	Passes model parameters into the model from the circuit. Declares data type and data range
variables.inc	Defines variables for internal equations of model
tscaling.inc	Defines temperature scaling equations
evaluate.inc	Defines all equations in Mextram

Table 1.6: The structure of Mextram 505.00 code.

the model card name of bjt505tva, which calls a Verilog-A code for a BJT including substrate terminal and self-heating modeling. The structure of the code [9] is listed in Table 1.6.

1.5 Measurements

For a reliable extraction of parameters, getting the measurements done over a large range of different bias conditions is very important. There are different measurement setups such as forward Early measurement, reverse Early measurement, forward Gummel measurement, reverse Gummel measurement and output characteristic measurement. An overview of the different measurement setups and bias conditions used to get the data in this thesis is shown in Table 1.7. The parameters can be extracted from appropriate measurements.

Table 1.7: The measurement setups in this thesis.

Measurement name	**Bias setting**	**Meas. data**
Forward Early	V_{BE} = 0.68V, V_{CB} = 0 ... 5.0V	I_C, I_B
Reverse Early	V_{BC} = 0.65V, V_{EB} = 0 ... 1.5V	I_E, I_B
Forward Gummel	V_{BC} = 0V, V_{BE} = 0.3V ...1.2V	I_C, I_B, I_{sub}
Reverse Gummel	V_{BE} = 0V, V_{BC} = 0.3V ...1.2V	I_E, I_B, I_{sub}
R_E flyback	I_c = 1μA, V_{BE} = 0.8V ...1.315V	I_E, V_{CE}

Measurement name	**Bias setting**	**Meas. data**
R_{Cc} active	V_{BC}= 0.6V, V_{BE} = 0.6V ...1.4V	I_C, I_B, I_{sub}
Output - characteristic	I_B = $2.44\mu A$, $13.84\mu A$, $23.82\mu A$, $37.69\mu A$, $57.72\mu A$	
	V_{CE} = 0...4.0V	I_C, I_{sub}, V_{BE}
Base-emitter depl. cap.	V_{BE} = 0...0.55V	C_{BE}
Base-collector depl. cap.	V_{BC} = -2.5V...1.0V	C_{BC}
Substrate-coll. depl. cap.	V_{SC} = -2.5V...1.0V	C_{SC}
S-parameters	V_{CB} =-0.5V, 0V, 1.0V, 2.0V	
	V_{BE} = 0.6V...1.1V	I_C, I_B, S-pars.

1.6 Temperature scaling basics

Temperature scaling parameters describe how characteristics of a transistor vary when temperature changes. This change may be due to self-heating, which can increase the local temperature of the transistor, or change of environment temperature. Table 1.8 shows temperature scaling parameters, and the electrical parameters each temperature scaling parameter affects.

The actual simulation temperature is denoted by TEMP (in °C). The temperature at which the parameters are determined is $\mathrm{T_{ref}}$ (also in °C). In this work $\mathrm{T_{ref}}$ is 26.85°C for the measurements at 300 K are used as reference to do temperature scaling extraction.

Conversion to Kelvin

$$T_K = \text{TEMP} + \text{DTA} + 273.15 + \mathrm{V_{dT}}, \tag{1.1a}$$

$$T_{\text{amb}} = \text{TEMP} + \text{DTA} + 273.15, \tag{1.1b}$$

$$T_{RK} = \mathrm{T_{ref}} + 273.15, \tag{1.2}$$

$$t_N = \frac{T_K}{T_{RK}}. \tag{1.3}$$

1	A_{QB0}	V_{er}, V_{ef}, I_s, R_{Bv}, τ_B, τ_R, dE_g
2	A_E	R_E,I_{BI}, I^s_{BI},
3	A_B	R_{Bv},I_s,I_k τ_B, τ_R, τ_E
4	A_{epi}	R_{c_v}, τ_{epi}, τ_R
5	A_{ex}	R_{B_C}
6	A_C	R_{C_C}
7	A_S	I_{S_S}, I_{ks}
8	A_{CX}	I_{BX}, I_{kBX}
9	A_{sub}	I_{CSs}
10	V_{g_B}	I_s, C_{j_E}, V_{d_E}, V_{er}
11	V_{g_C}	C_{j_C}, V_{d_C}, $V_{d_C ctc}$, X_p, I_{Br}, V_{ef}
12	V_{g_S}	I_{S_S}, I_{CSs}, C_{j_S}, V_{d_S}
13	V_{g_j}	I^s_{BF}, I^s_{SIBrel}
14	$V_{g_{CX}}$	I_{BX}
15	$dV_{g\tau_E}$	τ_E
16	T_{Bavl}	B_{avl}

Table 1.8: The temperature parameters in the temperature scaling rules of the electrical parameters.

Note that V_{dT} is the voltage of temperature node dT shown in Figure 1.3. The value of V_{dT} contributes to the increase in local temperature. DTA is the difference between device and ambient temperatures and its default value is 0. T_K is the actual temperature of the circuit.

Thermal voltage

$$V_T = (\frac{k}{q})T_K, \tag{1.4}$$

k is Boltzmann constant:

$$k = 1.38064852 \times 10^{-23}\,\mathrm{J/K}, \tag{1.5}$$

q is elementary charge:

$$q = 1.6021918 \times 10^{-19}\,\mathrm{C}, \tag{1.6}$$

$$V_{T_R} = (\frac{k}{q})T_{RK}, \tag{1.7}$$

$$\frac{1}{V_{\Delta T}} = \frac{1}{V_T} - \frac{1}{V_{T_R}}, \tag{1.8}$$

V_T is the thermal voltage at the actual temperature T_K. V_{T_R} is the thermal voltage at reference temperature T_{RK}.

In DC low current parameter extraction at the reference temperature, the temperature rise due to self-heating is negligible. However, there is still a temperature increase when bias gets larger. Some temperature scaling parameters can be obtained from low current parameter extraction in order to provide a good estimation for high current parameter extractions. To denote a temperature scaled parameter, a capital letter 'T' is added to the subscript. For example, I_{kT} and R_{CcT} are parameters after temperature scaling.

1.7 Outline

We have reviewed the background of the SiGe HBT, and given an overview of Mextram 505.00. The modeling tools are briefly introduced. The measurements required for parameter extraction and temperature scaling fundamentals are also discussed.

In chapter 2, the parameters are separated into several groups based on how they are extracted. Then an extraction strategy is proposed.

Parameter initialization is described in chapter 3. Extraction of low current parameters is presented in chapter 4. These parameters include the parameters of capacitances, the avalanche effect, Early effect, Gummel characteristics and their related temperature scaling parameters. In chapter 5, high current parameters, as well as related temperature scaling parameters are extracted from high current output characteristics and cut-off frequency. Finally, all the extraction results are shown in chapter 6.

Chapter 2

Parameter extraction strategy

For the sake of an accurate extraction result, a good strategy which considers the conflicts and sequences between parameters is necessary. The general strategy of parameter extraction is to separate the parameters into small groups and then extract the parameters simultaneously out of correlated measurement.

2.1 Grouping of parameters

As we mentioned before, some of the Mextram parameters are flag parameters which are used to switch on or off a part of the model, some are electrical parameters used to describe currents, and some are used to describe the temperature dependence of a transistor. Thus, the parameters could be classified as parameters extracted at low-injection and high-injection, of which the electrical parameters and temperature-scaling parameters could also be further separated [10]. A typical grouping of Mextram 505.00 parameters [8] is given in Table 2.1.

Table 2.1: A typical grouping of parameters in Mextram 505.00.

Base-emitter capacitance	: C_{j_E}, p_E, V_{d_E}
Base-collector capacitance	: C_{j_C}, p_C, X_p, V_{d_Cctc}
Collector-substrate capacitance	: C_{j_S}, p_S, V_{d_S}
Avalanche at small collector currents, high V_{CB}	: A_{avl}, B_{avl}, C_{avl}, V_{d_cavl}, T_{Bavl}
Avalanche at high collector currents	: I_{TOavl}

Reverse Early effect	: V_{er}
Forward Early effect	: V_{ef}
Forward and reverse Early effect	: dE_g
Forward Gummel I_C	: I_s, N_{FF}, I_k
Forward Gummel I_B	: I_{BI}, I_{BI}^s, I_{Bf}, I_{Bf}^s, N_{BI}, N_{BI}^s, m_{Lf}, m_{Lf}^s
Reverse Gummel I_E	: N_{FR}
Reverse Gummel I_B and I_{sub}	: I_{BX}, I_{kBX}, I_{Br}, m_{Lr}, I_{Ss}, I_{CSs}, I_{ks}
Giacoletto method	: R_E
From forward Gummel plot at large V_{BE}, Y-parameters, or scaling	: R_{Bc}, R_{Bv}
Substrate current in hard saturation	: R_{Cc}
Geometry scaling	: XC_{jE}, XC_{jC}
Temperature scaling	: Temperature parameters shown in Table 1.8
Decrease of V_{BE} for constant I_B at high V_{CE}	: R_{th}
Collector current up to high V_{CE}	: I_k
From the fall-off of h_{fe} and f_T at high currents	: R_{Cv}, V_{d_C}
From the f_T vs. I_C	: SCR_{Cv}, I_{hc}, τ_E, τ_{epi}, τ_B, a_{x_i}, m_τ, m_C
Reverse Gummel plot at large V_{BC}	: X_{ext}

Actually, it is not realistic to extract all the Mextram model parameters from one measured transistor. For instance, the determination of geometrical scaling parameters XC_{jE} and XC_{jC} needs more devices. The parameters describing the side wall, such as I_{BI}^s and I_{Bf}^s, also need more information about geometrical scaling and technology. Therefore, these parameters are not extracted in this work.

2.2 Extraction strategy

Some of these parameters could be extracted directly from the measurement. The extraction of low-current parameters is straightforward, but the extraction of high-current parameters demands much more efforts, for many physical effects occur in this regime. In general, low-current parameters are extracted before high-current parameters. Temperature-scaling parameters are extracted when temperature variation due to self-heating and environment changing cannot be ignored.

The collector-emitter saturation current I_S, which is a temperature-sensitive parameter used to describe the collector current, is used here to show the influence of temperature variation. I_S is extracted from forward Gummel measurement. The actual temperature T_K in this measurement is increased when the bias gets larger, as shown in Figure 2.1, for the $V_{CB} = 0$ Gummel measurement.

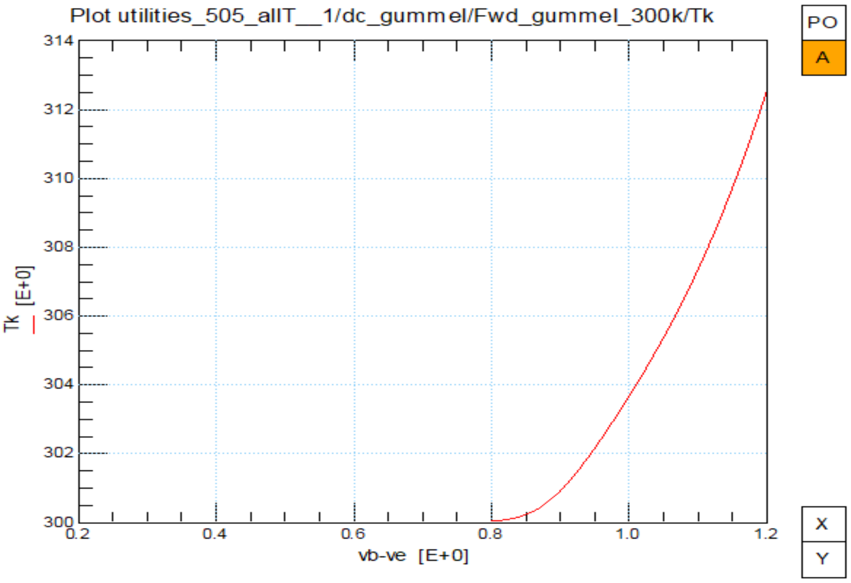

Figure 2.1: The actual temperature T_k of forward Gummel measurement at 300 K

T_K increases from 300 K to around 313 K in the measurement at TEMP = 300 K due to self-heating. Meanwhile, the curve of I_S - T_K is given in Figure 2.2, showing that as T_K

increasing, I_S increases several times. The situation is much worse for high current, high voltage measurements, where self-heating is much more significant.

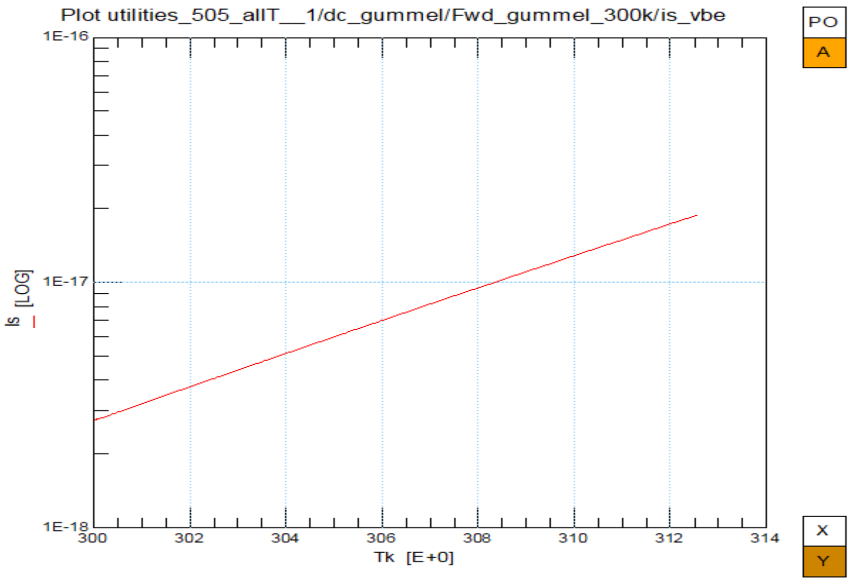

Figure 2.2: I_S - T_K

Therefore, the impact of temperature variation is so significant that the temperature scaling parameters need to be extracted properly. The extraction strategy of this work is shown in Figure 2.3.

Instead of extracting temperature scaling parameters after the extraction of all the electrical parameters as described in [11], most temperature scaling parameters are estimated in low-current parameter measurement and then be optimized when extracting high-current parameters in this work. To be more detailed, we first extract parameters of depletion capacitance from $C - V$ characteristics, then extract the electrical and temperature scaling parameters of the avalanche factor G_{em} and the parameters of Early effect in Early measurement. Next, the saturation currents are extracted and resistances are estimated from Gummel measurement, followed by their temperature scaling parameters. V_{dC} is estimated from the fall-off of forward current gain. After checking low current output plots we can start to extract high current electrical and temperature scaling parameters from high current output plots. Then we extract electrical parameters and temperature scaling parameters of cut-off frequency.

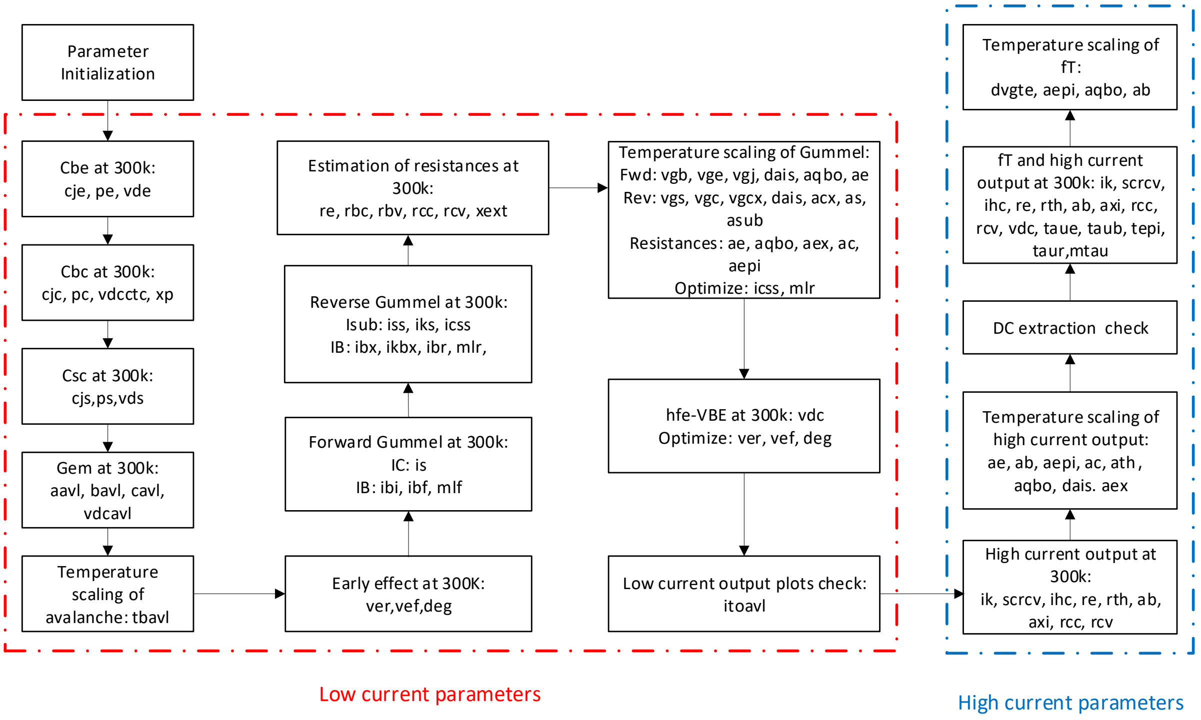

Figure 2.3: Parameter Extraction Strategy

Chapter 3

Parameter initialization

The first step in parameter extraction is to generate an initial parameter set. The initial values of the parameters are important because they could offer a good starting point. With the good estimation of these values, the optimizing process could be fast and accurate, and the chance of getting stuck with very unphysical parameter values is lowered.

In this section, the method of giving initial values of parameters is introduced. The parameters are separated into three categories here. One is immediately given as constant, such as LEVEL, TYPE, and flag settings. One is obtained directly from their measurements without optimizing, like C_{jE} and C_{jC}. The other one is calculated from layout and process data, like the knee currents and resistances.

3.1 Parameters that can be given as a constant value

Table 3.1 gives the parameters whose initial value is constant. Some of them are process dependent [11]. These values come from a realistic transistor [8] and are good indication of typical values.

Table 3.1: Parameters that can be set to a constant as initial value

Parameter	**value**	**remark**
TYPE	1	Flag for NPN (1) or PNP (-1) transistor type
$\mathrm{T}_{\mathrm{ref}}$	26.85	Reference temperature
DTA	0	T_{ref} already describes the actual temperature

Parameter	**value**	**remark**
EXMOD	1	Flag for extended modelling of the reverse current gain
EXPHI	1	Flag for the distrubuted high-frequency effects in transient
EXAVL	0	Flag for extended modelling of avalanche currents
EXSUB	1	Flag for extended modelling of substrate currents
SWAVL	1	Switch of avalanche factor G_{EM} model
SWVCHC	0	Switch of V_{ch} for CB depletion capacitance
SWVJUNC	0	Switch of V_{junc} for CB depletion capacitance
$\mathsf{N_{FF}}$	1	
$\mathsf{N_{FR}}$	1	
$\mathsf{N_{BI}}$	1	
$\mathsf{I_{BI}^{S}}$	0	
$\mathsf{N_{BI}^{S}}$	1	
$\mathsf{m_{Lf}}$	2	
$\mathsf{I_{Bf}^{S}}$	0	
$\mathsf{m_{Lf}^{S}}$	2	
$\mathsf{I_{kBX}}$	$14.29 \cdot 10^{-3}$	
$\mathsf{m_{Lr}}$	2	
$\mathsf{X_{ext}}$	0.63	
$\mathsf{I_{zEB}}$	0	
$\mathsf{N_{zEB}}$	22	
$\mathsf{I_{zCB}}$	0	
$\mathsf{N_{zCB}}$	22	
$\mathsf{A_{avl}}$	400	
$\mathsf{B_{avl}}$	25	
$\mathsf{C_{avl}}$	-0.37	
$\mathsf{V_{d_{C}avl}}$	0.1	
$\mathsf{I_{TOavl}}$	$500 \cdot 10^{-3}$	

Parameter	**value**	**remark**
$\mathsf{R_{cblx}}$	0	
$\mathsf{R_{cbli}}$	0	
$\mathsf{a_{x_i}}$	0.3	
$\mathsf{V_{d_E}}$	0.95	Somewhat depending on process
$\mathsf{p_E}$	0.4	
$\mathsf{C_{BEO}}$	0	
$\mathsf{C_{BCO}}$	0	
$\mathsf{m_\tau}$	1.0	
$\mathsf{dE_g}$	0	
$\mathsf{X_{rec}}$		
$\mathsf{K_E}$	0	
$\mathsf{X_{Q_B}}$	1/3	
$\mathsf{A_{Q_{B0}}}$	0.3	Somewhat depending on process
$\mathsf{A_E}$	0	Somewhat depending on process
$\mathsf{A_B}$	1.0	Somewhat depending on process
$\mathsf{A_{ex}}$	0.62	Somewhat depending on process
$\mathsf{A_{epi}}$	2.5	Somewhat depending on process
$\mathsf{A_C}$	2	Somewhat depending on process
$\mathsf{A_{CX}}$	1.3	Somewhat depending on process
$\mathsf{A_{cbl}}$	2	Somewhat depending on process
$\mathsf{V_{g_B}}$	1.17	
$\mathsf{V_{g_C}}$	1.18	
$\mathsf{V_{gcx}}$	1.125	
$\mathsf{V_{g_E}}$	1.12	
$\mathsf{V_{g_J}}$	1.15	
$\mathsf{V_{gzEB}}$	1.15	
$\mathsf{A_{VgEB}}$	$4.73 \cdot 10^{-4}$	

Parameter	**value**	**remark**
$\mathsf{T_{VgEB}}$	636	
$\mathsf{V_{gzCB}}$	1.15	
$\mathsf{A_{VgCB}}$	$4.73 \cdot 10^{-4}$	
$\mathsf{T_{VgCB}}$	636	
$\mathsf{dV_{g\tau_E}}$	0.05	
$\mathsf{dA_{I_s}}$	0	
$\mathsf{t_{NFF}}$	0	
$\mathsf{t_{NFR}}$	0	
$\mathsf{T_{Bavl}}$	$500 \cdot 10^{-6}$	
$\mathsf{A_f}$	2	
$\mathsf{A_{fN}}$	2	
$\mathsf{K_f}$	$20 \cdot 10^{-12}$	
$\mathsf{K_{fN}}$	$20 \cdot 10^{-12}$	
$\mathsf{K_{avl}}$	0	
$\mathsf{K_C}$	0	
$\mathsf{F_{taun}}$	0	
$\mathsf{I_{CSs}}$	0	
$\mathsf{V_{d_S}}$	0.62	Somewhat depending on process
$\mathsf{p_S}$	0.34	
$\mathsf{V_{g_S}}$	1.2	
$\mathsf{A_S}$	1.58	Somewhat depending on process
$\mathsf{A_{sub}}$	2.0	Somewhat depending on process
$\mathsf{R_{th}}$	1000	
$\mathsf{C_{th}}$	$3.0 \cdot 10^{-9}$	
$\mathsf{A_{th}}$	0	Somewhat depending on process
$\mathsf{I_{SIBrel}}$	0	
$\mathsf{N_{FIBrel}}$	2	

Parameter	**value**	**remark**
$\mathsf{G}_{\mathsf{min}}$	$1.0 \cdot 10^{-13}$	

The resistances R_{Cblx} and R_{Cbli} have values of zero, which means the internal node C_1 is connected directly to the extrinsic node C via constant collector resistor R_{Cc}.

3.2 Parameters estimated from measurements

Table 3.2 shows the parameters whose initial value are estimated from measured data. The methods of getting these initial values are also given [11].

Take $\mathrm{C_{jE}}$ to explain the method [12]. $\mathrm{C_{jE}}$ is used to describe base-emitter depletion capacitance. When $V_{BE} < V_{dE}$, the capacitance C_{BE} is given as:

$$C_{BE} = \frac{C_{jE}}{(1 - \frac{V_{BE}}{V_{dE}})^{p_E}}, \tag{3.1}$$

clearly, when V_{BE} = 0, we have C_{BE} = $\mathrm{C_{jE}}$. Therefore the initial value of $\mathrm{C_{jE}}$ is obtained.

The saturation currents are very important and they can be easily estimated from measurement data, so we explain their initialization here. Ignoring Early effect, currents can be estimated as:

$$I = I_{sat}\exp(\frac{V}{V_T}), \tag{3.2}$$

Param	Way of extraction
C_{jE}	Zero bias values of base-emitter capacitance
C_{jC}	Zero bias values of base-collector capacitance
C_{jS}	Zero bias values of substrate-collector capacitance
R_E	Numerical derivative in R_E-flyback measurement
V_{er}	Numerical derivative in reverse-Early measurement
V_{ef}	Numerical derivative in forward-Early measurement
I_S	From forward-gummel collector current without Early effect
I_{BI}	From forward-gummel base current
I_{Ss}	From reverse-gummel substrate current without Early effect
I_{BX}	From reverse-gummel base current
τ_E, τ_B	1/[10 π max(f_T)]

Table 3.2: Parameters that can be estimated from measurement.

I_{sat} is the saturation current of I, V is the corresponding control voltage, V_T is thermal voltage. Then the saturation current can be expressed as:

$$I_{sat} = \frac{I}{\exp\frac{V}{V_T}}. \tag{3.3}$$

Note that logarithm scale I needs to be linearly propotional to V when estimating I_{sat}. It is pretty easy to find this bias region when we look at $I-V$ plots. Take the initilization of collector saturation current I_S for example. Neglecting Early effect, the collector current can be given as:

$$I_C = I_S \exp\frac{V_{BE}}{V_T}, \tag{3.4}$$

from this expression we can have I_S as:

$$I_S = \frac{I_C}{\exp\frac{V_{BE}}{V_T}}. \tag{3.5}$$

Then we look at $I_C - V_{BE}$ curve to find the region where logarithm scale I_C is linearly propotional to V_{BE}, as shown in Figure 3.1.

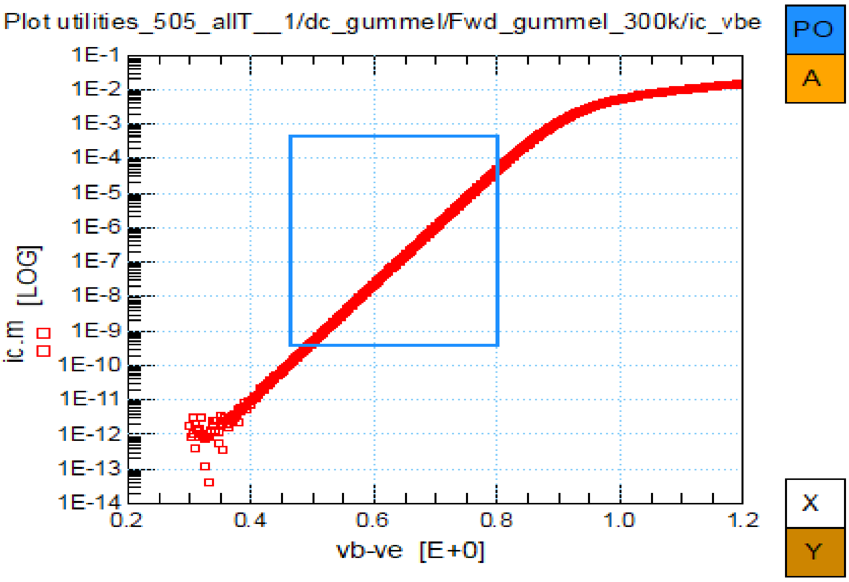

Figure 3.1: Measured $I_C - V_{BE}$ curve

The figure shows that it is suitable to use the collector current between $V_{BE} = 0.5V$ to $V_{BE} = 0.8V$ to estimate I_S. Next we look at the measurement data and find a point in this

MULT	Numbers of transistors measured in parallel
H_{em}	Emitter width (dimension on silicon)
L_{em}	Emitter strip length (dimension on silicon)
ρ_p	Pinched sheet resistance of the base
N_{base}	Number of base stripes
N_{epi}	Collector epilayer doping level
W_{epi}	Collector epilayer thickness

Table 3.3: The layout and process quantities

region, here we use the 185th point whose $V_{BE} = 0.67V$, and then write a program in IC-CAP to calculate I_S. The program is listed below:

```
Vt=(TEMP+273.15)*0.86171E-4


I=ic
V=vb-ve


Index=185
IS=I[Index]//exp(V[Index]//Vt)
```

Other saturation currents I_{BI}, I_{Ss} and I_{BX} are estimated in the same way.

3.3 Parameters that need to be calculated

The last group is the parameters whose initial value need to be calculated from layout and technology data. All parameters of this kind are initialized in this section whatever it's used or not. The layout and process quantities are given in Table 3.3 [11].

The following constants are also needed for the calculation.

Boltzmann constant is:

$$k = 1.38064852 \times 10^{-23}\,\mathrm{J/K}. \tag{3.6}$$

The elementary charge is:

$$q = 1.6021918 \times 10^{-19}\,\mathrm{C}. \tag{3.7}$$

Dielectric constant is:

$$\varepsilon = 1.036 \times 10^{-10}\,\mathrm{C/Vm}. \tag{3.8}$$

The saturated drift velocity is:

$$v_{sat} = 8.0 \cdot 10^{4}\,\mathrm{m/s}. \tag{3.9}$$

The quantities calculated from the reference temperature are [11]:

$$V_T = \frac{kT_{ref}}{q}, \tag{3.10}$$

$$n_i^2 = (9.61 \cdot 10^{32}\mathrm{cm}^{-6}\mathrm{K}^{-3}) \times \mathrm{T}_{\mathrm{ref}}^{3}\mathrm{e}^{-\mathrm{V_{gC}}/\mathrm{V_T}}. \tag{3.11}$$

Process quanties are :

$$H_{em} = 0.5\mu\mathrm{m}, \tag{3.12}$$

$$L_{em} = 2.5\mu\mathrm{m}. \tag{3.13}$$

Base doping is:

$$N_{base} = 1 \times 10^{18}\mathrm{cm}^{-3}. \tag{3.14}$$

Epilayer doping is:

$$N_{epi} = 3 \times 10^{17}\mathrm{cm}^{-3}. \tag{3.15}$$

Thus the emitter surface (A_{em}) and periphery (P_{em}) are calculated as:

$$A_{em} = H_{em} \cdot L_{em}, \tag{3.16}$$

$$P_{em} = 2(H_{em} + L_{em}). \tag{3.17}$$

The fraction of the BE depletion capacitance $\mathrm{XC_{jE}}$ and the fraction of the BC depletion capacitance $\mathrm{XC_{jC}}$ are then calculated from the layout and directly estimated data as [11]:

$$XC_{jE} = \frac{P_{em}}{P_{em} + 6A_{em}/\mu\mathrm{m}}, \tag{3.18}$$

$$XC_{jC} = XC_{jE}\frac{V_{er}}{V_{ef}}\frac{C_{jE}}{C_{jC}}. \tag{3.19}$$

Here $\mathrm{C_{jE}}$ is zero-bias emitter-base depletion capacitance; $\mathrm{C_{jC}}$ is zero-bias collector-base capacitance; $\mathrm{V_{er}}$ is reverse early voltage; $\mathrm{V_{ef}}$ is forward early voltage.

The zero bias value of the variable part of base resistance $\mathrm{R_{Bv}}$, the constant part of the base resistance $\mathrm{R_{Bc}}$ and the constant part of collector resistance $\mathrm{R_{Cc}}$ are calculated by equations [11]:

$$R_{Bv} = \frac{H_{em}\rho_p}{3N_{base}^2 L_{em}}, \tag{3.20}$$

$$R_{Bc} = R_{Cc} = \frac{300\Omega \cdot \mu\mathrm{m}}{L_{em}}. \tag{3.21}$$

The initial values of the knee current $\mathrm{I_K}$ and the knee current for Base-Collector-Substrate(BCS) transistor main current $\mathrm{I_{kS}}$ are [11]:

$$I_K = \frac{V_{er}(1 - XC_{je})C_{je}}{\tau_B}, \tag{3.22}$$

$$I_{kS} = (500\mu\mathrm{A}/\mu\mathrm{m}^2) \times \mathrm{A_{em}} \cdot \frac{\mathrm{I_{Ss}}}{\mathrm{I_S}}. \tag{3.23}$$

The saturation current of the non-ideal reverse base current $\mathrm{I_{Br}}$ and saturation current of the non-ideal forward base current $\mathrm{I_{Bf}}$ are given by [11]:

$$I_{Br} = 100 I_S, \tag{3.24}$$

$$I_{Bf} = 100 I_S. \tag{3.25}$$

The avalanche parameters $\mathrm{W_{epi}}$ and $\mathrm{V_{avl}}$ are from calculation [11]:

$$W_{avl} = W_{epi}, \tag{3.26}$$

$$V_{avl} = \frac{qN_{epi}W_{epi}^2}{2\varepsilon}. \tag{3.27}$$

We also need spreading parameter α_{l} and α_{h} for the calculation of epilayer [11]. The quantities are process and geometry dependent.

$$\tan \alpha_{\mathrm{l}} = 0.5, \tag{3.28}$$

$$\tan \alpha_{\mathrm{h}} = 1.0, \tag{3.29}$$

$$S_{Fl} = \tan \alpha_{\mathrm{l}} \mathrm{W}_{\mathrm{epi}} (\frac{1}{\mathrm{H}_{\mathrm{em}}} + \frac{1}{\mathrm{L}_{\mathrm{em}}}), \tag{3.30}$$

$$S_{Fh} = \frac{2}{3} \tan \alpha_{\mathrm{h}} \mathrm{W}_{\mathrm{epi}} (\frac{1}{\mathrm{H}_{\mathrm{em}}} + \frac{1}{\mathrm{L}_{\mathrm{em}}}). \tag{3.31}$$

The latter quantity is the current spreading factor for high injection, which is a parameter used in the high-current avalanche model. The epilayer parameters are calculated as below [11].

The collector-base diffusion voltage and collector-base diffusion voltage of depletion capacitance is calculated as:

$$V_{dc} = V_{d_C ctc} = V_T ln(N_{epi}^2/n_i^2). \tag{3.32}$$

Resistance of the un-modulated epilayer is calculated as:

$$R_{Cv} = \frac{W_{epi}}{q\mu_0 N_{epi} A_{em}} \frac{1}{(1+S_{Fl})^2}. \tag{3.33}$$

μ_0 is the mobility in the epilayer. Critical current for velocity saturation in the epilayer is evaluated from:

$$I_{hc} = q\mu_0 N_{epi} A_{em} v_{sat} (1+S_{Fl})^2. \tag{3.34}$$

The initial value of space charge resistance of the epilayer is calculated by:

$$SCR_{Cv} = \frac{W_{epi}^2}{2\varepsilon v_{sat} A_{em}} \frac{1}{(1+S_{Fh})^2}, \tag{3.35}$$

$\mathrm{X_p}$ is the constant part of $\mathrm{C_{jC}}$, $\mathrm{p_C}$ is collector-base grading coefficient, $\mathrm{m_C}$ is coefficient for the current modulation of the collector-base depletion capacitance. These quantities are calculated by [11]:

$$xd_0 = \sqrt{\frac{2\varepsilon V_{dc}}{qN_{epi}}}, \tag{3.36}$$

$$X_p = xd_0/W_{epi}, \tag{3.37}$$

$$p_C = 0.3/(1 - X_p), \tag{3.38}$$

$$m_C = (1 - X_p)/2. \tag{3.39}$$

The transit time of stored epilayer charge and transit time of reverse extrinsic stored base charge are calculated using [11]:

$$\tau_{epi} = \frac{W_{epi}^2}{4\mu_0 V_T}, \tag{3.40}$$

$$\tau_R = (\tau_B + \tau_{epi}\frac{1 - XC_{jc}}{XC_{jc}}). \tag{3.41}$$

3.4 Plots after initialization

The parameters are initialized based on what we discussed in this chapter. After initialization, the important characteristics of 300 K including characteristics of Early effect and avalanche effect, forward and reverse Gummel characteristics, output curves and cut-off frequency, are shown in Figure 3.2. As we can see, although all the parameters have physical initial values, the curves of measured and the simulated values are still much different.

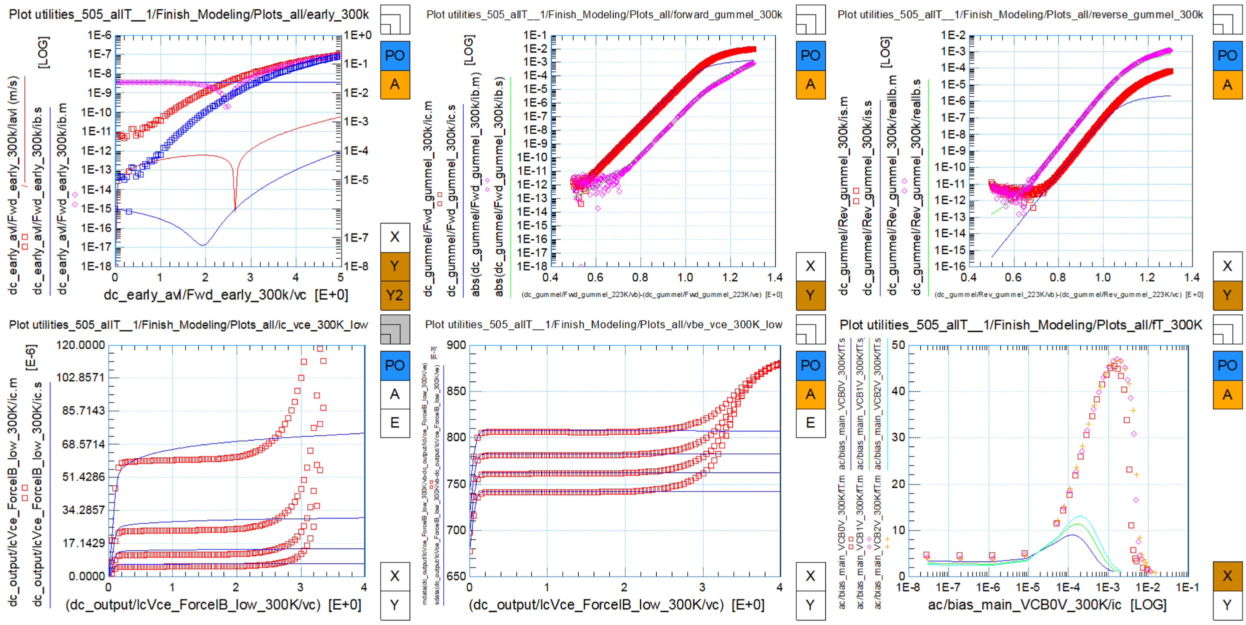

Figure 3.2: Plots of important characteristics at 300 K after initialization.

The forward and reverse currents in Gummel measurement at different temperatures are shown in Figure 3.3, the output characteristics and cut-off frequency curves at different temperatures are shown in Figure 3.4. The curves of their measured values and simulated values are also very different.

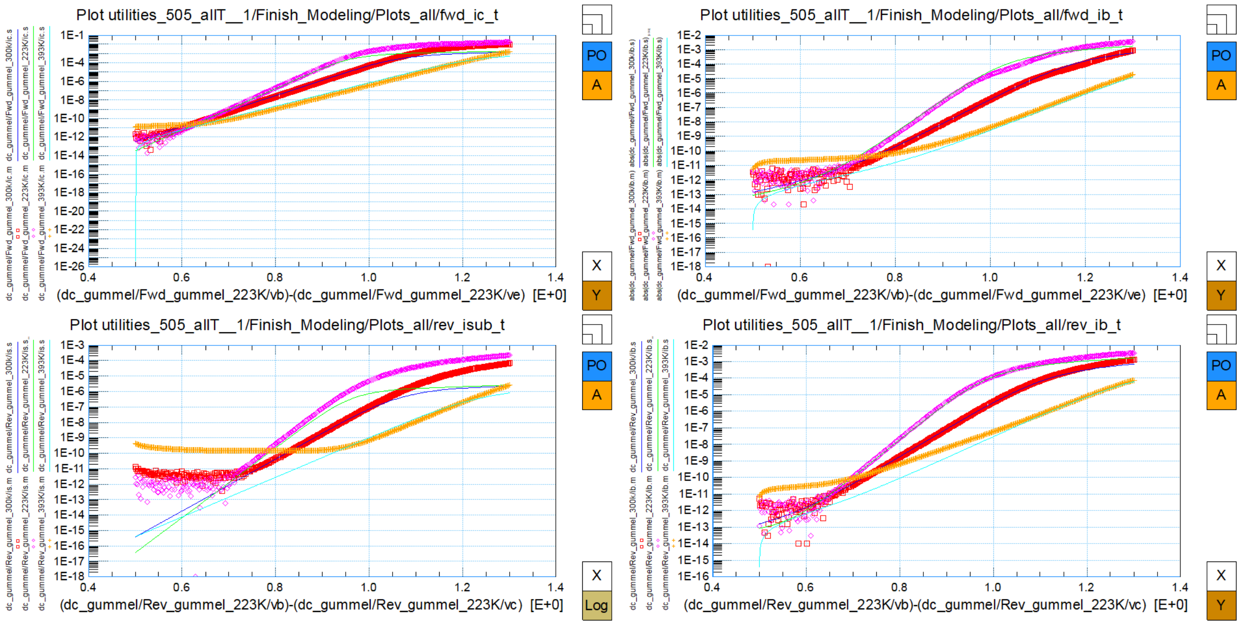

Figure 3.3: Currents at different temperature after initialization.

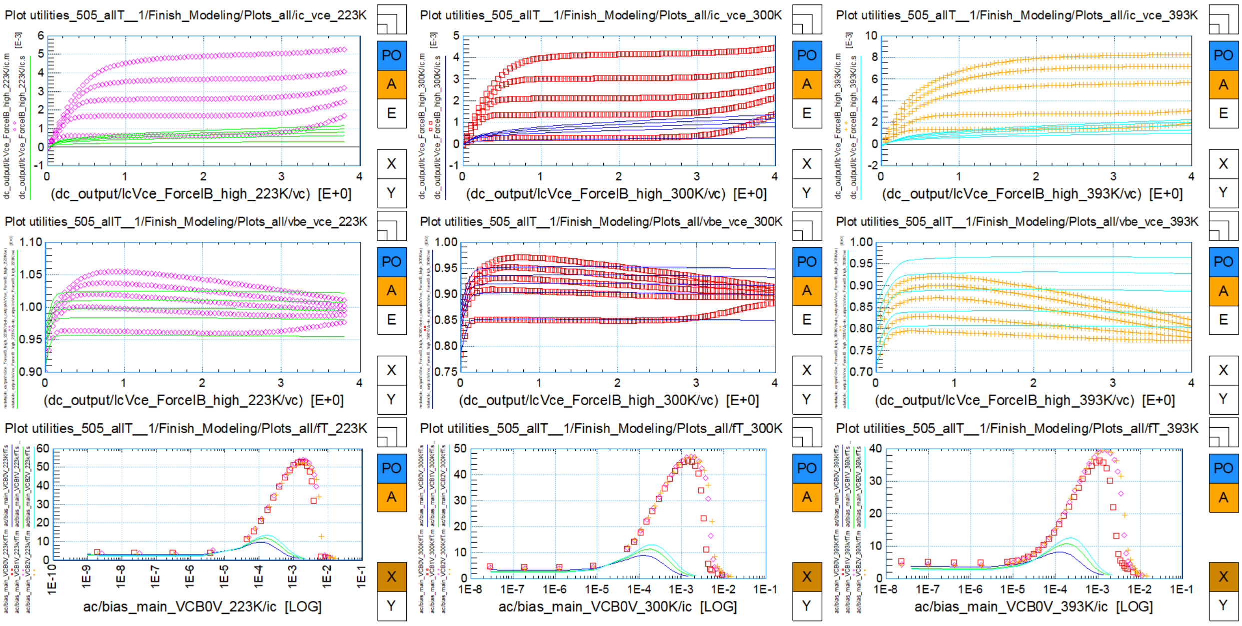

Figure 3.4: Plots of important characteristics at different temperature after initialization.

Chapter 4

Extraction of Low Current Parameters

As discussed earlier in 2.2, a logical starting step is to extract low current parameters, which are relatively straightforward as self-heating is negligible. Low current parameters include the parameters of depletion capacitances, avalanche effect, Early effect, and Gummel characteristics. Resistances are high current parameters but they can be estimated from high current region in Gummel plots. Temperature scaling parameters related to these parameters are also extracted here in order to provide a better description of low current parameters and a reasonable starting point for high current parameters. The reference temperature is 26.85 $^\circ C$ (300 K).

4.1 Depletion capacitance

The descriptions of capacitances contain some parameters which are essential for follow-up works, so the parameters of capacitances are extracted at the first step.

4.1.1 Base-emitter depletion capacitance

The measured base-emitter capacitance C_{BE} contains three parts: a depletion capacitance, an overlap capacitance and a diffusion capacitance. The contribution of diffusion capacitance can be ignored as long as base-emitter voltage V_{BE} is not too high in forward. The base-emitter depletion capacitance C_{BE} is given by the formula [11]:

$$C_{BE} = \frac{s_E C_{jE}}{(1 - \frac{V_{jE}}{V_{dE}})^{p_E}} + \frac{(1 - s_E) C_{jE}}{(1 - \frac{V_{FE}}{V_{dE}})^{p_E}} + C_{BEO}, \tag{4.1}$$

#	parameter	value	comment
1	C_{j_E}	12.14f	
2	p_E	561.9m	
3	V_{d_E}	2.158	
4	C_{BEO}	0	Use default value

Table 4.1: Parameters used in base-emitter depletion capacitance extraction.

this equation describes the transition between a depletion capacitance(when s_E = 1) to a constant capacitance(when s_E = 0). C_{j_E} is the zero-bias emitter base depletion capacitance. V_{d_E} is diffusion voltage. p_E represents emitter-base grading coefficient.

V_{j_E} is the effective junction bias which is given by:

$$V_{jE} = V_{BE} + 0.1V_{dE} \ln s_E, \tag{4.2}$$

s_E describes the transition between the ideal and the constant part and it is given by:

$$s_E = \frac{1}{1 + e^{\frac{V_{BE}-V_{FE}}{0.1V_{dE}}}}. \tag{4.3}$$

The voltage V_{FE} describes the point where the transition takes place and it is defined by the quantity a_{j_E},

$$V_{FE} = V_{dE}(1 - a_{jE}^{-\frac{1}{PE}}), \tag{4.4}$$

a_{jE} is a constant 3 here. The capacitance C_{BEO} is constant, which describes the overlap capacitances between base and emitter. C_{BEO} is set to zero here due to lack of geomery scaling and process information. The extracted C_{j_E} is actually a sum of real C_{j_E} and C_{BEO}. C_{j_E} , p_E and V_{d_E} are extracted by fitting plot $C_{BE} - V_{BE}$. The extraction result is shown in Figure 4.1. The values of parameters extracted in this section are given in Table 4.1.

4.1.2 Base-collector depletion capacitance

The extraction of the base-collector depletion capacitance and base-emitter depletion capacitance are similar. Parameter X_p is introduced here to describe the constant part of the capacitance, which indicates that the collector epilayer has a finite thickness. The base-collector

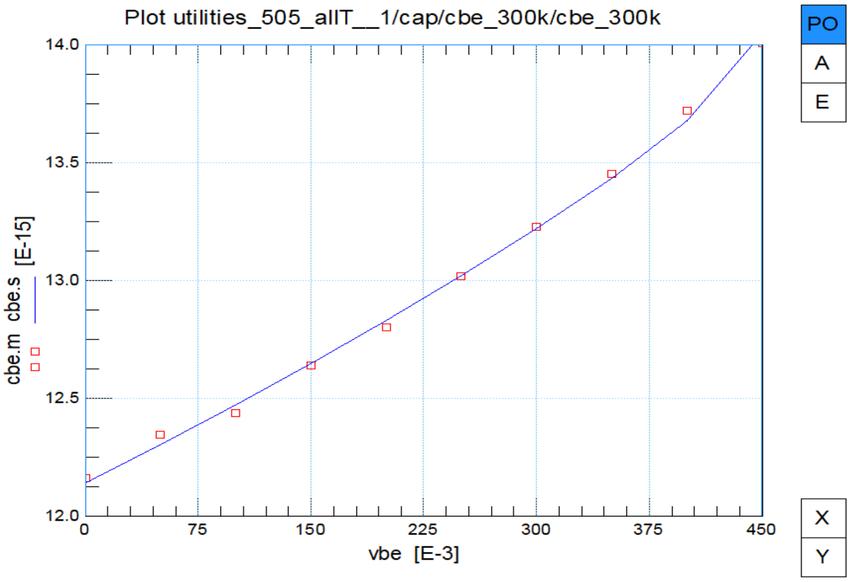

Figure 4.1: Measured (markers) and calculated (line) BE depletion capacitance at 300 K

depletion capacitance is given as [11]:

$$C_{BC} = \frac{S_C(1-X_p)C_{jC}}{(1-V_{jC}/V_{d_C ctc})^{p_C}} + \frac{(1-S_C)(1-X_p)C_{jC}}{(1-V_{FC}/V_{d_C ctc})^{p_C}} + X_P C_{jC} + C_{BCO}, \tag{4.5}$$

$$V_{jC} = V_{BC} + 0.1 V_{d_C ctc} \ln s_C, \tag{4.6}$$

$$s_C = \frac{1}{1 + e^{\frac{V_{BC}-V_{FC}}{0.1 V_{d_C ctc}}}}, \tag{4.7}$$

$$b_{jC} = \left(\frac{a_{jC} - X_P}{1 - X_P}\right), \tag{4.8}$$

$$V_{FC} = V_{d_C ctc}\left(1 - b_{jC}^{-\frac{1}{p_C}}\right). \tag{4.9}$$

Here we have a_{jC} = 2. Parameter C_{jC} is zero bias collector-base depletion capacitance, p_C is collector-base grading coefficient, $V_{d_C ctc}$ is collector-base diffusion voltage of depletion capacitance. C_{BCO} is the base-collector overlap capacitance and it is also set to zero, for the extracted C_{jc} is actually a sum of real C_{jc} and C_{BCO} for they cannot be separated here. V_{jc} is the effective junction bias. The transition between the ideal and the constant part is described by s_C. The voltage V_{FC} describes the point where the transition takes place. C_{jc}, p_C, $V_{d_C ctc}$

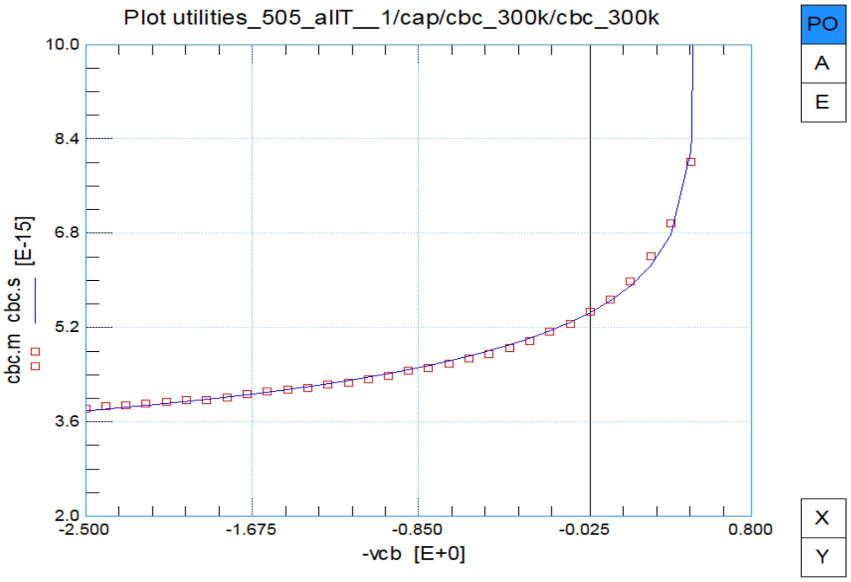

Figure 4.2: Measured (markers) and calculated (line) BC depletion capacitance at 300 K

#	**parameter**	**value**	**comment**
1	C_{jc}	5.452f	
2	p_C	368.9m	
3	V_{dcctc}	719.5m	
4	X_p	210.0m	
5	C_{BCO}	0	Use default value

Table 4.2: Parameters used in base-collector depletion capacitance extraction.

and X_p are extracted by fitting the $C_{BC} - V_{BC}$ curve as shown in Figure 4.2. The values of parameters extracted in this section are given in Table 4.2.

4.1.3 Collector-substrate depletion capacitance

The extraction of collector-substrate capacitance is also similar to C_{BE}. The equations of collector-substrate depletion capacitance are :

$$C_{SC} = \frac{s_S C_{jS}}{(1 - \frac{V_{jS}}{V_{dS}})^{p_S}} + \frac{(1 - s_S) C_{jS}}{(1 - \frac{V_{FS}}{V_{dS}})^{p_S}}, \tag{4.10}$$

$$V_{jS} = V_{SC} + 0.1 V_{dS} \ln s_S, \tag{4.11}$$

$$s_S = \frac{1}{1 + e^{\frac{V_{SC} - V_{FS}}{0.1 V_{dS}}}}, \tag{4.12}$$

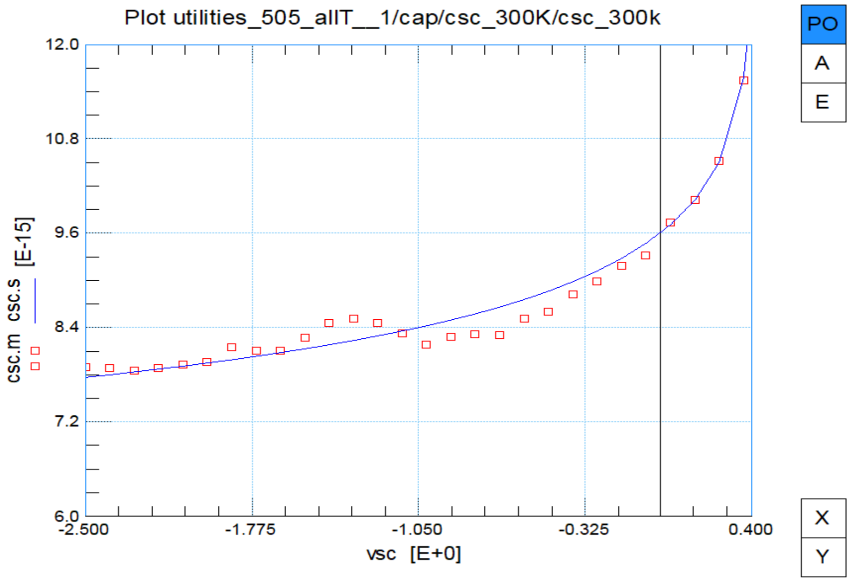

Figure 4.3: Measured (markers) and calculated (line) SC depletion capacitance at 300 K

$$V_{FS} = V_{dS}(1 - a_{jS}^{-\frac{1}{PS}}). \tag{4.13}$$

V_{j_S} is the effective junction bias. s_S describes the transition between the ideal and the constant part. The voltage V_{FS} is used to describe the point where the transition takes place and it's defined by a_{jS} whose value is 2. C_{jS} is zero bias collector-substrate depletion capacitance. p_S is collector-substrate grading coefficient. V_{dS} is collector-substrate diffusion voltage. C_{jS}, V_{dS} and p_S can be extracted by fitting $C_{SC} - V_{SC}$ curve. Figure 4.3 shows the extracted result. The values of parameters extracted in this section are given in Table 4.3.

#	**parameter**	**value**	**comment**
1	C_{js}	9.598f	
2	p_S	119.1m	
3	V_{d_S}	509.1m	

Table 4.3: Parameters used in collector-substrate depletion capacitance extraction.

4.2 Avalanche

Modern transistors have lower breakdown voltage, making the avalanche effect of a transistor more of a concern. The avalanche current I_{avl}, which is caused by impact ionization, could cause a decrease of base current when the collector-base bias is sufficiently high.

4.2.1 Extraction of avalanche parameters at 300 K

The low current avalanche parameters are extracted from base current under forward Early measurement shown in Figure 4.4, V_{BE} is set to 0.68V, V_{CB} is swept from 0 to 5.0V.

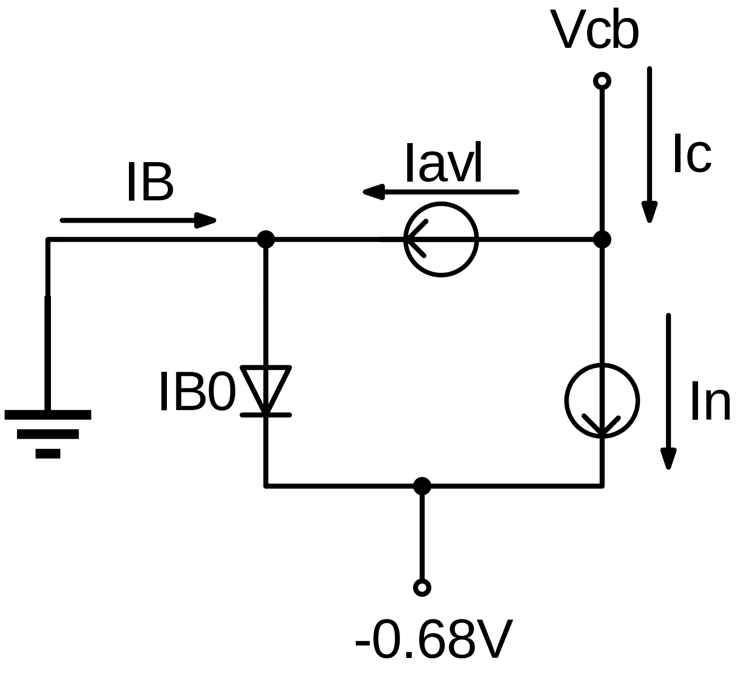

Figure 4.4: Simplified forward Early measurement circuit

In Mextram 505.00, switch parameter SWAVL for avalanche factor is added. When SWAVL = 0, there is no avalanche current. SWAVL = 1 is the default value and the new avalanche model is used at this time. When SWAVL is 2, Mextram 504 avalanche model is used. EXAVL is only meaningful when SWAVL is 2. In this work, SWAVL is the default value 1.

Since avalanche current leads to the decrease of base current when V_{CB} increases, it could be expressed as the difference between the base current at V_{CB} = 0 and at higher V_{CB}. The avalanche current is written as:

$$I_{avl} = I_{B0} - I_B. \tag{4.14}$$

I_{B0} is the base current at V_{CB} = 0. As V_{CB} increasing, the base current may drop below zero because avalanche effect occurs.The avalanche current can also be expressed as:

$$I_{avl} = I_N G_{EM}, \tag{4.15}$$

G_{EM} is the generation coefficient, which is given by equation in Mextram 505.00 as:

$$G_{EM} = \frac{A_{avl}}{B_{avl}} \phi \text{exp}(-B_{avl}\phi^{C_{avl}}), \tag{4.16}$$

$$\phi = (V_{dC_{avl}} + V_{CB}) \exp(-\frac{I_N}{I_{TOavl}}), \tag{4.17}$$

A_{avl}, B_{avl}, C_{avl}, $V_{dC_{avl}}$, and I_{TOavl} are avalanche parameters for this model. From equation (4.15), G_{EM} can also be expressed as:

$$G_{EM} = \frac{I_{avl}}{I_N}, \tag{4.18}$$

As shown in Figure 4.4, I_C = $I_{avl} + I_N$. G_{EM} can be rewritten as:

$$G_{EM} = \frac{I_{avl}}{I_C - I_{avl}}. \tag{4.19}$$

As I_{avl} is already obtained from I_B, G_{EM} can now be calculated from measured I_C and I_B.

Using (4.19), a transform for calculating G_{EM} is written in IC-CAP. The program code is listed below:

```
Ib0m=ib.m[0]
Ib0s=ib.s[0]
iavl=ib
i=0
while i<size(vc)
        iavl.m[i]=Ib0m-ib.m[i]
        iavl.s[i]=Ib0s-ib.s[i]
        i=i+1
end while
gem=ic
q=0
while q<size(vc)
        gem.m[q]=iavl.m[q]//(ic.m[q]-iavl.m[q])
        gem.s[q]=iavl.s[q]//(ic.s[q]-iavl.s[q])
        q=q+1
end while
return gem + 1e-6
```

A_{avl}, B_{avl}, C_{avl}, and V_{dCavl} are extracted here by fitting G_{EM}-V_{cb} curve. I_{TOavl} cannot be extracted here, but we need to set its value large enough compared to the collector current in question so that it does not affect low current avalanche parameters. That is, the exponential term in (4.17) needs to be essentially unity. I_{TOavl} describes the decrease of G_{EM} with increasing I_C at high current, and will be extracted later in a region of high I_C from output curves.

G_{EM} versus V_{CB} are shown in Figure 4.5 in both linear and logarithmic scales for G_{EM}. The values of avalanche parameters used in this step are given in Table 4.4.

#	parameter	value	comment
1	A_{avl}	237.3	
2	B_{avl}	14.51	
3	C_{avl}	-528.1m	
4	$V_{d_{C}avl}$	192.2m	
5	I_{TOavl}	500m	To be extracted from output plots

Table 4.4: Parameters used in avalanche factor extraction.

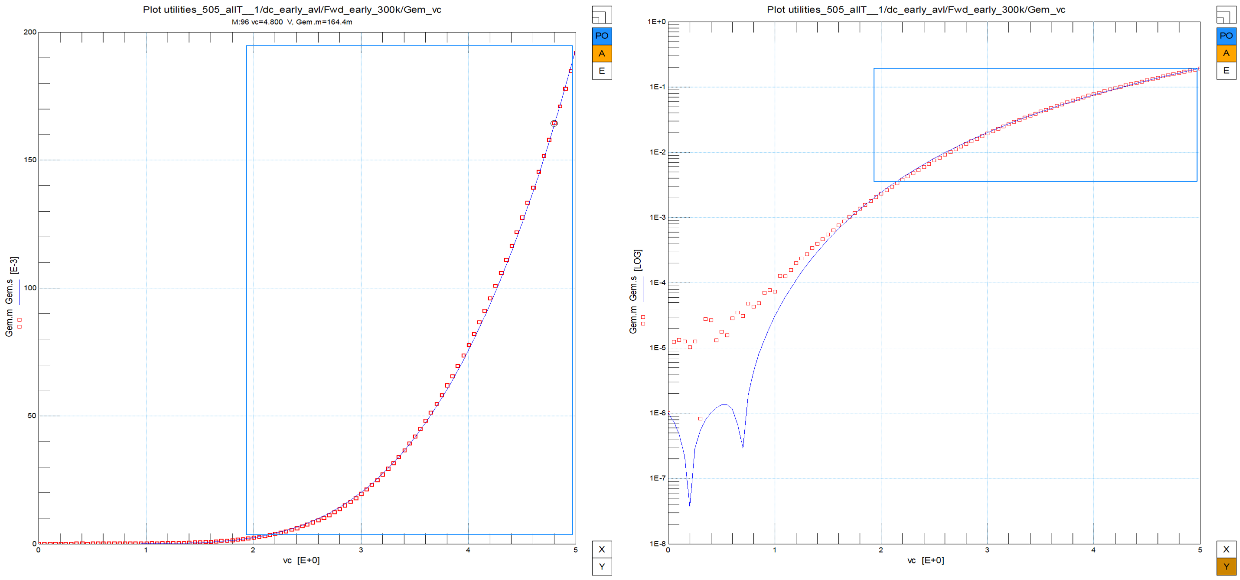

Figure 4.5: Linear scale and log scale G_{EM} versus V_{CB} at 300 K

#	parameter	value	comment
1	$\mathrm{T_{Bavl}}$	473.9μ	

Table 4.5: Temperature scaling parameter of avalanche factor.

4.2.2 Temperature scaling of avalanche effect

B_{avl} has temperature dependence given by:

$$B_{avl_T} = B_{avl}(1 + T_{Bavl}(T_K - T_{ref})), \tag{4.20}$$

where T_{Bavl} is temperature scaling parameter. By fitting G_{EM}-V_{cb} curve under differet temperatures at 223 K, 300 K and 393 K, T_{Bavl} is extracted. The extraction results are shown in Figure 4.6. The parameter extracted here is shown in Table 4.5.

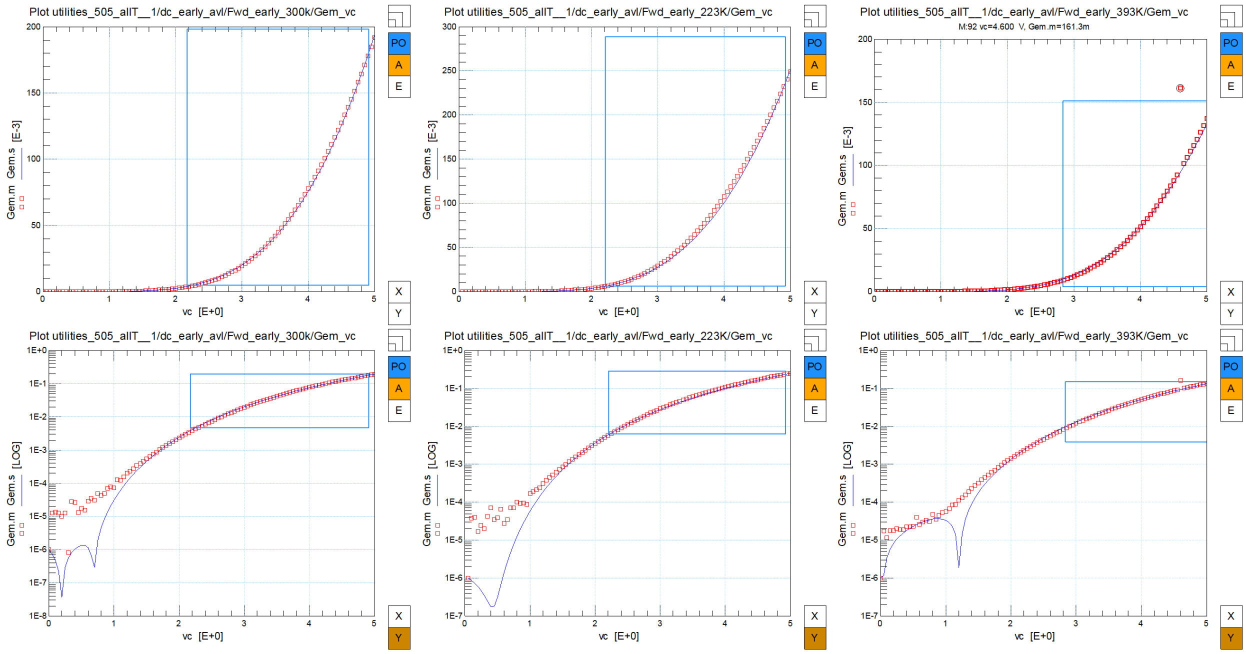

Figure 4.6: Linear scale and log scale $G_{EM} - V_{CB}$ at different temperatures

4.3 Early Effect

Early effect is the variation in the base width of a BJT due to the applied base-collector and base-emitter bias variation. In Mextram we have two parameters, reverse Early voltage V_{er} and forward Early voltage V_{ef}, to describe this bias-dependet effect. V_{er} is extracted from reverse Early measurement and V_{ef} is extracted from forward Early measurement. In SiGe transistors Ge mole fraction has a non-zero slope, which means we have a non-zero base bandgap difference dE_g. Thus, Mextram redefines the coefficient q_1^I to describe Early effect for the currents [8] as:

$$q_1^I = \frac{\exp([\frac{V_{tE}}{V_{er}} + 1]\frac{dE_g}{V_T}) - \exp(\frac{-V_{tC}}{V_{ef}}\frac{dE_g}{V_T})}{\exp(\frac{dE_g}{V_T}) - 1}. \tag{4.21}$$

Neglecting the voltage drop over resistances, the normalized charges V_{tE} and V_{tC} are evaluated from:

$$V_{tE} = \frac{V_{dE}}{1 - p_E}[1 - (1 - V_{jE}/V_{dE})^{1-p_E}] + a_{jE}(V_{BE} - V_{jE}), \tag{4.22}$$

$$V_{tC} = (1 - X_p)(\frac{V_{dC}}{1 - p_C}[1 - (1 - V_{jC}/V_{dC})^{1-p_C}] + b_{jC}(V_{BC} - V_{jC})) + X_p V_{BC}. \tag{4.23}$$

V_{tE} and V_{tC} are calculated using parameters extracted in $C - V$ characteristics. The emitter current for the reverse Early effect measurement setup is written as:

$$I_E = I_{E0}\frac{\exp(\frac{dE_g}{V_T}) - \exp(\frac{-V_{tC}}{V_{ef}}\frac{dE_g}{V_T})}{\exp([\frac{V_{tE}}{V_{er}} + 1]\frac{dE_g}{V_T}) - \exp(\frac{-V_{tC}}{V_{ef}}\frac{dE_g}{V_T})}. \tag{4.24}$$

I_{E0} is the emitter current at V_{BE} = 0. The collector current for the forward Early effect measurement setup can be written as:

$$I_C = I_{C0}\frac{\exp([\frac{V_{tE}}{V_{er}} + 1]\frac{dE_g}{V_T})}{\exp([\frac{V_{tE}}{V_{er}} + 1]\frac{dE_g}{V_T}) - \exp(\frac{-V_{tC}}{V_{ef}}\frac{dE_g}{V_T})} + I_{B0} - I_B, \tag{4.25}$$

where I_{C0} is the collector current at V_{BC} = 0, I_{B0} is the base current at V_{CB} = 0. It is clear from inspection of these equations that the emitter current depends on forward Early voltage, reverse Early voltage and bandgap difference dE_g, and the collector current also depends on both voltages and bandgap difference. Therefore, we extract them at the same time.

The fractions containing V_{er}, V_{ef} and dE_g in above expressions are current change factors due to Early effect. In our extraction, rather than fitting currents, we fit these current change factors calculated using:

$$F_{revEarly} = \frac{I_E}{I_{E0}}, \tag{4.26}$$

$$F_{fwdEarly} = \frac{I_C - I_{avl}}{I_{C0}}, \tag{4.27}$$

where I_{avl} is avalanche current defined in (4.14). V_{er}, V_{ef} and dE_g are extracted by fitting $F_{revEarly}$ and $F_{fwdEarly}$ together. $F_{revEarly} - V_{EB}$ and $F_{fwdEarly} - V_{CB}$ are shown in Figure 4.7.

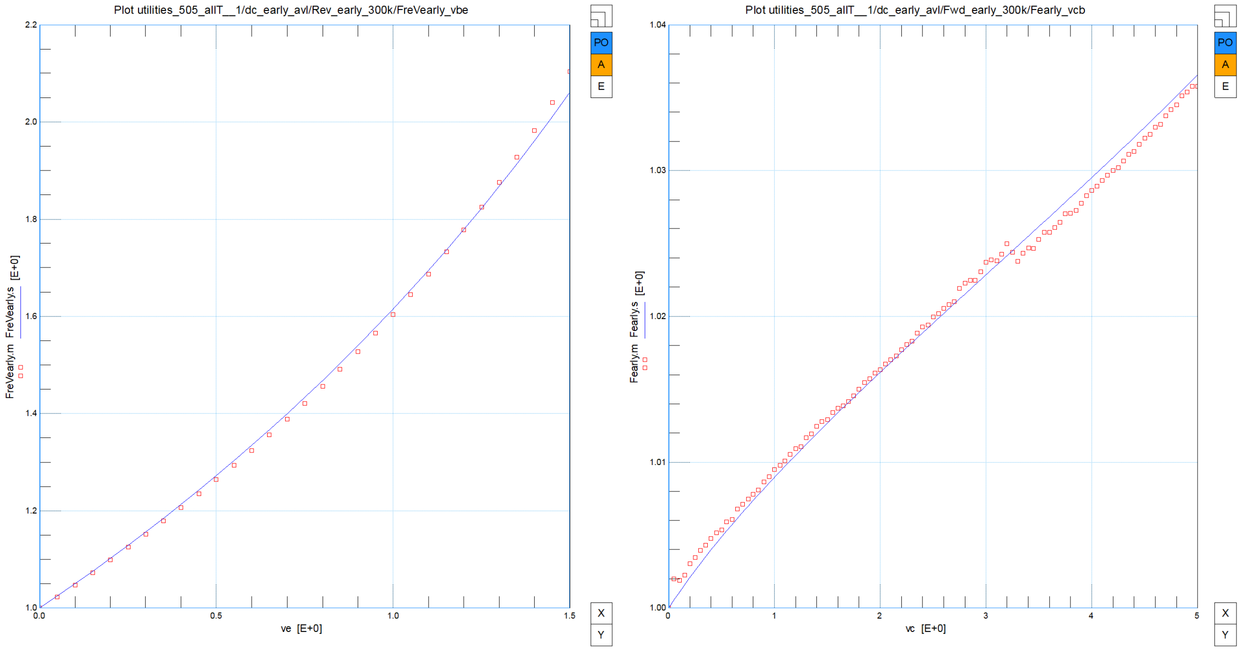

Figure 4.7: $F_{revEarly} - V_{EB}$ and $F_{fwdEarly} - V_{CB}$ at 300 K

From equation (4.25) we can see that V_{er}, V_{ef} and dE_g have the ability of influencing I_C and therefore influence the current gain. Thus, these parameters should be optimized later in current gain plot. The values of V_{er}, V_{ef} and dE_g extracted from this step are listed in Table 4.6.

#	parameter	value	comment
1	V_{er}	3.146	To be optimized in current gain plot
2	V_{ef}	47.35	To be optimized in current gain plot
3	dE_g	25.59m	To be optimized in current gain plot

Table 4.6: Parameters used in Early effect extraction.

4.4 DC Gummel parameters

We now proceed with extracting forward and reverse Gummel related model parameters as well as related temperature scaling parameters.

4.4.1 Extraction of forward Gummel parameters

The collector saturation current I_S, a crucial parameter describing the main current, is extracted at medium-low base-emitter voltages, to avoid high-injection, quasi-saturation, series resistance effects, as well to avoid non-ideal leakage currents. At such bias, I_C is approximately given by:

$$I_C = \frac{I_S \exp \frac{V_{BE}}{N_{FF} V_T}}{q_1^I}, \tag{4.28}$$

where q_1^I, the current change factor due to Early effect, is given by (4.21). Its value has to do with the C-V parameters and Early effect parameters, which have been extracted. In future extraction steps, any adjustment to those parameters will require adjustment of I_S as well. N_{FF} is the non-ideality factor of forward main current. In this work, N_{FF} is set to its default value 1, which is found to be sufficient. The extraction result is shown in Figure 4.8.

Figure 4.8 shows that at medium V_{BE}, logarithm scale I_C is approximately a linear function of the base-emitter bias as the equation (4.28) described. However, when the bias becomes larger, the measured I_C and simulated I_C split. This is in part due to the series resistance voltage drops. The intrinsic junction voltage $V_{B_2E_1}$ becomes considerably smaller than the bias we apply, V_{BE}. We can minimize this difference later by extracting reasonable resistances in section 4.4.3. Here we only focus on the medium V_{BE} range from 0.5V to 0.8V, to extract I_S. The values of parameter used here are shown in Table 4.7.

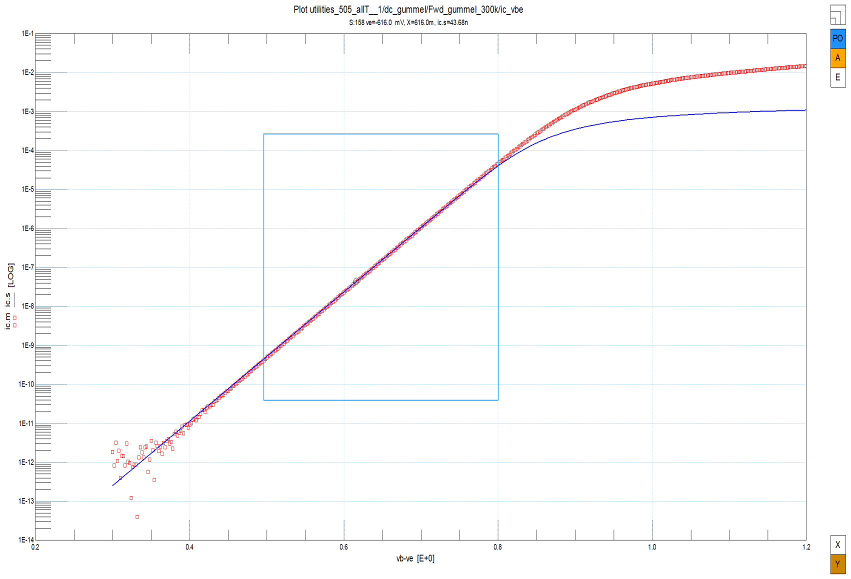

Figure 4.8: Measured (markers) and simulated (line) collector current in forward Gummel measurement at 300 K

#	**parameter**	**value**	**comment**
1	I_S	2.699a	
2	N_{FF}	1.0	Use default value

Table 4.7: Parameters used in forward I_C in Gummel measurement.

The parameters of forward base current are also extracted in forward Gummel measurement. Ideal base current is evaluated by:

$$I_{B_1} = I_{BI}(e^{V_{B_2E_1}/N_{BI}V_T} - 1). \tag{4.29}$$

Ideal side-wall base current is written as:

$$I^S_{B_1} = I^S_{BI}(e^{V_{B_1E_1}/N^S_{BI}V_T} - 1). \tag{4.30}$$

Non-ideal base current is:

$$I_{B_2} = I_{Bf}(e^{V_{B_2E_1}/m_{Lf}V_T} - 1). \tag{4.31}$$

Non-ideal side-wall base current is:

$$I^S_{B_2} = I^S_{Bf}(e^{V_{B_2E_1}/m^S_{Lf}V_T} - 1). \tag{4.32}$$

I_{BI} is the saturation current of ideal base current, N_{BI} is the non-ideality factor of ideal base current and it keeps its default value here. I_{BI}^S is the saturation current of ideal side-wall base current and N_{BI}^S is the non-ideality factor of ideal side-wall base current. Saturation current of non-ideal forward base current is represented by I_{Bf} and the non-ideality factor of non-ideal forward base current is m_{Lf}. I_{Bf}^S and m_{Lf}^S are saturation current and the non-ideality factor of non-ideal side-wall forward base current. The total base current I_B is the sum of currents in equation (4.29) - (4.32). Actually, the parameters of $I_{B_1}^S$ and $I_{B_2}^S$ are not extracted, since we just have one transistor so it is not possible to have any information of side-wall currents. The extraction result is shown in Figure 4.9.

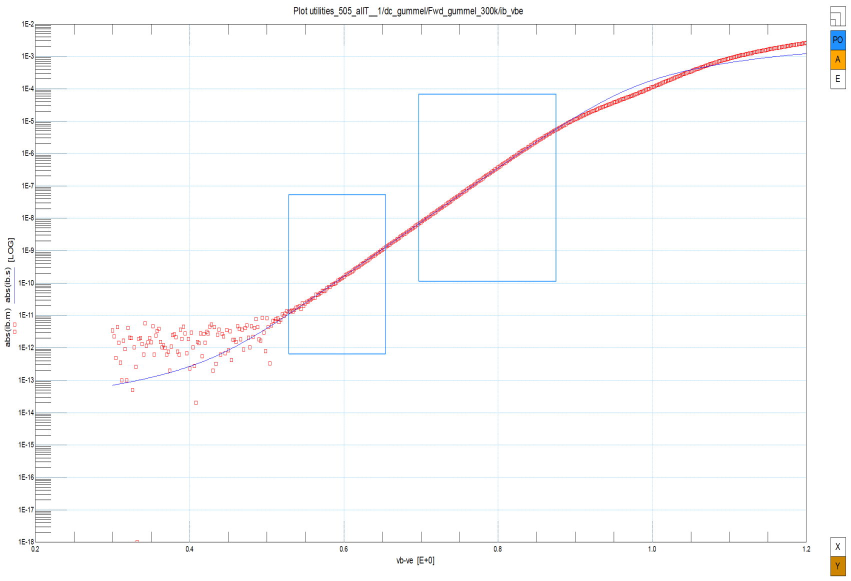

Figure 4.9: Measured (markers) and simulated (line) base current in forward Gummel measurement at 300 K

Similar to the extraction of I_S, we extract forward base current parameters at medium-low bias in order to avoid the region where high current effects and resistance effect may occur. The values of parameter used here are shown in Table 4.8.

4.4.2 Extraction of reverse Gummel parameters

First, we extract the parameters of I_{sub}, which is the main current of the parasitic Base-Collector-Substrate(BCS) transistor. In this work EXSUB = 1, so the substrate current is given by:

#	parameter	value	comment
1	$\mathsf{I_{Bl}}$	1.325E-20	
2	$\mathsf{N_{Bl}}$	1.0	Use default value
3	$\mathsf{I^S_{Bl}}$	0.0	Use default value
4	$\mathsf{N^S_{Bl}}$	1.0	Use default value
5	$\mathsf{I_{Bf}}$	562.8a	
6	$\mathsf{m_{Lf}}$	2.741	
7	$\mathsf{I^S_{Bf}}$	0.0	Use default value
8	$\mathsf{m^S_{Lf}}$	2.0	Use default value

Table 4.8: Parameters used in forward I_B in Gummel measurement.

$$I_{sub} = (1 - X_{ext}) \frac{2I_{Ss}(e^{V_{B_1C_4}/V_T} - e^{V_{SC_4}/V_T})}{1 + \sqrt{1 + 4\frac{I_{Ss}}{I_{Ks}} e^{V_{B_1C_4}/V_T}}}, \tag{4.33}$$

I_{Ss} is the saturation current of parasitic BCS transistor main current. I_{Ks} is the knee current of this parasitic transistor's collector-substrate junction. X_{ext} is the partitioning factor of the extrinsic region.

The substrate-collector diode current is calculated by:

$$I_{sf} = I_{CSs}(e^{V_{SC_1}/V_T} - 1), \tag{4.34}$$

I_{CSs} is the ideal saturation current of collector-substrate junction. We also extract the parameters of reverse I_B in this measurement. The reverse I_B contains an ideal part and a non-ideal part. Ideal reverse base current is:

$$I_{ex} = (1 - X_{ext}) \frac{2I_{BX}(e^{V_{B_1C_4}/V_T} - 1)}{1 + \sqrt{1 + 4\frac{I_{BX}}{I_{kBX}} e^{V_{B_1C_4}/V_T}}}. \tag{4.35}$$

Non-ideal reverse base current is generated from the depleted base-collector region by recombination and it is expressed by equation:

$$I_{B_3} = I_{Br}(e^{V_{B_1C_4}/m_{Lr}V_T} - 1), \tag{4.36}$$

I_{BX} is the saturation current of ideal reverse base current I_{ex}. I_{kBX} is the knee current of I_{ex}. I_{Br} is the saturation current of non-ideal reverse base current. m_{Lr} is the non-ideality factor of I_{B_3}.

Reverse I_{sub} and I_B have strong correlation so their parameters are extracted by fitting I_{sub}, I_{ex} and I_{B_3} together . Again, we only focus on the extraction of low V_{BC} region so that we could neglect those undesired effects. X_{ext} is the fraction of external charges and currents between B and C_1 instead of B_1 and C_1. From Figure 1.5 we can know that over the resistance R_{BC} the reverse base currents are split in a part with X_{ext} and a part with $(1 - X_{ext})$, therefore X_{ext} and R_{BC} should be extracted together from high V_{BC} where the reverse currents are high. Here X_{ext} uses its initialized value. The values of parameter used are shown in Table 4.9. Due to the voltage drop over resistances, the simulated currents and the measured currents split at high V_{BC}.

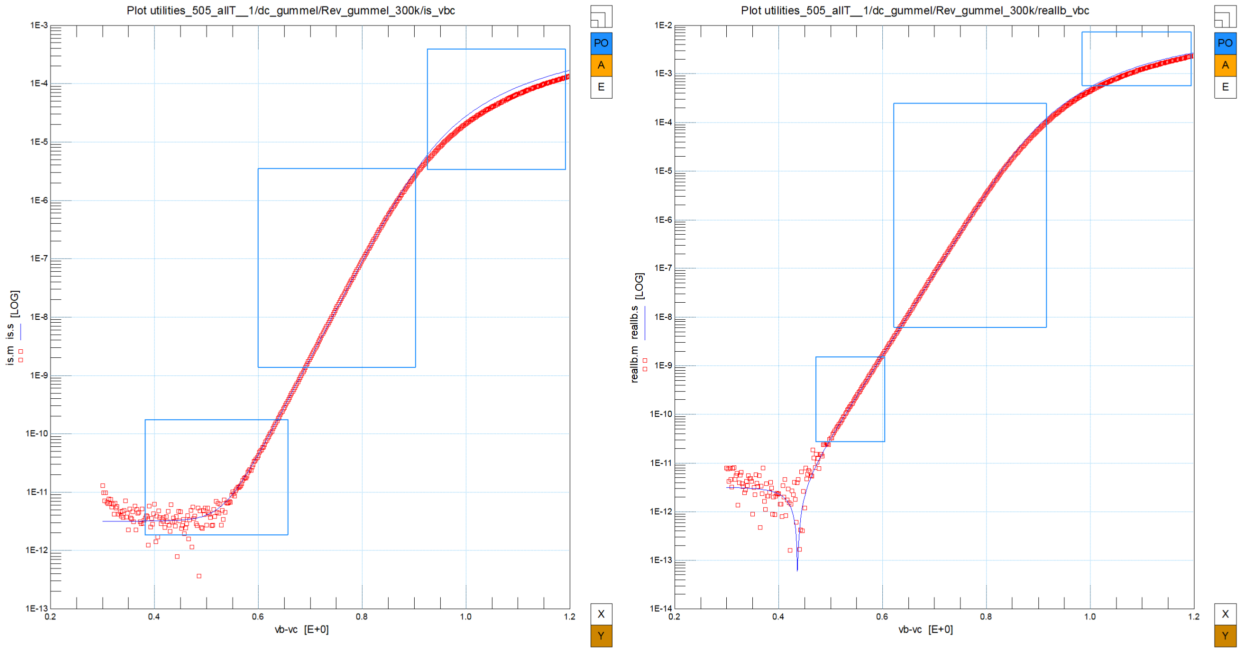

Figure 4.10: $I_{sub} - V_{BC}$ and $I_B - V_{BC}$ in reverse Gummel measurement at 300 K

#	parameter	value	comment
1	I_{Ss}	3.449E-21	Extracted at high V_{BC} together with R_{BC}
2	I_{Ks}	21.28u	
3	X_{ext}	630m	
4	I_{CSs}	3.202p	
5	I_{BX}	1.633E-19	
6	I_{kBX}	155.4u	
7	I_{Br}	562.8a	
8	m_{Lr}	2.851	

Table 4.9: Parameters used in reverse Gummel measurement.

#	parameter	value	comment
1	R_E	11.39	Optimized in high current output plot
2	R_{BC}	16.47	
3	R_{BV}	20.34	
4	R_{CC}	9.729	Optimized in high current output plot
5	R_{CV}	25.96	Optimized in high current output plots
6	X_{ext}	585.2m	

Table 4.10: Resistances estimated in Gummel measurement.

4.4.3 Estimation of resistances

From former extractions of Gummel plots we know that the simulated data and the measured data cannot fit well, one of the reasons is that resistances have influence on the currents especially when the bias is high, so a good estimation of resistances is very important.

First we look at R_E, R_{BC}, R_{BV}, R_{CC} and R_{CV}, which have a large influence on high bias Gummel characteristics. R_E is the emitter resistance between node E and $E1$. R_{BC} and R_{BV} are the constant part and the variable part of base resistance. R_{CC} is the constant collector resistance. For low base-collector bias, R_{CV} determines the ohmic voltage drop over the epilayer. Forward currents I_C and I_B are strongly affected by R_E, and also influenced by R_{BC} and R_{BV}. R_{CC} has large impact on reverse currents I_{sub} and I_B, and its influence on forward I_C is not negligible. R_{CV} mainly influences forward I_C and reverse I_{sub}. Moreover, the partitioning factor of the extrinsic region X_{ext}, is extracted from high reverse currents.

Therefore, R_E, R_{BC}, R_{BV}, R_{CC}, R_{CV} and X_{ext} are extracted by fitting forward currents and reverse currents together. Figure 4.11 shows $I_C - V_{BE}$, $I_B - V_{BE}$, $I_{sub} - V_{BC}$ and $I_B - V_{BC}$ after parameter extraction. Values of parameter used here are shown in Table 4.10.

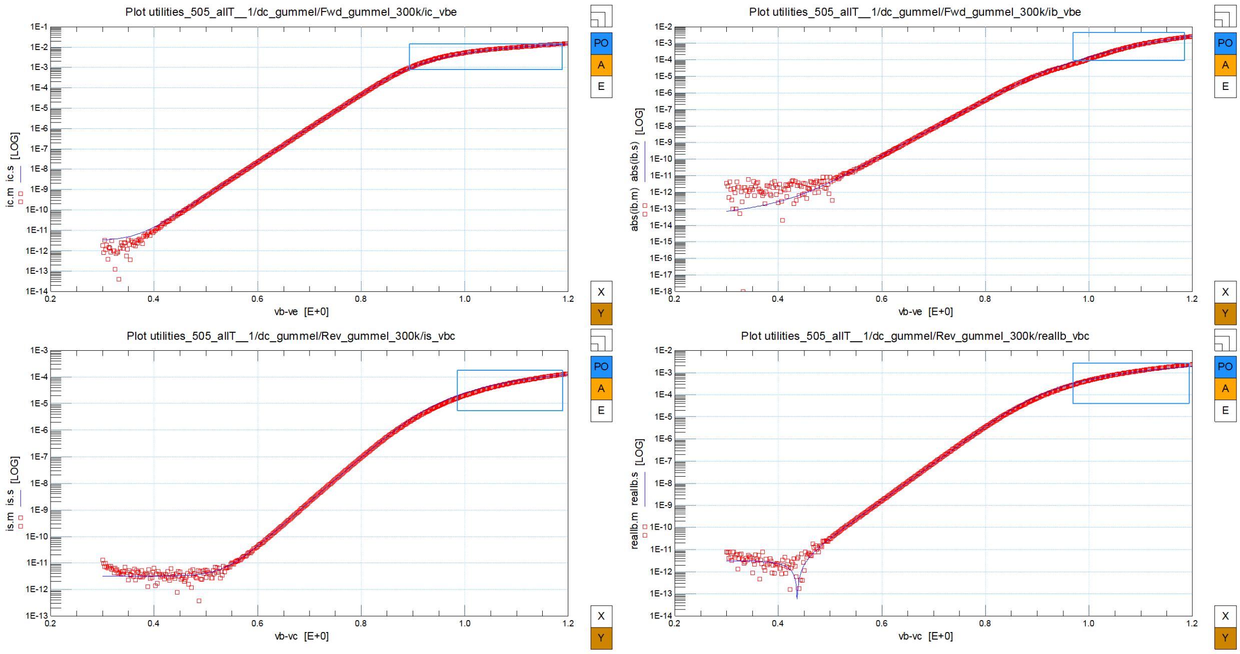

Figure 4.11: Forward I_C and I_B and reverse I_{sub} and I_B in Gummel measurement at 300 K

It is obvious that after the extraction of resistances the currents at higher bias fit much better than before. Actually, when the bias and currents become larger, the effect of self-heating also needs to be taken into consideration, so the temperature scaling of these curves are done later in section 4.4.4.

4.4.4 Temperature scaling of Gummel parameters

The junction temperature T_K in the forward and reverse Gummel measurement at 300 K are shown in Figure 4.12 and Figure 4.13.

As we can see, T_K increases as the bias gets higher. In forward Gummel measurement the value of T_K increases from 300 K to around 313 K, and in reverse mode it ends up around 307 K. This allows us to get an more intuitive aware that we cannot neglect the temperature scaling at high bias. Therefore, the temperature scaling parameters related to Gummel characteristics are extracted here.

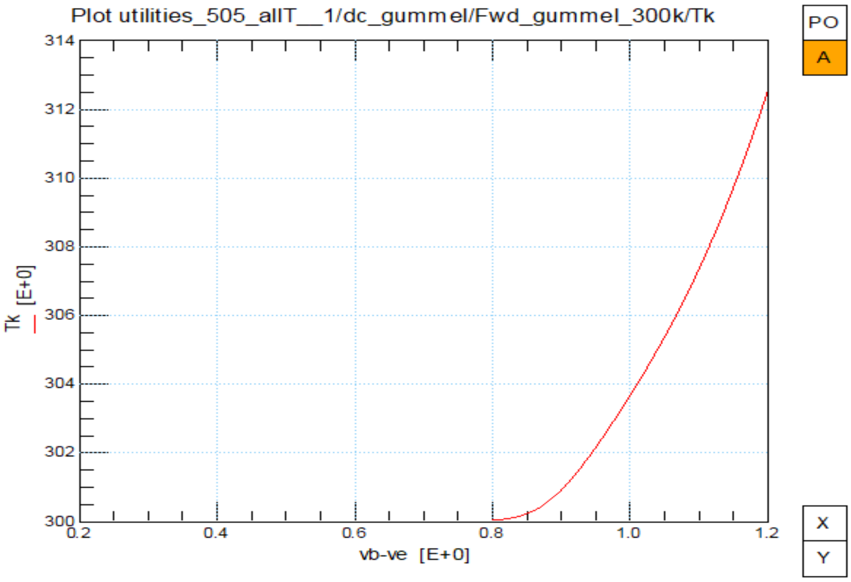

Figure 4.12: T_K of forward Gummel measurement at 300 K

Temperature scaling of low injection forward Gummel I_C is primarily determined by the temperature scaling of the collector current saturation current:

$$I_{sT} = I_s t_N^{\frac{4 - A_B - A_{Q_{B0}} + DAIS}{N_{FF}}} \exp[-\frac{V_{gB}}{N_{FF} V_{\Delta T}}]. \tag{4.37}$$

N_{FF} is also linearly scaled with temperature, with a coefficient t_{NFF} that defaults to zero, which we use here. That is, N_{FFT} = N_{FF}. The same A_B parameter is also used for temperature scaling of the knee current I_k, which is important for high injection Gummel I_C:

$$I_{kT} = I_k t_N^{1 - A_B}. \tag{4.38}$$

Low injection temperature scaling of forward ideal I_B comes from temperature dependence of I_{BI}:

$$I_{BIT} = I_{BI} t_N^{\frac{4 - A_E + DAIS}{N_{BI}}} \exp[-\frac{V_{gE}}{N_{BI} V_{\Delta T}}]. \tag{4.39}$$

Similarly, temperature scaled forward side-wall ideal I_B saturation current is given by:

$$I_{BIT}^S = I_{BI}^S t_N^{\frac{4 - A_E + DAIS}{N_{BI}^S}} \exp[-\frac{V_{gE}}{N_{BI}^S V_{\Delta T}}]. \tag{4.40}$$

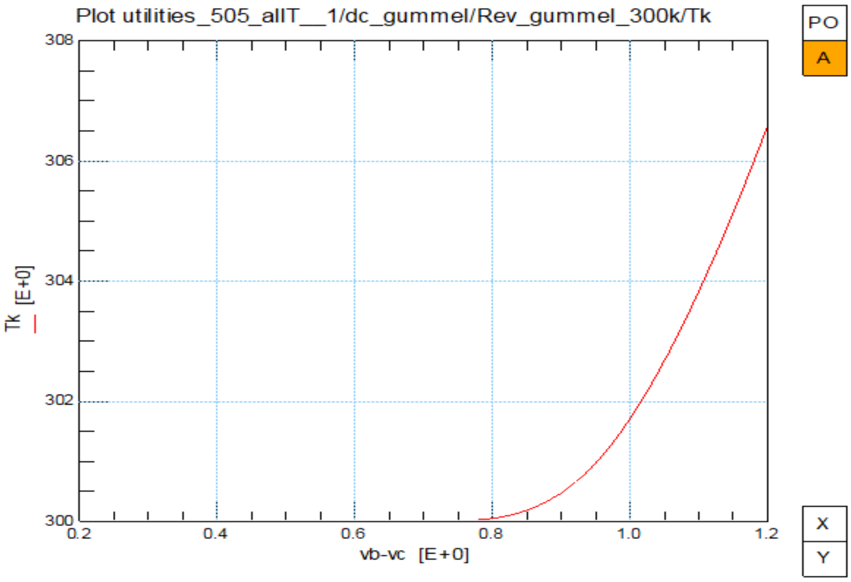

Figure 4.13: T_K of reverse Gummel measurement at 300 K

Temperature scaled forward non-ideal I_B saturation current is given by:

$$I_{BFT} = I_{BF} t_N^{6-2m_{Lf}} \exp[-\frac{V_{gJ}}{m_{Lf} V_{\Delta T}}]. \tag{4.41}$$

Temperature scaled forward non-ideal side-wall I_B saturation current is given by:

$$I_{BFT}^S = I_{BF}^S t_N^{6-2m_{Lf}^S} \exp[-\frac{V_{gJ}}{m_{Lf}^S V_{\Delta T}}]. \tag{4.42}$$

As we discussed in section 4.4.1, I_{BI}^S and I_{BF}^S are using the default value 0, so they are not used to extract temperature parameters.

The temperature scaled saturation currents relevant for reverse Gummel I_B, strictly speaking, $I_B + I_{sub}$, are:

$$I_{BXT} = I_{BX} t_N^{4-A_{CX}+DAIS} \exp[-\frac{V_{gCX}}{V_{\Delta T}}], \tag{4.43}$$

$$I_{kBXT} = I_{kBX} t_N^{1-A_{CX}}, \tag{4.44}$$

$$I_{BrT} = I_{Br} t_N^{6-2m_{Lr}} \exp[-\frac{V_{gC}}{m_{Lr} V_{\Delta T}}]. \tag{4.45}$$

The temperature dependence of substrate current I_{sub} is given by:

$$I_{SsT} = I_{Ss} t_N^{4-A_S} \exp[-\frac{V_{gS}}{V_{\Delta T}}], \tag{4.46}$$

$$I_{CS_sT} = I_{CS_s} t_N^{3.5-0.5A_{sub}} \exp[-\frac{V_{gS}}{V_{\Delta T}}], \tag{4.47}$$

$$I_{ksT} = I_{ks} t_N^{1-A_S}. \tag{4.48}$$

The parameters describing the temperature dependence of resistances are also extracted in Gummel plots to provide a reasonable basis for the extraction of output curves. The scaled resistances are given by:

$$R_{ET} = R_E t_N^{A_E}, \tag{4.49}$$

$$R_{BVT} = R_{BV} t_N^{A_B-AQ_{B0}}, \tag{4.50}$$

$$R_{BCT} = R_{BC} t_N^{A_{EX}}, \tag{4.51}$$

$$R_{CCT} = R_{CC} t_N^{A_C}, \tag{4.52}$$

$$R_{CVT} = R_{CV} t_N^{A_{epi}}. \tag{4.53}$$

Table 4.11 summerizes temperaure scaling parameters of Gummel characteristics. Parameters V_{gE}, V_{gB}, V_{gJ} can be extracted by fitting forward I_B and I_C together for $DAIS$ is used in both currents. A_B is not extracted here for the influence of I_K is not so significant here that it will be extracted later in DC output curves. Here we use the initialized value of A_B to estimated $DAIS$, V_{gB} and A_{QBO}, these parameters are going to be optimized when we extract A_B.

V_{gS}, V_{gC}, V_{gCX}, A_S, A_{sub} and A_{CX} are extracted by fitting reverse I_{sub} and I_B together. Temperature scaling parameters describing resistances and $DAIS$ need to be extracted by fitting all Gummel plots together for they have the influence on both forward and reverse currents. Therefore, the parameters of forward and reverse Gummel characteristics are extracted together by fitting $I - V$ curves at 223 K, 300 K and 393 K together. When we are fitting these curves, it appears that the leakage current of substrate current is too large so I_{CS_sT} is adjusted along with its temperature coefficient A_{sub}. m_{Lr} is also adjusted since the non-ideal current I_{B3} is not

forward Gummel	I_{sT}	1. $A_B + A_{Q_{B0}} - DAIS$ 2. V_{gB}
	I_{kT}	A_B
	I_{BIT}	1. $A_E - DAIS$ 2. V_{gE}
	I_{BFT}	V_{gJ}
reverse Gummel	I_{BXT}	1. $A_{CX} - DAIS$ 2. V_{gCX}
	I_{kBXT}	A_{CX}
	I_{BrT}	V_{gC}
	I_{SsT}	1. A_S 2. V_{gS}
	I_{CS_sT}	1. A_{sub} 2. V_{gS}
	I_{ksT}	A_S
resistance	R_E	A_E
	R_{BC}	A_{EX}
	R_{BV}	$A_B - AQ_{B0}$
	R_{CC}	A_C
	R_{CV}	A_{epi}

Table 4.11: Temperaure scaling parameters of Gummel characteristics.

good. The $I - V$ curves before temperature scaling and optimizing I_{CS_sT} and m_{Lr} are shown in Figure 4.14, the optimized curves are shown in Figure 4.15. Values of parameters used here are shown in Table 4.12.

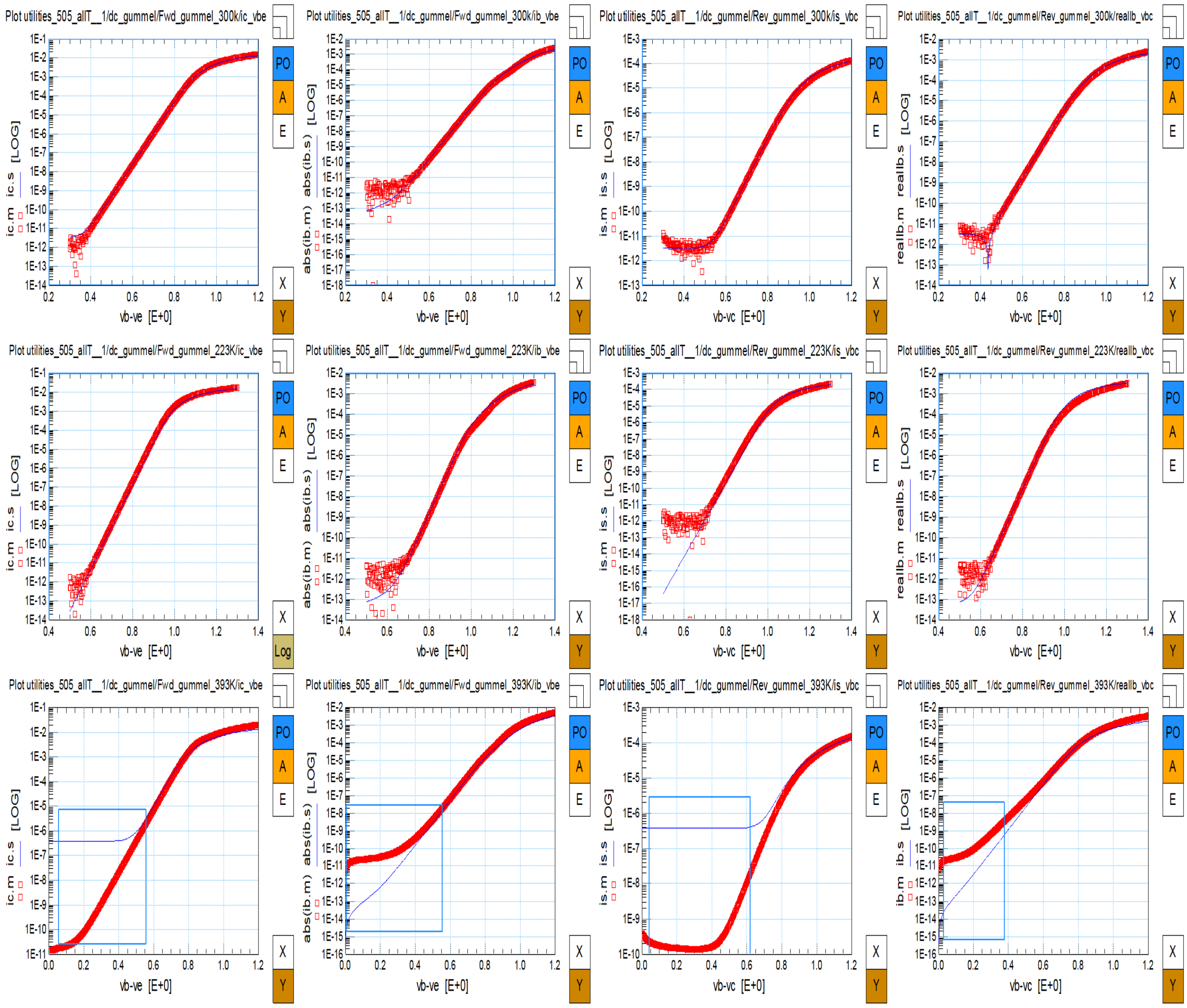

Figure 4.14: $I - V$ curves of Gummel measurement before temperature scaling and optimizing I_{CS_sT} and m_{Lr}.

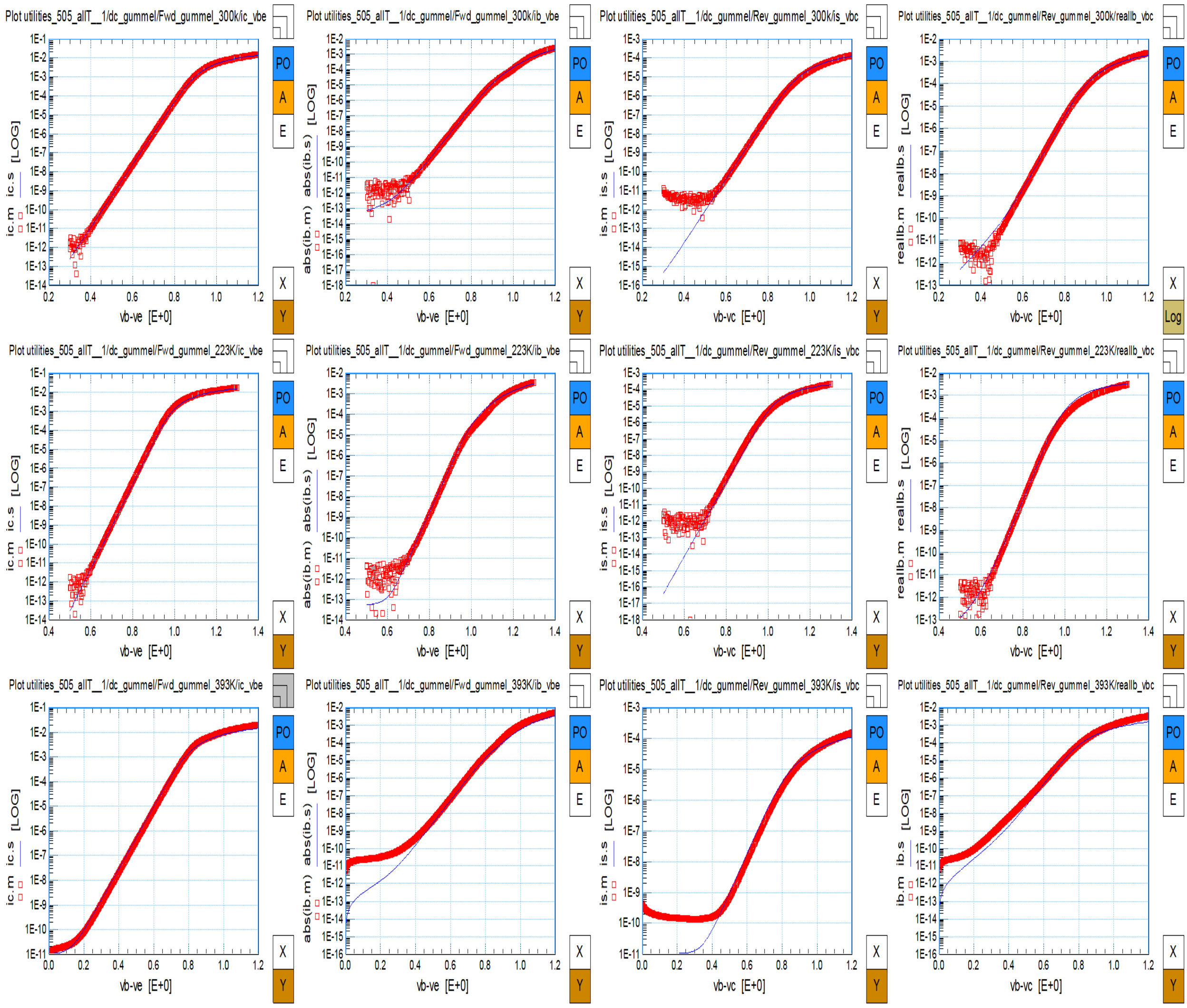

Figure 4.15: $I - V$ curves of Gummel measurement after temperature scaling and optimizing I_{CS_sT} and m_{Lr}, generated by parameters in Table 4.12.

#	parameter	value	comment
1	$\mathsf{A_B}$	1	Extracted in high current output plot
2	$\mathsf{A_{Q_{B0}}}$	356.9m	Need to be optimized with $\mathsf{A_B}$
3	DAIS	12.94m	Optimized in high current output plot
4	$\mathsf{V_{gB}}$	1.169	
5	$\mathsf{A_E}$	-35.31m	Optimized in high current output plot
6	$\mathsf{V_{gE}}$	1.114	
7	$\mathsf{V_{gJ}}$	1.611	
8	$\mathsf{A_{CX}}$	1.268	
9	$\mathsf{V_{gCX}}$	1.124	
10	$\mathsf{V_{gC}}$	1.23	
11	$\mathsf{A_S}$	1.66	
12	$\mathsf{V_{gS}}$	1.199	
13	$\mathsf{A_{sub}}$	1.967	
14	$\mathsf{A_C}$	1.951	Optimized in high current output plot
15	$\mathsf{A_{EX}}$	366.8m	Optimized in high current output plot
16	$\mathsf{A_{epi}}$	2.745	Optimized in high current output plot
17	$\mathsf{I_{CSs}}$	89.26a	
18	$\mathsf{m_{Lr}}$	2.741	

Table 4.12: Parameters used in temperature scaling parameter extraction of Gummel characteristics, used to gerenate Figure 4.15.

4.4.5 Estimation of V_{dC}

With good extraction results of the parameters used to calculate currents, the current gain is supposed to be described well. The forward current gain h_{fe} is calculated from I_B and I_C in forward Gummel measurement:

$$h_{fe} = \frac{I_C}{I_B}, \tag{4.54}$$

h_{fe} is shown in Figure 4.16. The simulated and measured h_{fe} does not fit so well. We can optimize V_{er}, V_{ef}, I_S and dE_g to get a better description of currents. Compared to V_{er}, we care more about V_{ef} for most of time transistors work in forward mode. Therefore we optimize V_{er}, V_{ef}, I_S and dE_g by fitting h_{fe} and $F_{fwdEarly}$ together.

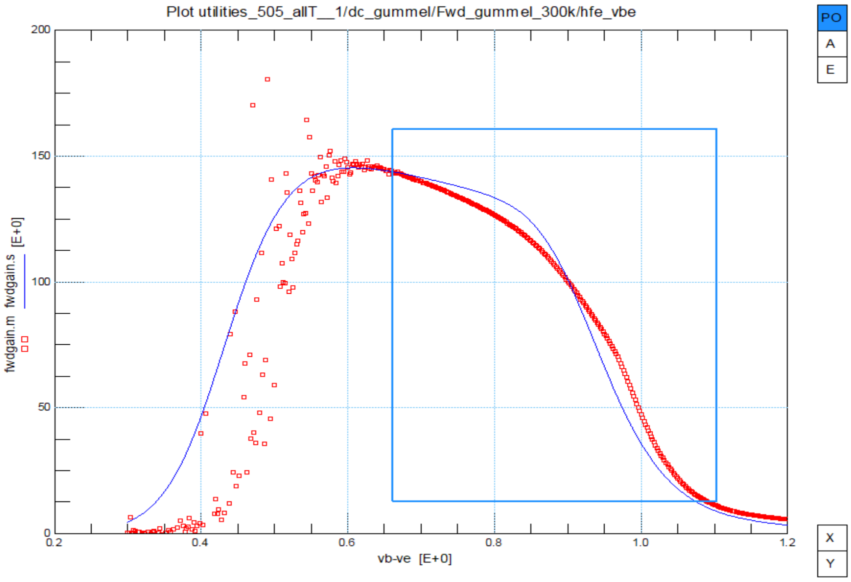

Figure 4.16: Measured (markers) and simulated (line) forward current gain h_{fe}

When bias gets higher, the current gain starts to fall. Diffusion voltage V_{dC} is one of the parameters contributing to the decrease of the current gain. As we discussed before, the collector resistance R_{CC} and R_{CV} can lead to a voltage drop between the external collector and the internal collector. When this voltage drop is sufficiently high, the internal junction bias $V_{B_2C_2}$ can be comparable to the value of V_{dC} and this internal base-collector junction is therefore forward biased. Then it is time to speak of quasi-saturation. Thus, the diffusion voltage V_{dC} is extracted in the region where the forward current gain is falling. V_{dC} also needs to

#	parameter	value	comment
1	V_{er}	2.775	
2	V_{ef}	46.82	
3	dE_g	21.82m	
4	V_{dc}	897.3m	Optimized the cut-off frequency plot
5	I_S	2.618m	

Table 4.13: Parameters used in fitting h_{fe}, used to generate Figure 4.17.

be optimized later when we extract cut-off frequency, for cut-off frequency strongly depends on the current gain. Figure 4.17 shows the forward current gain after extracting V_{dC} and optimizing V_{er}, V_{ef}, I_S and dE_g, their values are given in Table 4.13.

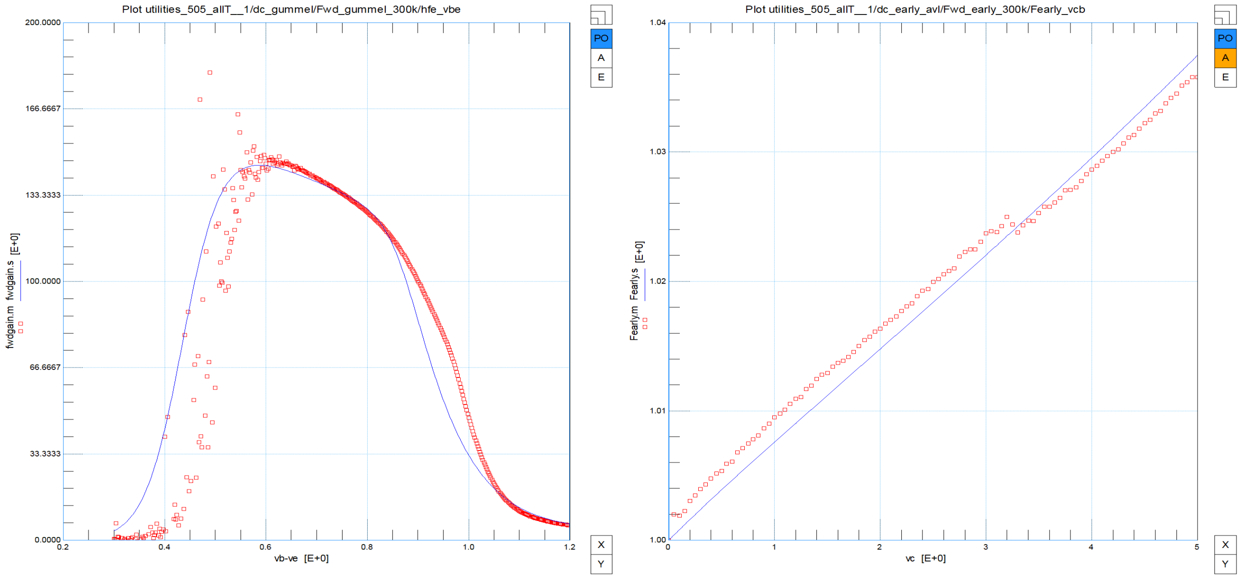

Figure 4.17: Measured (markers) and simulated (line) forward current gain h_{fe} after the extraction of V_{dC}, generated by parameters in Table 4.13.

We also want to make sure that the temperature dependence of h_{fe} is good, for they can give correct current at different temperatures. The temperature scaling rules of I_S is given in equation (4.37). The temperature dependence of V_{er}, V_{ef} and dE_g are given as:

$$V_{efT} = V_{ef}\, t_N^{A_{QB0}} \left[(1 - X_p)\left(\frac{V_{d_C}}{V_{d_CT}}\right)^{p_C} + X_p\right]^{-1}, \tag{4.55}$$

$$V_{erT} = V_{er}\, t_N^{A_{QB0}} \left(\frac{V_{d_E}}{V_{d_ET}}\right)^{-p_E}, \tag{4.56}$$

#	parameter	value	comment
1	V_{gB}	1.162	
2	V_{gC}	1.137	
3	V_{gE}	1.113	
4	A_{QB0}	366.3m	

Table 4.14: Temperature scaling parameters optimized here, used to generate Figure 4.18 and Figure 4.19.

$$dE_{gT} = dE_g t_N^{A_{QB0}}, \tag{4.57}$$

therefore the temperature scaling parameters V_{gB}, V_{gC}, V_{gE} and A_{QB0} are optimized by fitting h_{fe} at different temperatures as shown in Figure 4.18.

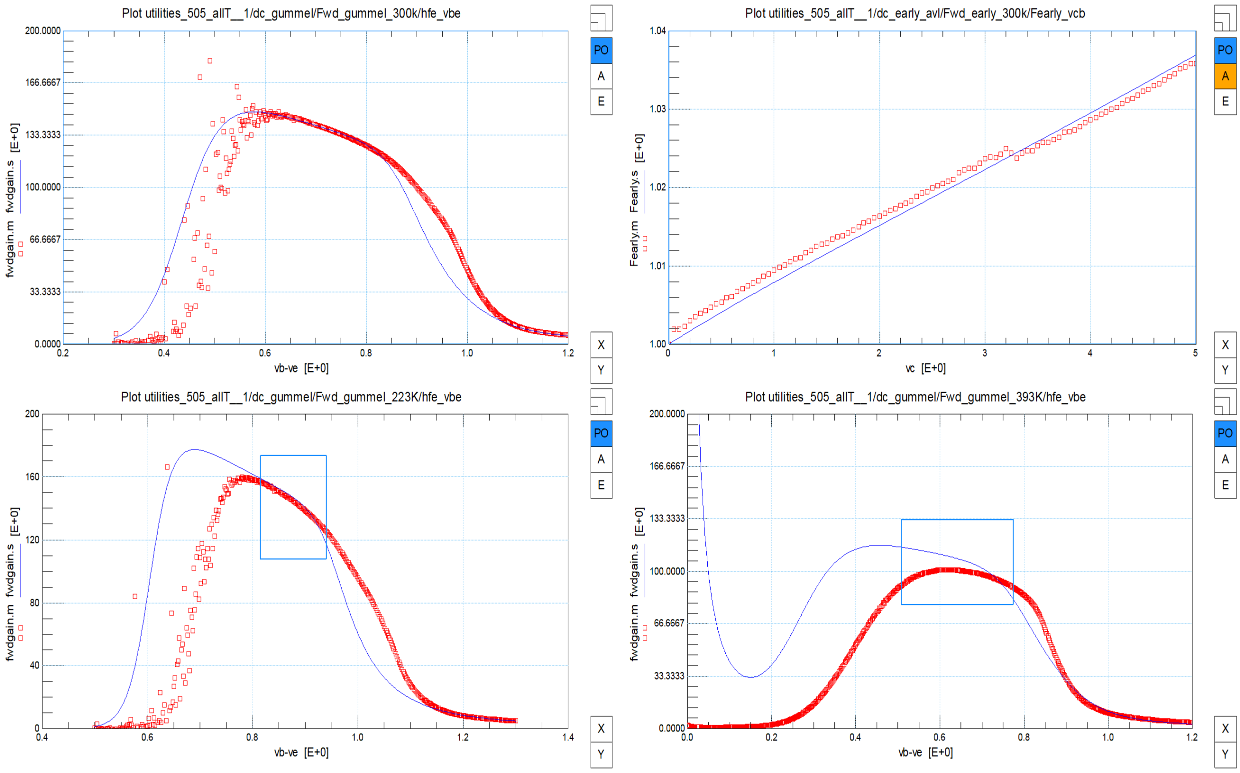

Figure 4.18: h_{fe} at different temperatures, generated by parameters in Table 4.14.

We also need to check forward collector current at different temperatures because I_S has been changed. I_C barely changes as shown in Figure 4.19. The parameters used here are shown in Table 4.14.

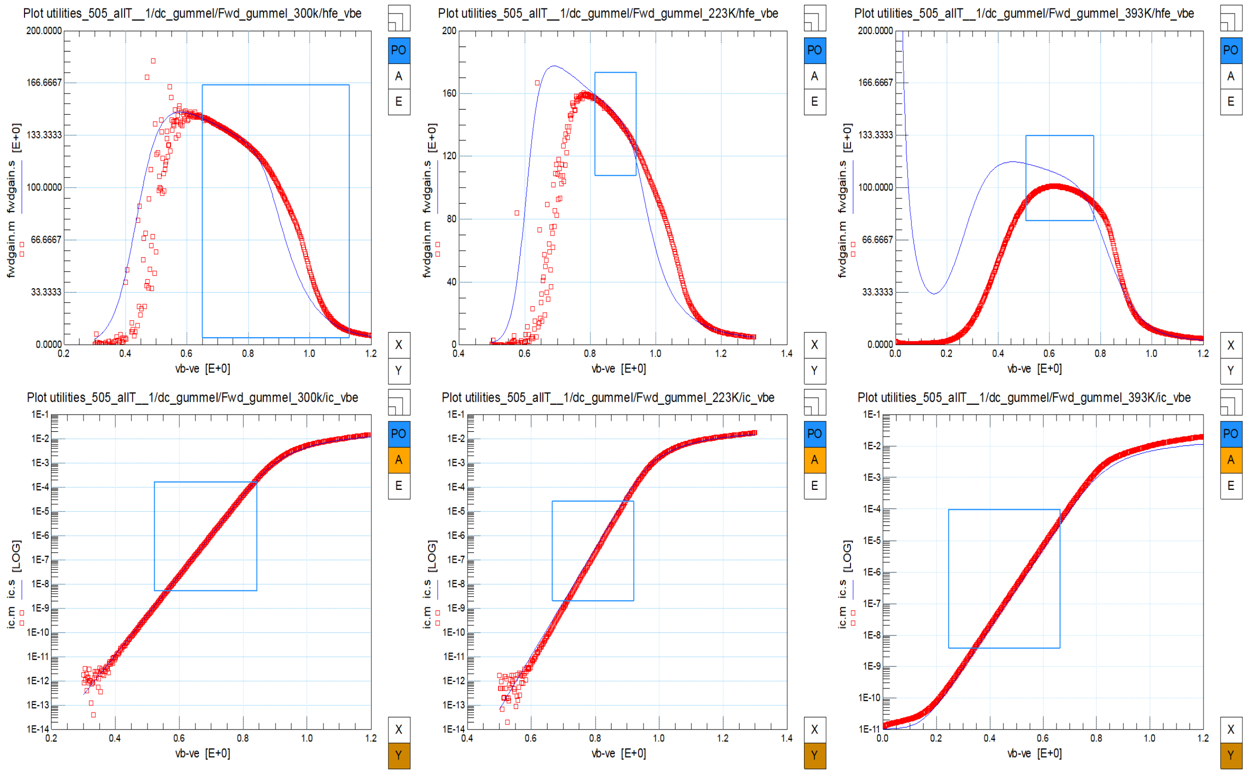

Figure 4.19: Gummel plots check after extracting parameters of h_{fe}, generated by parameters in Table 4.14.

4.5 Low current output plots check

Output curves are important since they are used to extract the self-heating parameters and high current parameters. In this section, the output curves of forced low I_B and forced low V_{BE} are inspected in order to verify the extraction results of former parameters. The results are shown in Figure 4.20.

I_C curve is not good in forced-V_{BE} $I_C - V_{CE}$ plot, so the parameters used to describe I_C, which are I_S, V_{er}, V_{ef} and dE_g, need to be optimized. When adjusting these parameters, we also need to optimize I_{BI} to keep forced-I_B $I_C - V_{CE}$ fitted. Thus I_S, I_{BI}, V_{er}, V_{ef} and dE_g are optimized by fitting these output curves of low currents, forward collector and base currents, hfe as well as $F_{fwdearly}$ as shown in Figure 4.21. The value of I_S, I_{BI}, V_{er}, V_{ef} and dE_g are listed in Table 4.15.

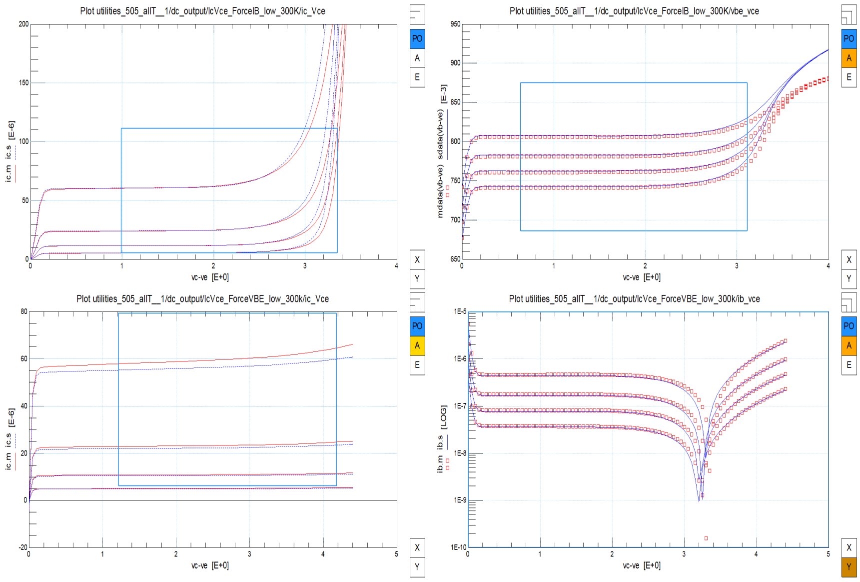

Figure 4.20: Low current output characteristics at 300 K.

#	parameter	value	comment
1	$\mathsf{I_S}$	3.429a	
2	$\mathsf{I_{BI}}$	1.449e-20	
3	$\mathsf{V_{ef}}$	10.77	
4	$\mathsf{V_{er}}$	5.183	
5	$\mathsf{dE_g}$	90.02m	

Table 4.15: Parameters used to fit low current output curves, used to generate Figure 4.21.

Since the value of I_S, I_{BI}, V_{er}, V_{ef} and dE_g have been changed, their related temperature scaling coefficients are also optimized here, as shown in Figure 4.22. Here we optimize V_{gB}, V_{gE} and A_{QB0} by fitting forward I_C and I_B as well as current gain. The value of V_{gB}, V_{gE} and A_{QB0} are given in Table 4.16.

At high V_{CE}, the simulated I_C and V_{BE} and their measured data split. It is because the avalanche parameter I_{TOavl} which is used for high currents is not extracted yet. Therefore

#	parameter	value	comment
1	$\mathsf{V_{gB}}$	1.123	
2	$\mathsf{V_{gE}}$	1.125	
3	$\mathsf{A_{QBO}}$	716.2m	

Table 4.16: Temperature scaling parameters used in fitting low current output curves, used to generate Figure 4.22.

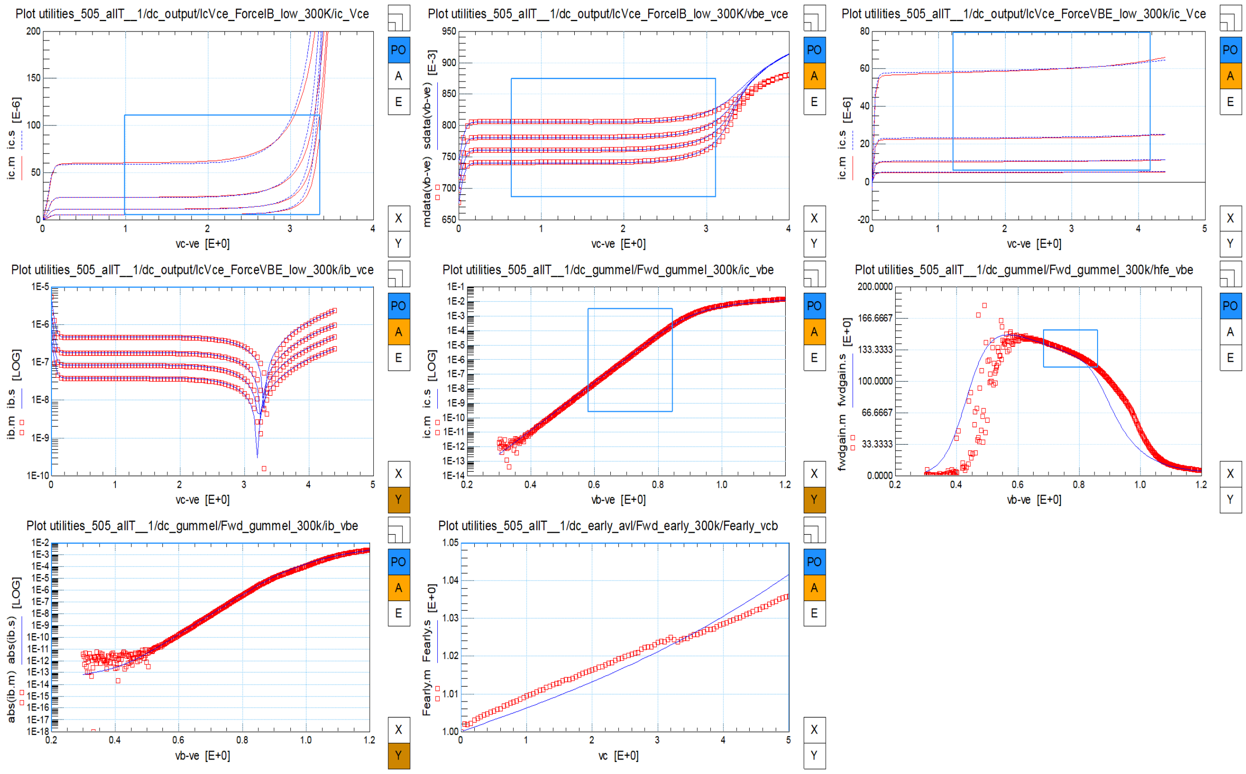

Figure 4.21: Fitting low current output characteristics at 300 K, generated by parameters in Table 4.15.

#	parameter	value	comment
1	I_{TOavl}	6.54m	

Table 4.17: Parameter I_{TOavl} used to generate Figure 4.23.

I_{TOavl} is optimized by fitting these output curves of low currents, along with I_{avl} and G_{EM}, as shown in Figure 4.23. The value of I_{TOavl} is given in Table 4.17.

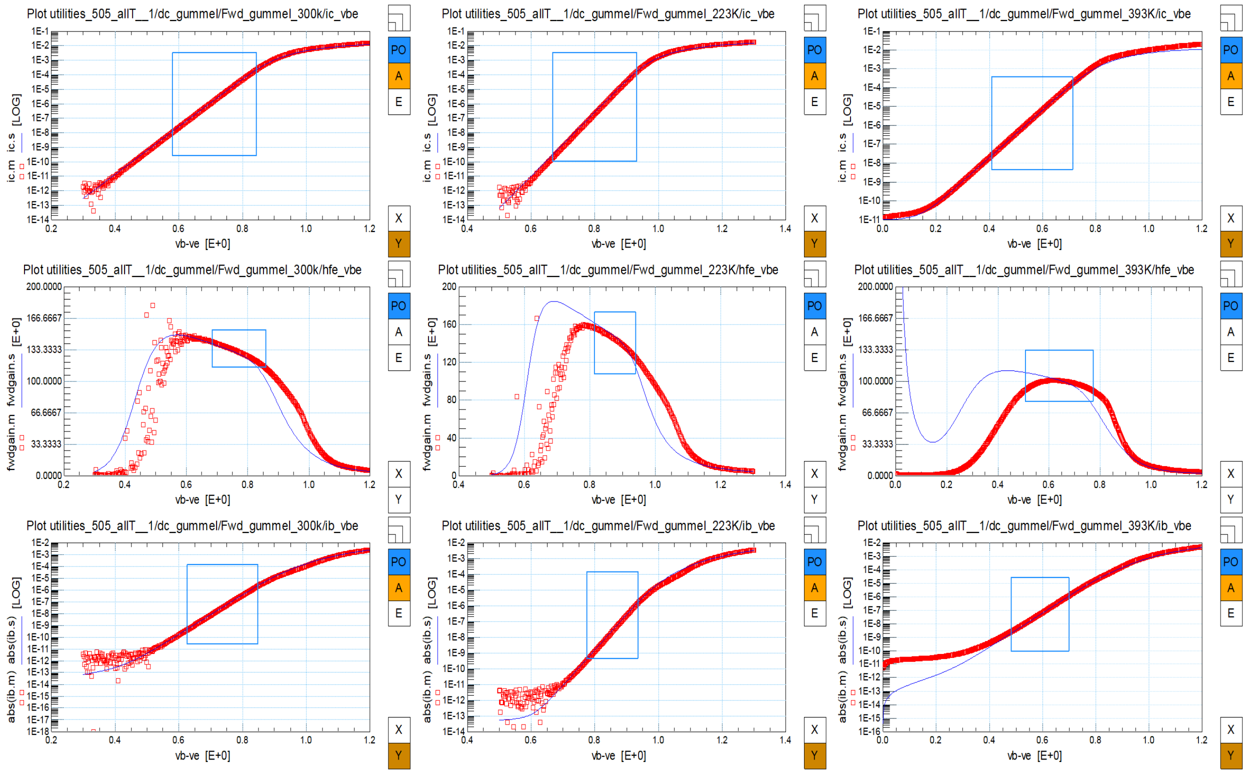

Figure 4.22: Gummel plots check and current gain check after extracting parameters of low current output characteristics, generated by parameters in Table 4.16.

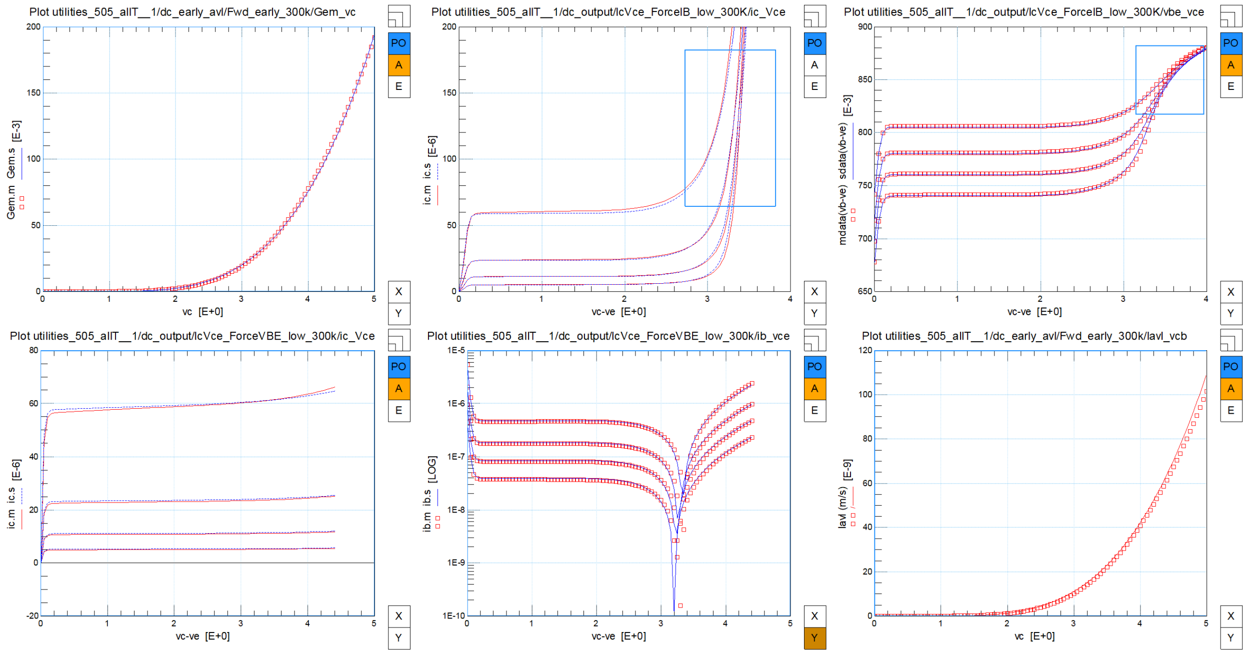

Figure 4.23: Low current output characteristics fitting, generated by parameter in Table 4.17.

Chapter 5

Extraction of High Current Parameters

The extraction of high current parameters is not as straightforward as that of low current parameters. In this chapter, we first discuss self-heating, then we extract the parameters of forced high I_B and forced high V_{BE} output curves and the related temperature scaling parameters. Last, parameters of cut-off frequency and temperature scaling of those parameters are extracted.

5.1 Extraction of parameters of self-heating and output characteristics at 300 K

The extraction of self-heating parameters should be done properly in order to extract the high-current parameters correctly, for self-heating can distort the measurement at high currents and voltages as we discussed in former steps. The thermal resistance R_{TH} is critical for the modeling of self-heating because the junction temperature is determined by R_{TH}, and therefore the temperature characteristics of the whole device. R_{TH} is extracted from the base-emitter voltage in the output curve V_{BE}-V_{CE}, of which the base current is a constant value.

The temperature will rise due to self-heating by an amount given as:

$$\Delta T = R_{TH}(I_B V_{BE} + I_C V_{CE}). \tag{5.1}$$

Obviously, the collector part contributes significantly to self-heating. At small V_{CE} and I_B, self-heating can be neglected so the base-emitter voltage is a constant. As V_{CE} and I_B increase, self-heating effect becomes more and more important. I_B is dominated by the ideal base current

I_{BI} and it can be approximated by:

$$I_B = I_{BIT} e^{V_{B_2E_1}/(N_{BI}V_T)}. \tag{5.2}$$

From now on, we need to temperature scaled model parameters, because the currents and voltages are high. I_{BIT}, as we discussed in 4.4.4, increases with increasing temperature. V_{CE} increases rapidly in output measurement and causes the increase of temperature, which leads to the increase of I_{BIT}. Then V_{BE} needs to be decrease to keep I_B constant for a forced I_B output measurement. R_{TH} is extracted from this decrease of V_{BE}.

From equation (5.2) the internal junction voltage $V_{B_2E_1}$ can be expressed as:

$$V_{B_2E_1} = N_{BI}V_T \ln(\frac{I_B}{I_{BIT}}). \tag{5.3}$$

The external base-emitter voltage V_{BE} also includes voltage drops over resistance, of which the most important is R_E, and it can be approximated by:

$$V_{BE} = N_{BI}V_T \ln(\frac{I_B}{I_{BIT}}) + I_C R_{ET}, \tag{5.4}$$

R_E is the emitter resistance we extracted in 4.4.3. Since it presents in the equation of V_{BE}, we need to optimize its value here for a good description of output curves. Thus, R_{TH} and R_E are both extracted from output measurement V_{BE}-V_{CE} as shown in Figure 5.1.

Other parameters used to describe output characteristics are extracted from forced I_B I_C-V_{CE} curves. To understand extraction of these parameters, we consider calculating the collector current in terms of the base current I_B and the collector bias V_{CE}, following [11]. The collector current I_C is written as:

$$I_{C_1C_2} = I_N = I_S \frac{e^{V_{B_2E_1}/V_T} - e^{V^*_{B_2C_2}/V_T}}{q^I_B}. \tag{5.5}$$

q^I_B, $V_{B_2E_1}$ and $V^*_{B_2C_2}$ should be calculated to get $I_{C_1C_2}$. $V^*_{B_2C_2}$ is the bias considering quasi-saturation. $V_{B_2E_1}$ can be obtained by equation 5.2 from base current. q^I_B can be calculated

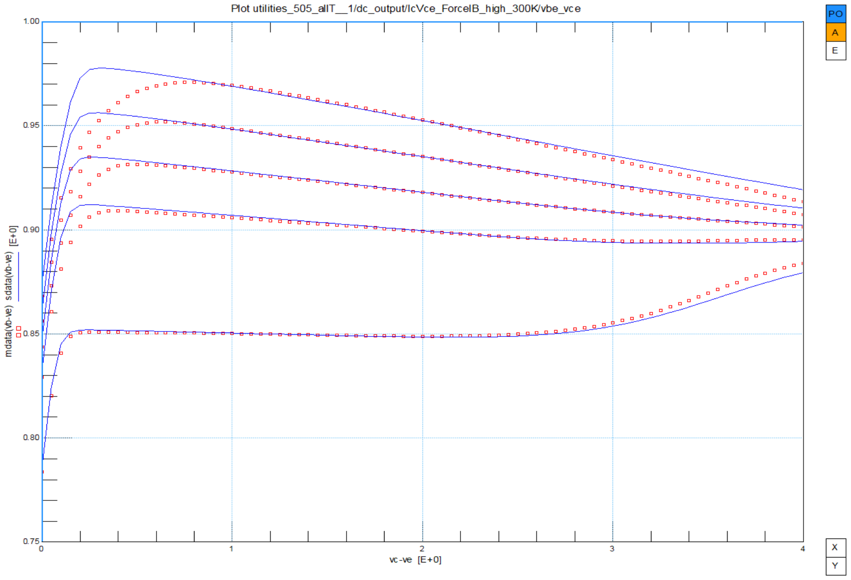

Figure 5.1: V_{BE} - V_{CE} under forced high I_B

by:

$$q_B^I = q_1^I(1 + 0.5n_0 + 0.5n_B), \tag{5.6}$$

q_1^I is defined in (4.21). n_0 and n_B are the base minority electron densities at the emitter edge and at the collector edge, and they are given by:

$$f_1 = 4\frac{I_S}{I_K}e^{V_{B_2E_1}/N_{FF}V_T}, \tag{5.7}$$

$$n_0 = \frac{f_1}{1 + \sqrt{1 + f_1}}, \tag{5.8}$$

$$f_2 = 4\frac{I_S}{I_K}e^{V^*_{B_2C_2}/N_{FR}V_T}, \tag{5.9}$$

$$n_B = \frac{f_2}{1 + \sqrt{1 + f_2}}. \tag{5.10}$$

$V^*_{B_2C_2}$ is solved iteratively from $I_{C_1C_2}$. First, the voltage and current at which quasi-saturation start are given as

$$V_{qs}^{th} = V_{dCT} + 2V_T \ln(\frac{I_{C_1C_2}R_{CVT}}{2V_T} + 1) - V_{B_2C_1}, \tag{5.11}$$

$$V_{qs} = 0.5(V_{qs}^{th} + \sqrt{(V_{qs}^{th})^2 + 4(0.1V_{dCT})^2}), \tag{5.12}$$

$$I_{qs} = \frac{V_{qs}}{SCR_{CV}} \frac{V_{qs} + I_{hc}SCR_{CV}}{V_{qs} + I_{hc}R_{CVT}}, \tag{5.13}$$

SCR_{CV} is the space charge resistance of epilayer. I_{hc} is the critical current for velocity saturation in the epilayer. The internal voltage $V_{B_2C_1}$ in equation 5.11 is calculated by:

$$V_{B_2C_1} = V_{B_2E_1} + I_C R_{CCT} + (I_B + I_C)R_{ET} - V_{CE}. \tag{5.14}$$

Then we can get α expressed as:

$$\alpha = \frac{1 + a_{Xi} \ln(1 + \exp[(I_{C_1C_2}/I_{qs} - 1)/a_{Xi}])}{1 + a_{Xi} \ln(1 + \exp[-1/a_{Xi}])}, \tag{5.15}$$

a_{Xi} is the smoothness parameter for onset of quasi-saturation.

We need to solve

$$\alpha I_{qs} = \frac{V_{qs}}{SCR_{CV} y_i^2} \frac{V_{qs} + I_{hc}SCR_{CV} y_i}{V_{qs} + I_{hc}R_{CVT}}, \tag{5.16}$$

which leads to

$$v = \frac{V_{qs}}{I_{hc}SCR_{CV}}, \tag{5.17}$$

$$y_i = \frac{1 + \sqrt{1 + 4\alpha v(1 + v)}}{2\alpha(1 + v)}. \tag{5.18}$$

The injection thickness is given by:

$$\frac{x_i}{W_{epi}} = 1 - \frac{y_i}{1 + p_W y_i}, \tag{5.19}$$

the hole density p_0^* at the base-collector junction is expressed by:

$$g = \frac{I_{C_1C_2} R_{CVT}}{2V_T} \frac{x_i}{W_{epi}}, \tag{5.20}$$

$$p_0^* = \frac{g - 1}{2} + \sqrt{(\frac{g - 1}{2})^2 + 2g + p_W(p_W + g + 1)}, \tag{5.21}$$

$$e^{V^*_{B_2C_2}/V_T} = p_0^*(p_0^* + 1)e^{V_{d_CT}/V_T}. \tag{5.22}$$

The internal base-collector bias is obtained from equations involved for finding I_C from a given I_B, outlined above. We see that I_K, SCR_{CV},R_{CV}, I_{hc}, and a_{Xi} are most important parameters. R_{CV}, V_{d_C}, R_E, R_{CC}, which are parameters estimated in former steps, need to be optimized here in order to give good description of output characteristics, while I_K, SCR_{CV}, I_{hc}, and a_{Xi} are extracted the first time.

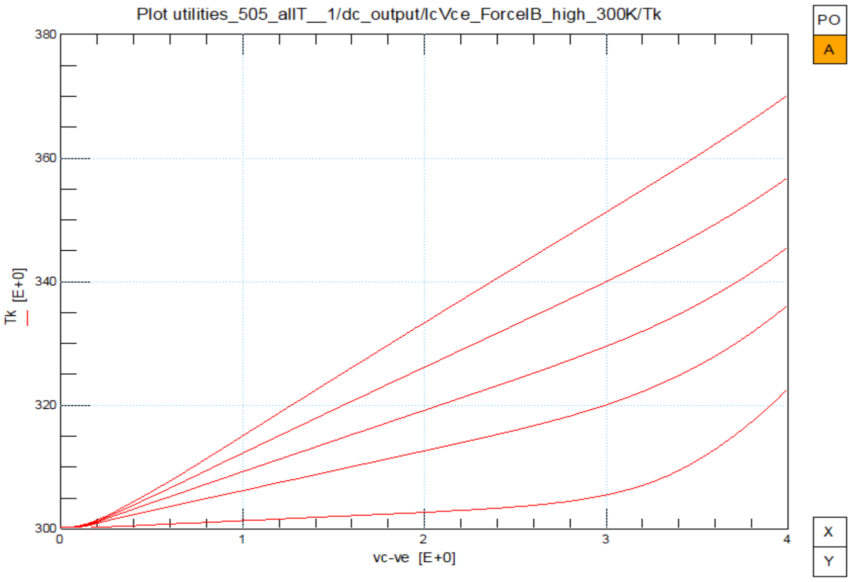

Figure 5.2: T_k of forced high I_B at 300 K

T_K shown in Figure 5.2 illustrates that self-heating needs to be taken into account in high bias output measurement. Therefore, temperature-scaling needs to be done here. Since all the related temperature scaling parameters except A_B already have good estimation from former extractions, A_B, which is fairly important, is extracted here. The significance of A_B can be seen in equations:

$$I_{sT} = I_s t_N^{\frac{4-A_B-A_{QB0}+DAIS}{N_{FF}}} \exp[-\frac{V_{gB}}{N_{FF}V_{\Delta T}}], \tag{5.23}$$

$$I_{kT} = I_k t_N^{1-A_B}. \tag{5.24}$$

Actually, high current parameters have strong correlations between each other, so it is not possible to extract them individually. The parameters such as I_K, R_{CV} and I_{hc} which are important in extracting the parameters of I_C also have obvious influences on V_{BE}. Therefore, we extract output parameters by fitting I_C-V_{CE} and V_{BE}-V_{CE} curves together as shown in

Figure 5.3. Then we need to check the output plots of forced V_{BE}. The curves are shown in Figure 5.4.

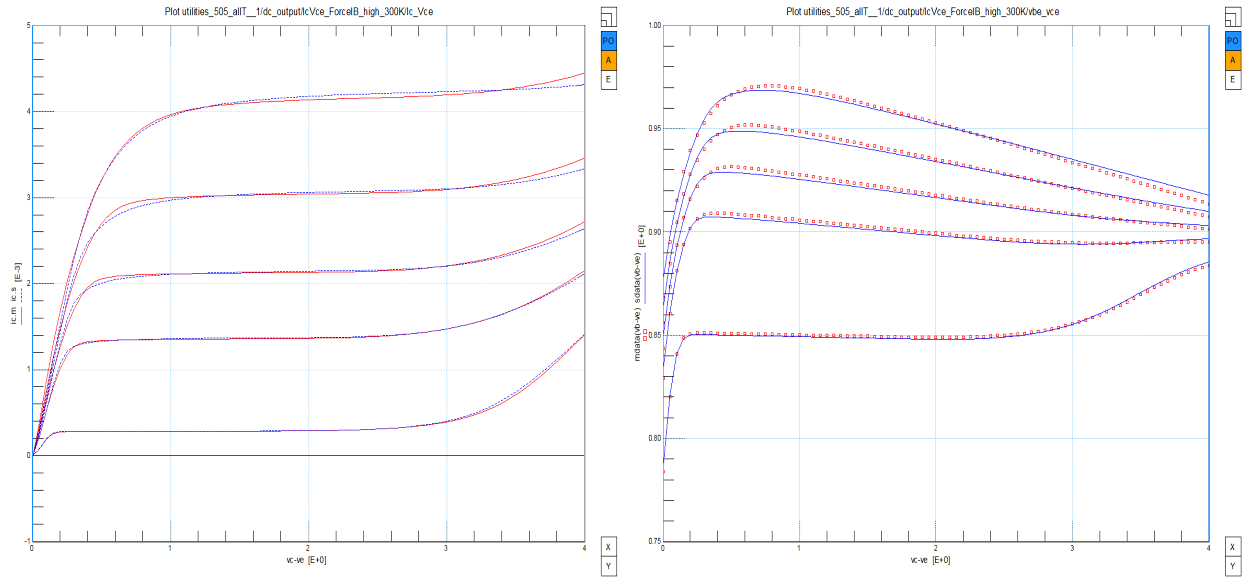

Figure 5.3: I_C-V_{CE} and V_{BE}-V_{CE} plots of forced high I_B at 300 K

As we can see, at low V_{CE} (around 0V-2V) the simulated I_C and I_B fit well with the measured data in forced V_{BE} measurement. When V_{CE} further rises, the simulated data increases rapidly and then reaches to a plateau. This is because the thermal resistance R_{th} is overestimated so that the voltage of temperature node V_{dT} reaches its upper limit defined by the Mextram 505 code and it cannot be increased any more. T_K, therefore, also stops rising. T_K of forced high V_{BE} is shown in Figure 5.5.

The value of T_k is too high and reaches its limit as shown in Figure 5.5. Figure 5.4 shows that in forced V_{BE} $I_C - V_{CE}$ curves, the simulated data is larger than measured data at high V_{CE}, so the value of R_{th} is a bit large. Therefore R_{th} is reduced and all the other parameters are adjusted to fit output plots. The extraction results are shown in Figure 5.6.

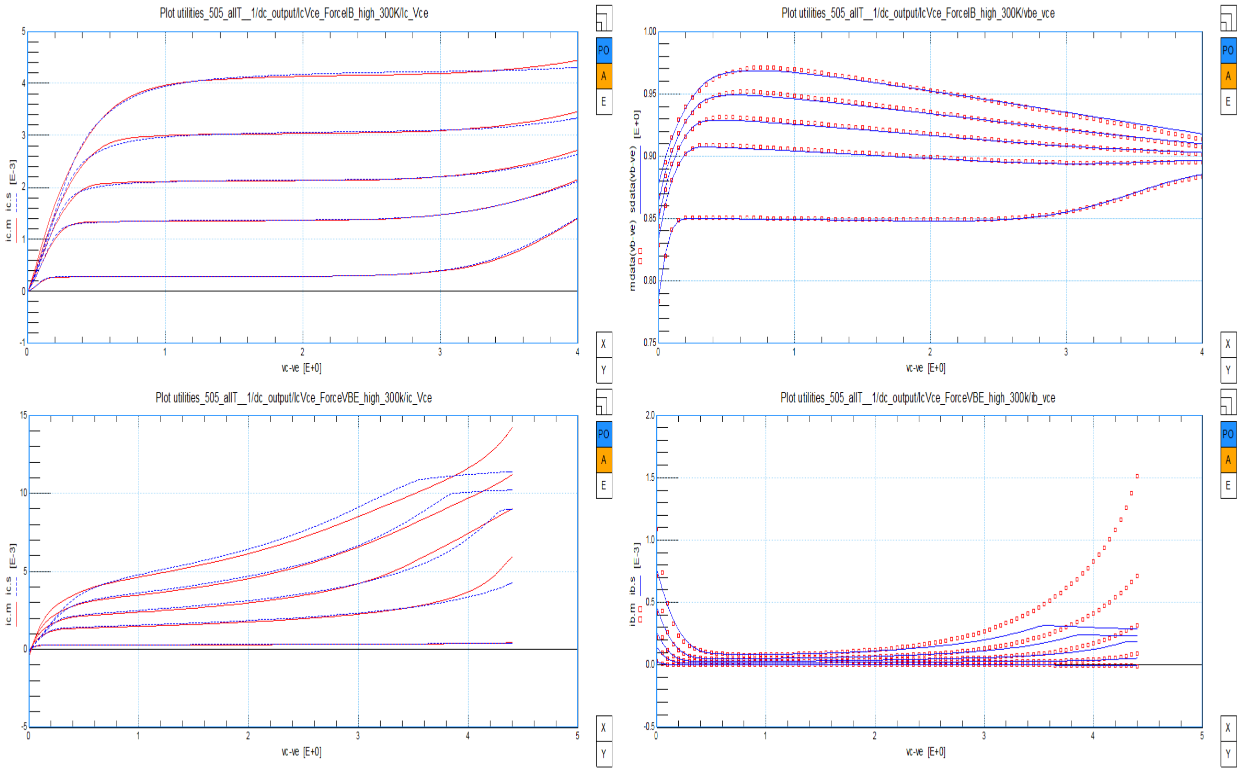

Figure 5.4: Output plots of forced high I_B and forced high V_{BE} at 300 K

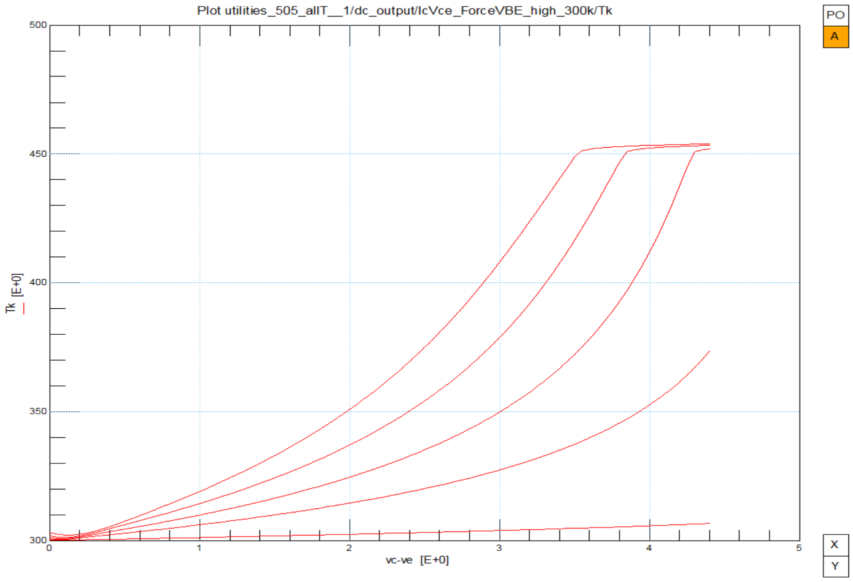

Figure 5.5: T_k of forced high V_{BE} at 300 K

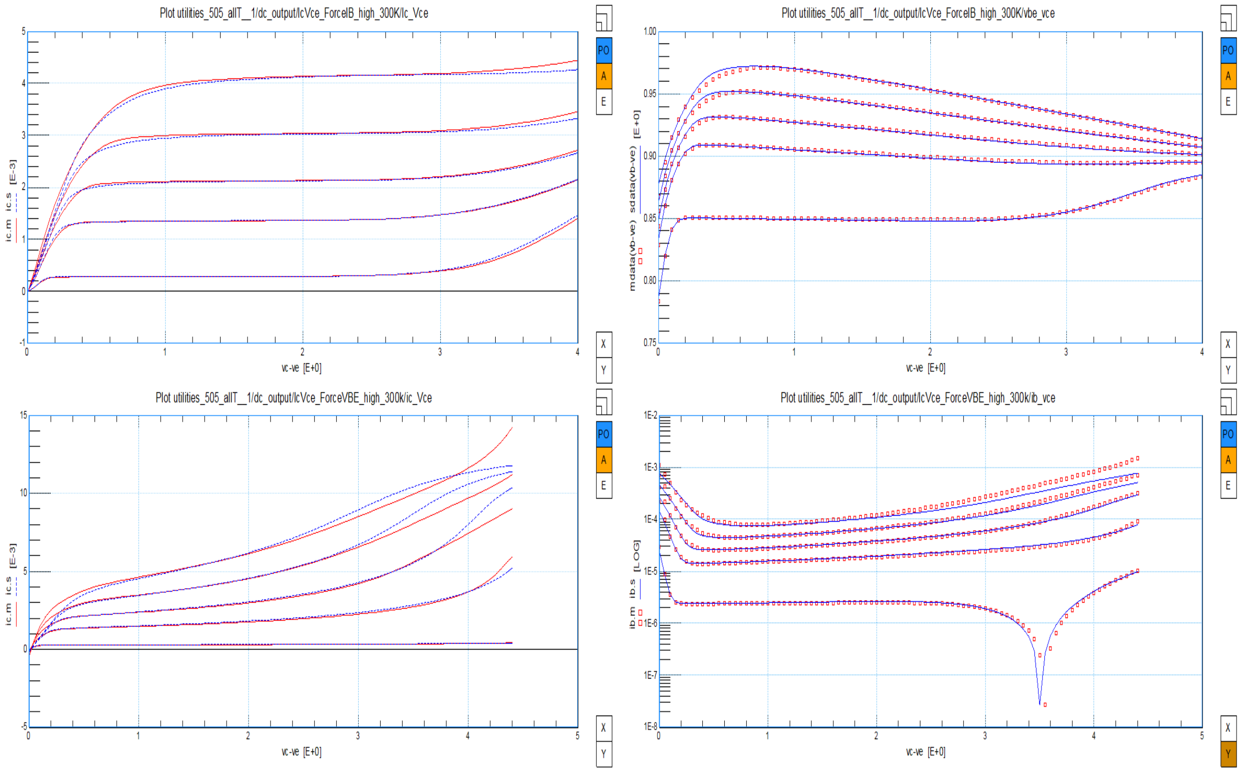

Figure 5.6: Output plots of forced high I_B and forced high V_{BE} at 300 K

After extracting all output parameters, it is necessary to look back at the Gummel plots, for resistance R_E, R_{CC} and R_{CV} have been changed to fit output curves. The Gummel plots are shown in Figure 5.7.

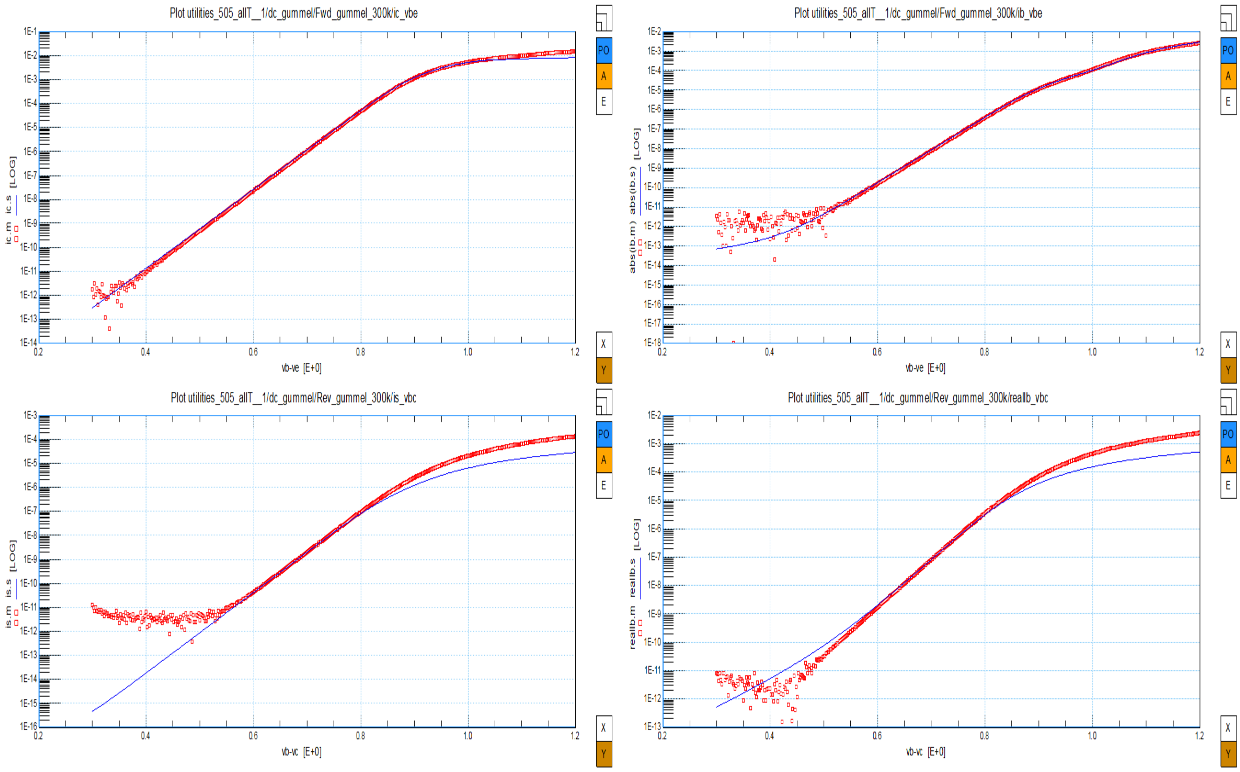

Figure 5.7: Gummel plots after extraction of output plots at 300 K

As can be seen from the figure, there is just a small change in the forward Gummel plots, but the reverse Gummel plots are quite different from the previous ones. This is because the resistance R_E, R_{CV} and R_{CC} are used in the extraction of both Gummel measurement and output measurement. The influence of R_{CC} and R_{CV} in reversed Gummel plots is greater than that of forward Gummel plots. The effect of R_E is opposite. However, the variation of R_E is small so the influence of R_E on forward Gummel plots could be ignored. Therefore, the changes of reverse Gummel plots are more apparent. Trying to fit all plots more desirable, the resistance R_{CV} and R_{CC} are optimized by fitting the reverse Gummel plots at high V_{BC} and output plots together as shown in Figure 5.8. The values of parameters used here are listed in Table 5.1.

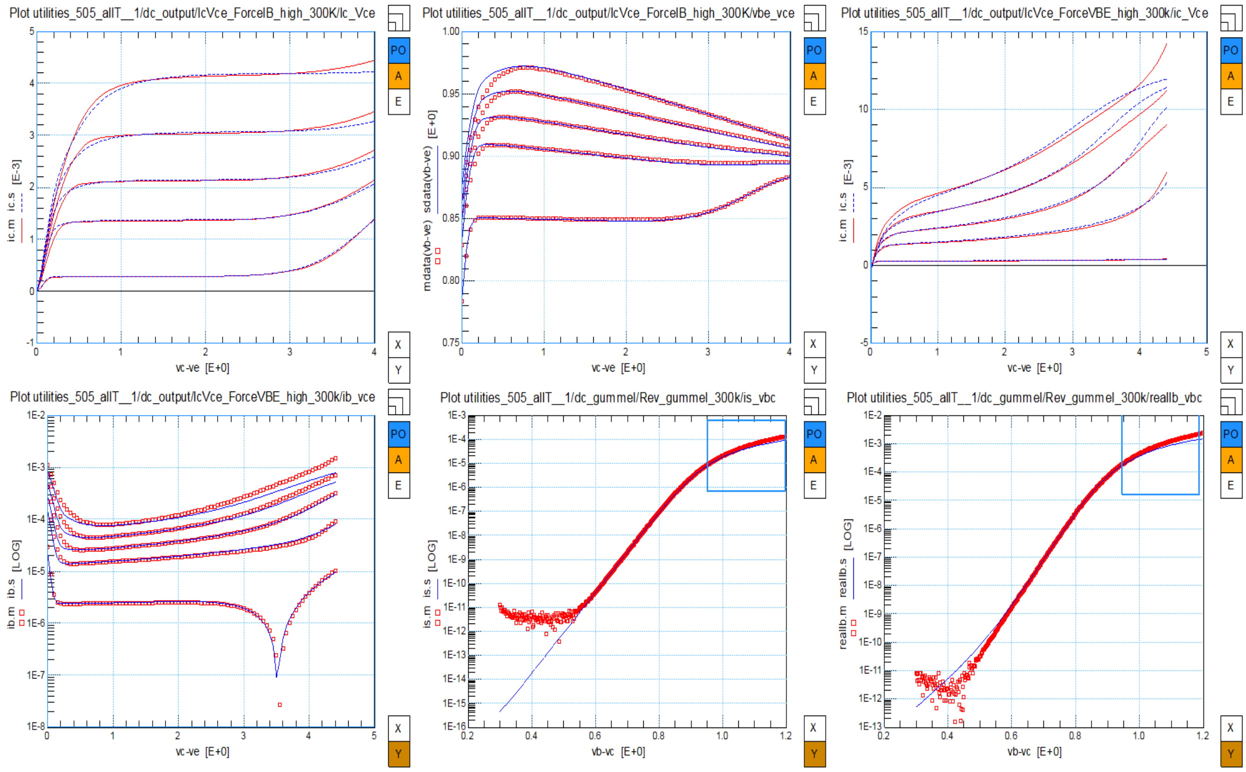

Figure 5.8: Optimize R_{CV} and R_{CC} by fitting reverse Gummel plots and high current output plots together at 300 K, generated by parameters in Table 5.1.

#	parameter	value	comment
1	$\mathsf{R_E}$	14.83	
2	$\mathsf{R_{th}}$	4.543k	
3	$\mathsf{R_{CC}}$	28.98	
4	$\mathsf{R_{CV}}$	101.6	
5	$\mathsf{A_B}$	799.3m	
6	$\mathsf{I_K}$	17.08m	
7	$\mathsf{SCR_{CV}}$	76.14	
8	$\mathsf{I_{hc}}$	18.82m	
9	$\mathsf{a_{Xi}}$	181.4m	

Table 5.1: Parameters extracted from high current output curves and reverse currents in Gummel measurement, used to generate Figure 5.8.

5.2 Temperature scaling of DC high current parameters

After extracting parameters of output characteristics at 300 K, the temperature scaling parameters are extracted by fitting all the I_C - V_{CE} and V_{BE} - V_{CE} plots at different temperatures at the same time, as shown in Figure 5.9. The parameters optimized in high current output plots include A_C, A_B, A_{EPI}, A_{EX}, $DAIS$, A_{QBO} and A_E from former extractions in section 4.4.4. A_{TH}, which is used to describe the temperature dependence of thermal resistance R_{TH}, needs to be extracted here. The values of parameters used here are given in Table 5.2.

$$R_{TH,Tamb} = R_{TH}(\frac{T_{amb}}{T_{RK}})^{A_{TH}}. \tag{5.25}$$

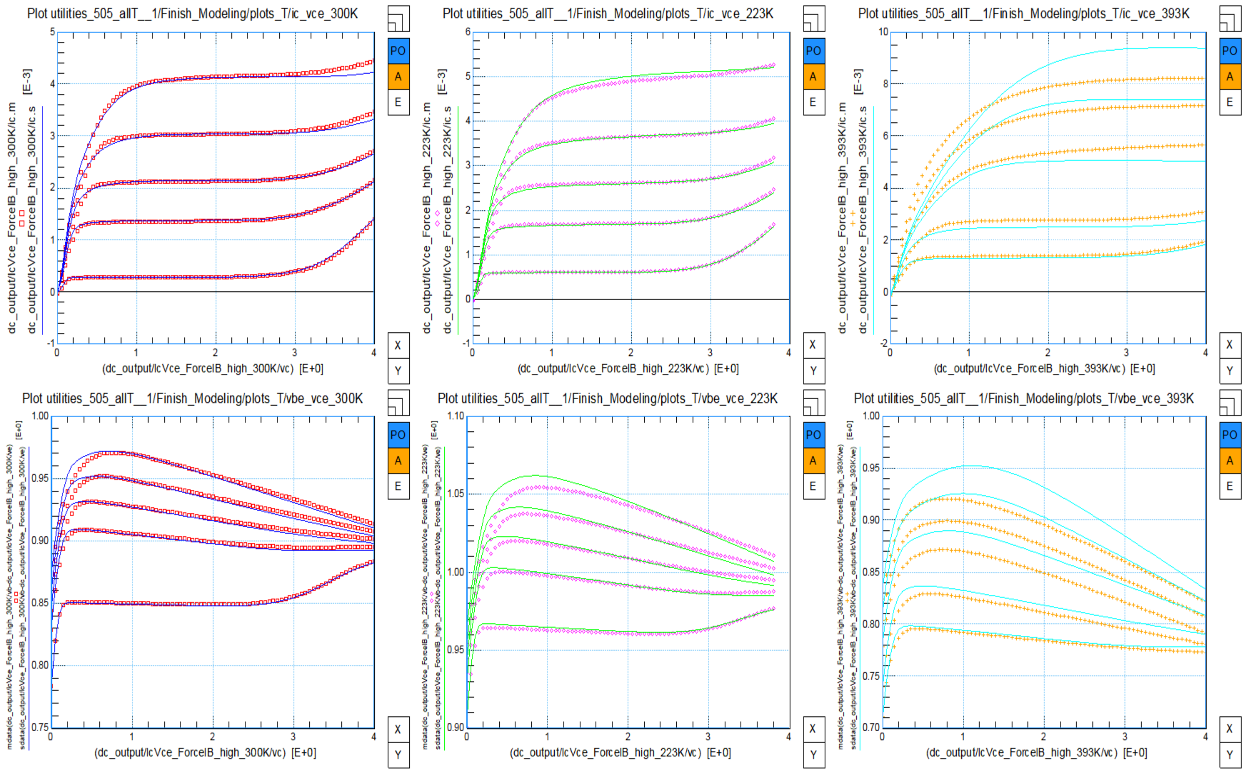

Figure 5.9: Forced high I_B output curves at different temperatures, generated by parameters in Table 5.2.

Again, we need to check Gummel plots since the temperature scaling parameters have been changed here. As shown in Table 4.11, the change of A_B, $DAIS$ and A_{QBO} will lead to the change of V_{gB}; the change of $DAIS$ and A_E will lead to the change of V_{gE}; the change

#	parameter	value	comment
1	A_{epi}	1.346	
2	A_C	-1.467	
3	A_B	1.485	
4	A_{EX}	366.8m	
5	A_{QBO}	10.77m	
6	DAIS	399.9m	
7	A_E	-753.0u	
8	A_{th}	431.8m	

Table 5.2: Temperature scaling parameters used in fitting high current output curves to generate Figure 5.9.

#	parameter	value	comment
1	V_{gB}	1.139	
2	V_{gE}	1.136	
3	A_{CX}	1.674	
4	V_{gCX}	1.136	

Table 5.3: Temperature scaling parameters extracted from Figure 5.10.

of $DAIS$ will lead to the change of A_{CX} and V_{gCX}. Therefore, V_{gB}, V_{gE}, A_{CX} and V_{gCX} are optimized by fitting high current output curves and Gummel plots at different temperatures as shown in Figure 5.10. The values of these parameters are given in Table 5.3.

Since V_{gB}, V_{gE} and A_{QBO}, A_B, $DAIS$ and A_E have been changed here, we also need to check the values of I_{ST} and I_{BIT}, which are saturation currents influenced by these parameters. We inspect I_{ST} and I_{BIT} from low current output curves at different temperatures as shown in Figure 5.11.

The figure shows that at 300 K the low current output curves fit well, but at 223 K and 393 K their fittings need to be improved. Therefore, V_{gB}, V_{gE}, A_{QBO}, A_B, $DAIS$, and A_E, which are temperature scaling parameters used to describe base and collector currents are optimized by fitting low current output plots with high current output curves, as well as forward I_B and I_C from Gummel measurement at different temperatures simultaneously, as shown in Figure 5.12. The values of parameters optimized here are also given in Table 5.4.

Since $DAIS$ has been changed again, A_{CX} and V_{gCX} may also have been changed either or not. These two parameters are optimized by fitting I_S and I_B in reverse Gummel measurement at different temperatures as shown in Figure 5.13. In this figure we also plot high current

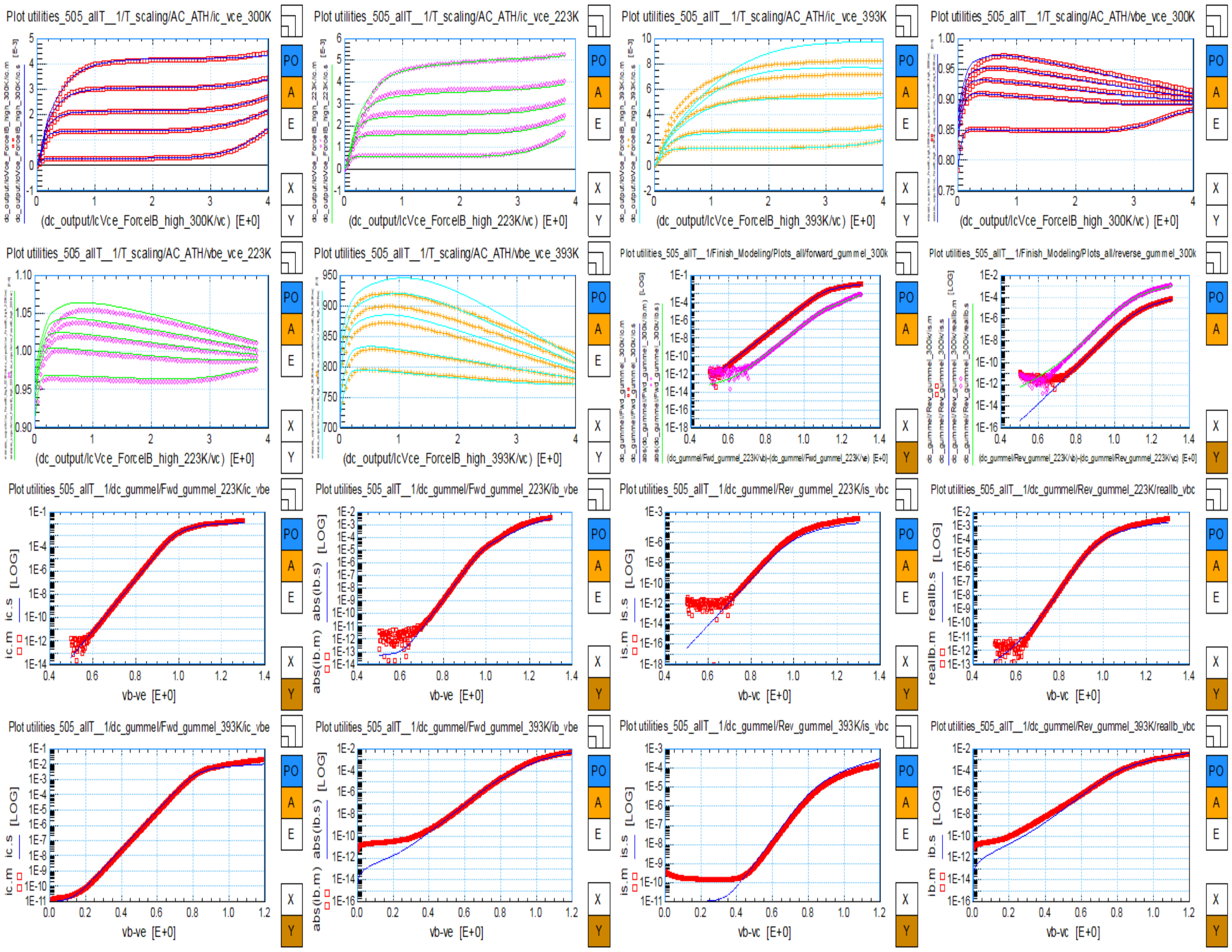

Figure 5.10: Gummel plots check with output curves at different temperatures, generated by parameters in Table 5.3.

output curves to show that A_{CX} and V_{gCX} have small impacts on them. The values of A_{CX} and V_{gCX} are given in Table 5.5.

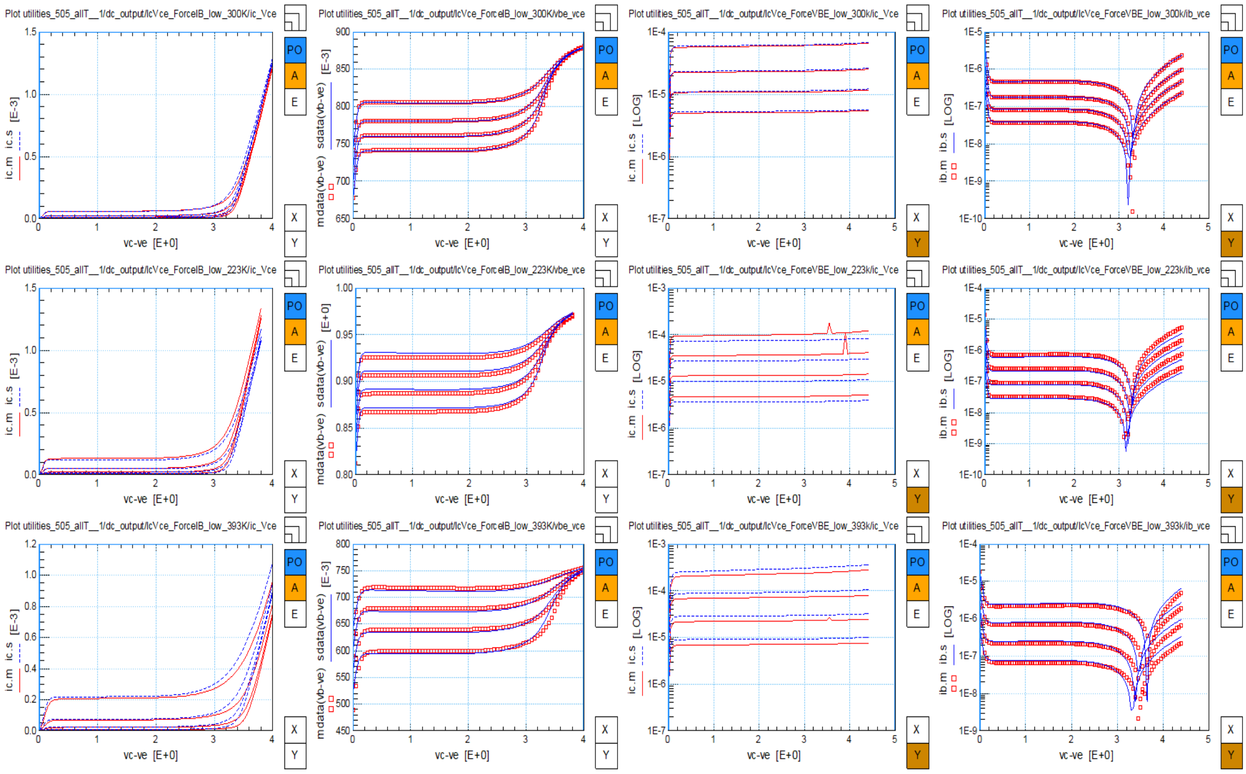

Figure 5.11: Low current output plots check at different temperatures.

#	parameter	value	comment
1	$\mathrm{A_B}$	1.487	
2	$\mathrm{A_{QBO}}$	144.4m	
3	DAIS	20.38m	
4	$\mathrm{A_E}$	-589.3u	
5	$\mathrm{V_{gB}}$	1.142	
6	$\mathrm{V_{gE}}$	1.149	

Table 5.4: Parameters used in low current output plots fitting with high current output plots and forward Gummel curves at different temperatures, used to generate Figure 5.12.

#	parameter	value	comment
1	$\mathrm{A_{CX}}$	1.39	A_{CX} in Figure 5.13
2	$\mathrm{V_{gCX}}$	1.133	V_{gCX} in Figure 5.13

Table 5.5: Parameters used in fitting I_S and I_B in reverse Gummel measurement with high current output curves at different temperatures, extracted from Figure 5.13.

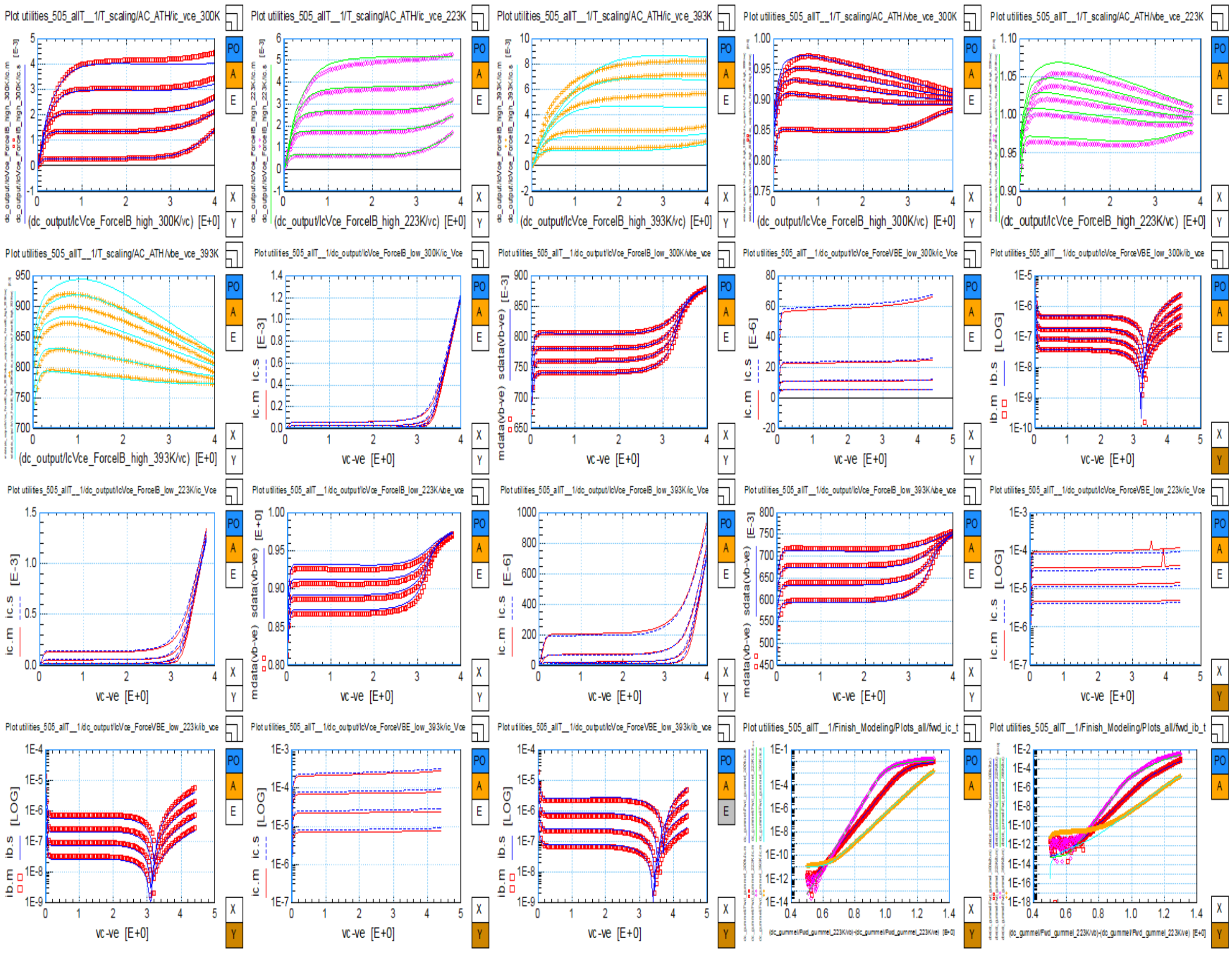

Figure 5.12: Low current output plots fitting with high current output plots and forward Gummel curves at different temperatures, generated by parameters in Table 5.4.

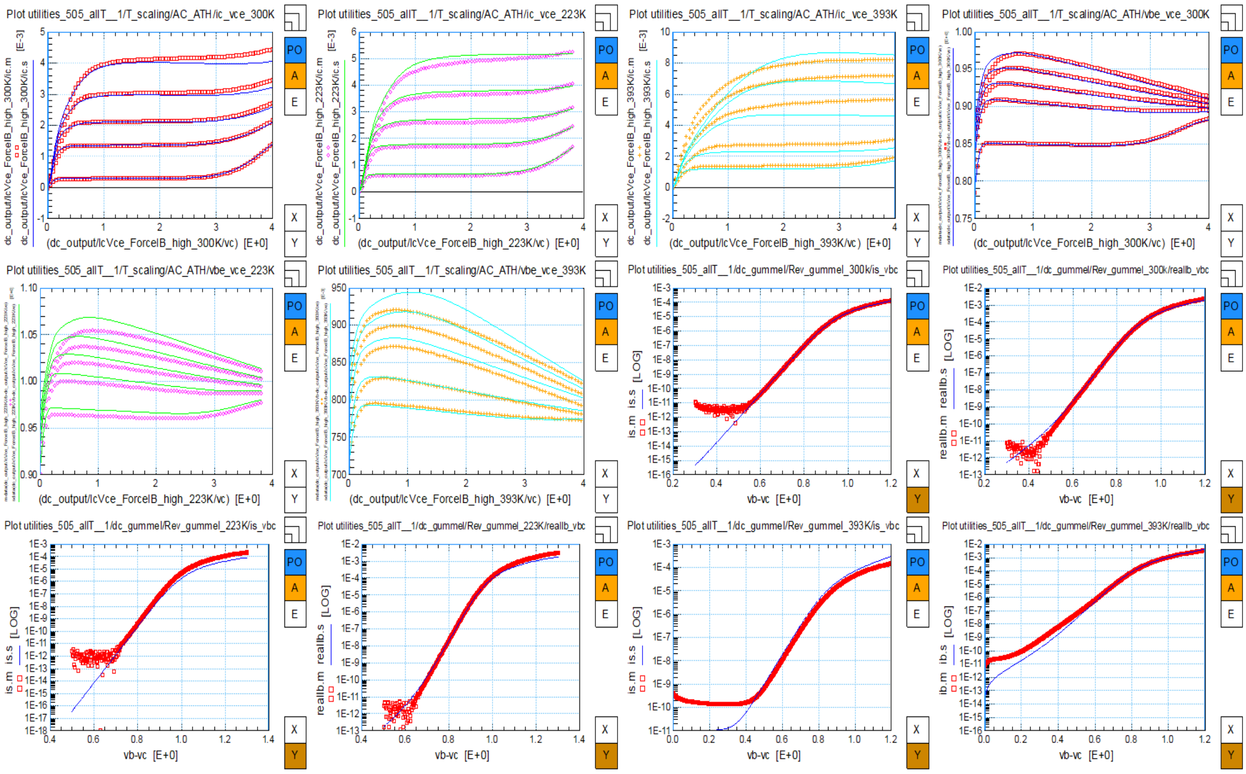

Figure 5.13: Fitting I_S and I_B in reverse Gummel measurement with high current output curves at different temperatures, generated by parameters in Table 5.5.

5.3 DC extraction check

It is necessary to take a look at all the extraction results at the same time after extracting all DC electric and temperature-scaling parameters, to make sure that all DC parameters have reasonable value. First, we look at important plots of DC low current extraction at 300 K shown in Figure 5.14. The Gummel characteristics after temperature scaling are shown in Figure 5.15. The output curves under forced low I_B and forced low V_{BE} aftter temperature scaling are shown in Figure 5.16. The output curves of forced high I_B and forced high V_{BE} aftter temperature scaling are shown in Figure 5.17.

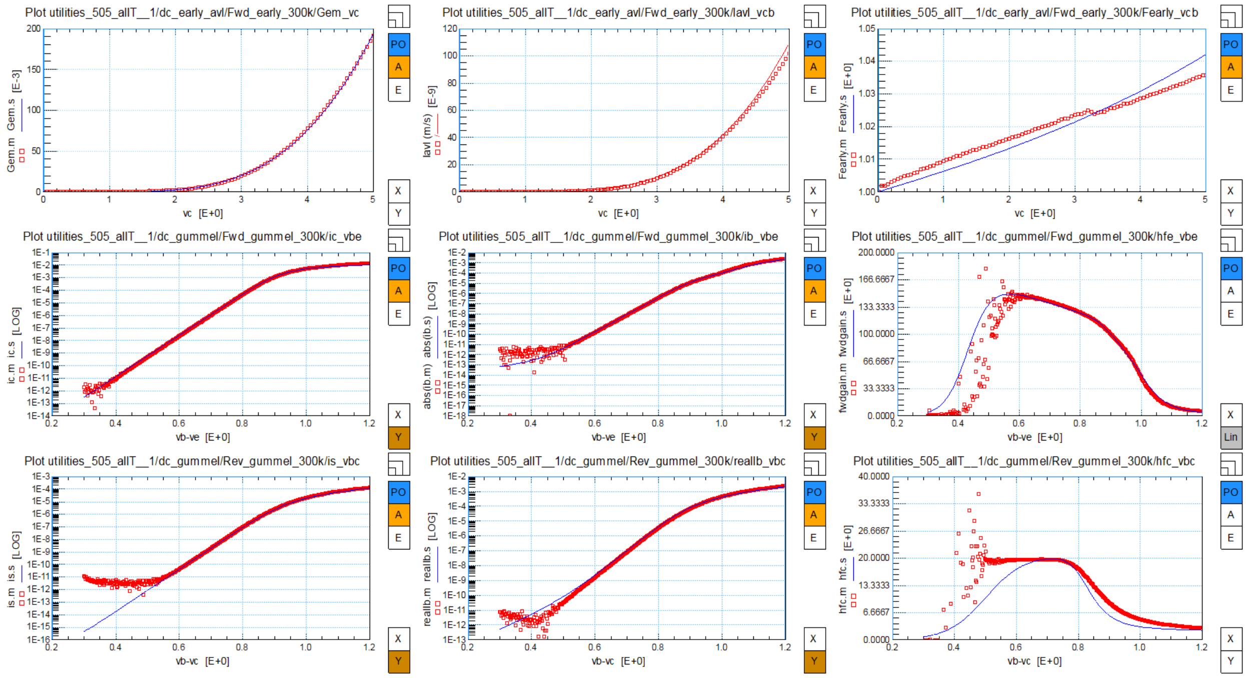

Figure 5.14: DC low current extraction results at 300 K.

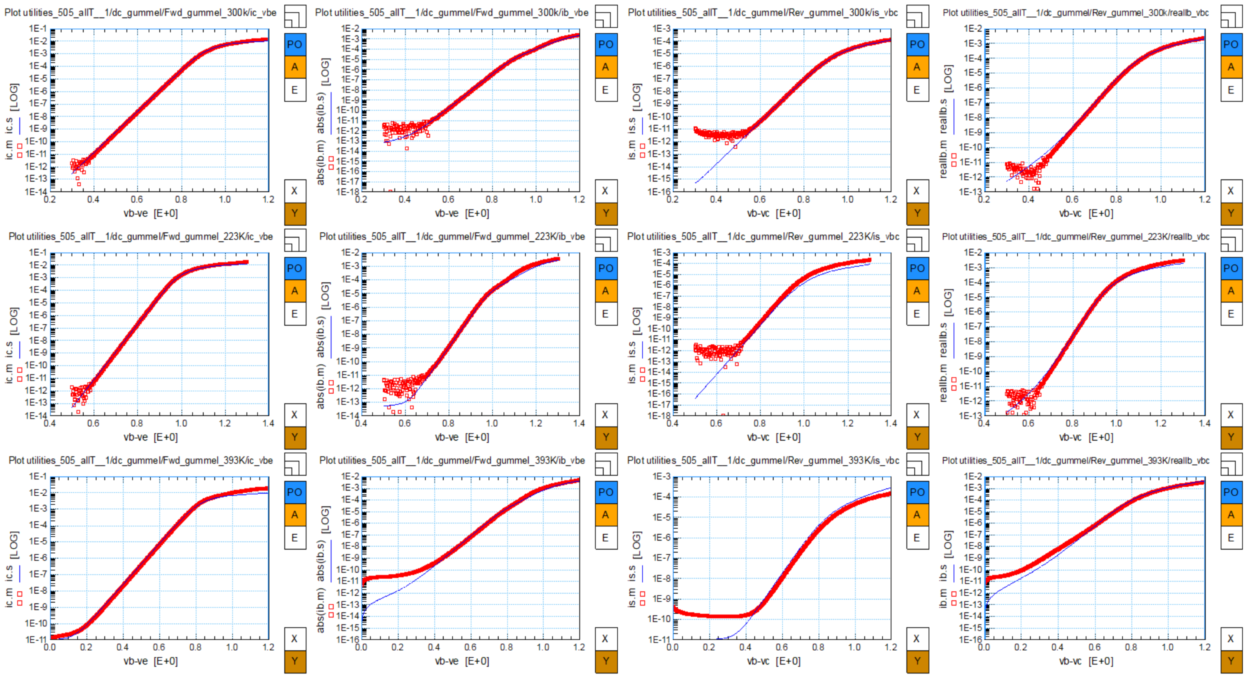

Figure 5.15: Gummel plots after temperature scaling.

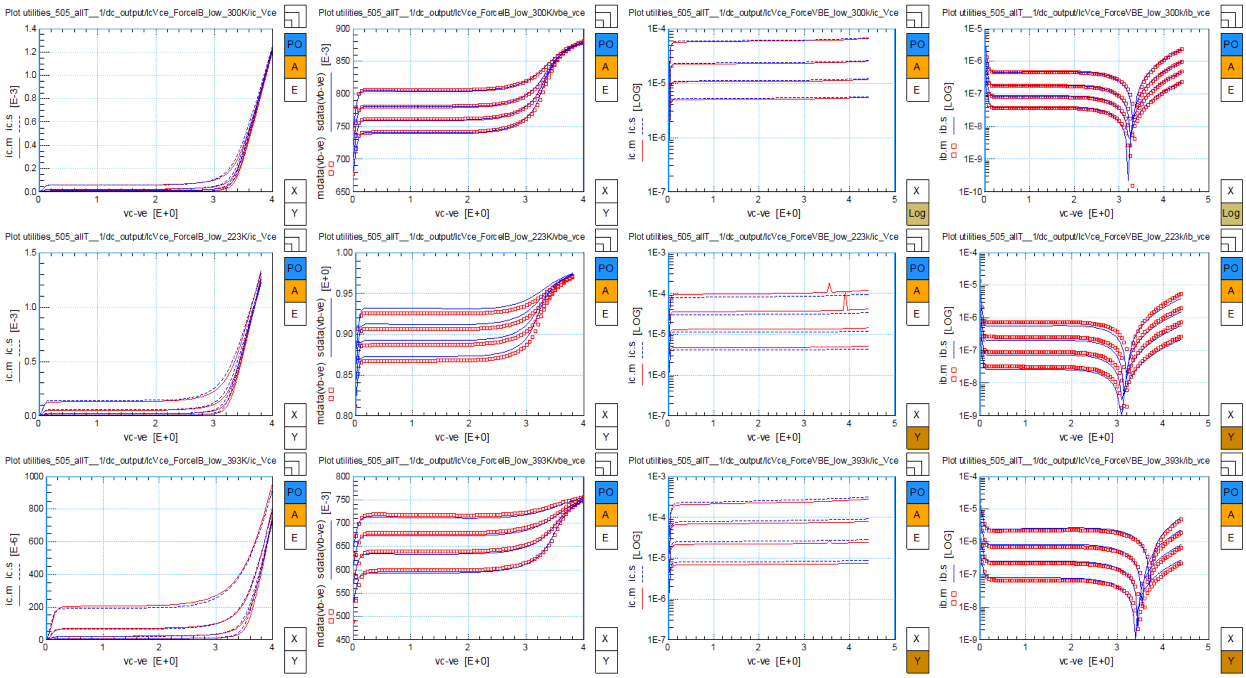

Figure 5.16: Low current output curves after temperature scaling.

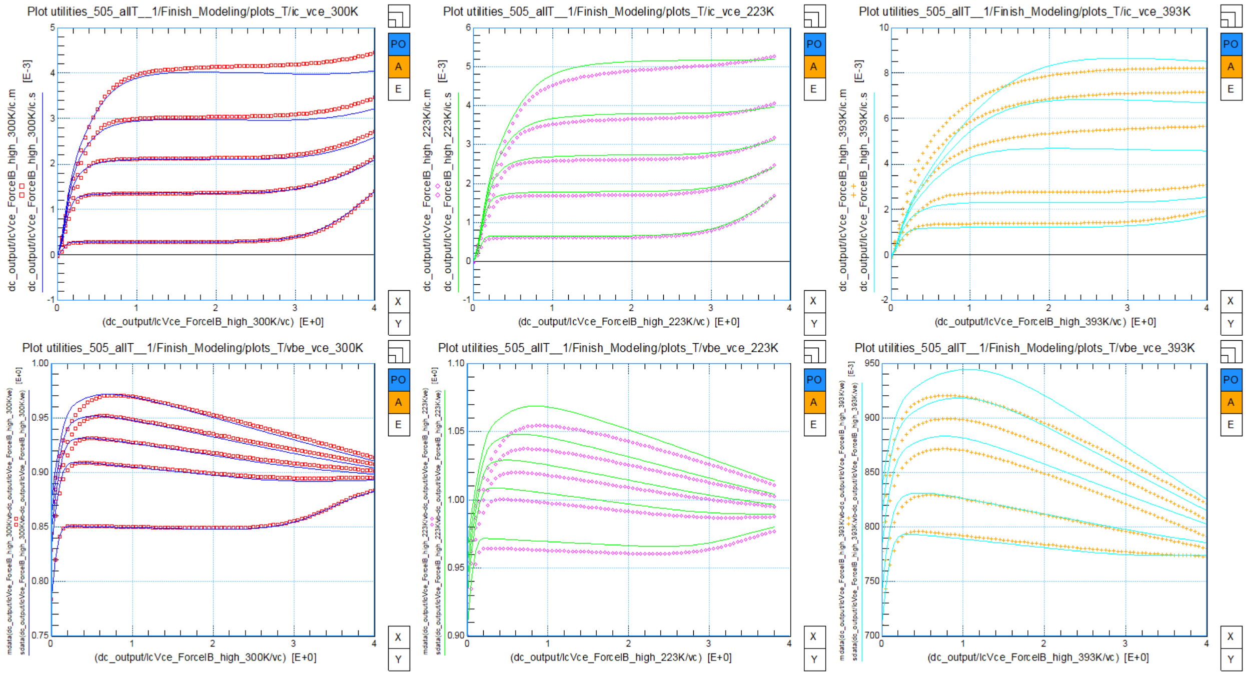

Figure 5.17: High current output curves after temperature scaling.

5.4 Cut-off frequency at 300 K

The cut-off frequency f_T is defined as the frequency at which the current gain h_{fe} reduces to unity. The current gain can be expressed in terms of Y-parameters as:

$$h_{fe} = h_{21} = \frac{Y_{21}}{Y_{11}}, \tag{5.26}$$

f_T is calculated by:

$$f_T = \frac{f}{Im(1/h_{fe})}, \tag{5.27}$$

this equation is used to calculate f_T for both high and intermediate frequencies. Again, to understand how to extract transit times we need to caluculate f_T following [11]. f_T can be determined in terms of I_C as:

$$\frac{1}{2\pi f_T} = \tau_T = \frac{dQ}{dI_C}|_{V_{CE}}, \tag{5.28}$$

τ_T is the total emitter-collector transit time. It is related to the differential charge dQ and the differential current dI_C, both under a constanct collector-emitter bias V_{CE}. To solve this equation, we first need to know the variation of the internal biases $V_{B_2E_1}$, $V_{B_2C_1}$ and the collector current $I_{C_1C_2}$. $V_{B_2E_1}$ is calculated by equation(5.2), $V_{B_2C_1}$ is evaluated from equation(5.14), the collector current $I_{C_1C_2}$ is discribed by equation (5.5). Thus we have:

$$dV_{CE} = \frac{\partial V_{CE}}{\partial V_{B_2E_1}} dV_{B_2E_1} + \frac{\partial V_{CE}}{\partial V_{B_2C_1}} dV_{B_2C_1} + \frac{\partial V_{CE}}{\partial I_{C_1C_2}} dI_{C_1C_2} = 0, \tag{5.29}$$

$$dI_N = \frac{\partial I_N}{\partial V_{B_2E_1}} dV_{B_2E_1} + \frac{\partial I_N}{\partial V_{B_2C_1}} dV_{B_2C_1} + \frac{\partial I_N}{\partial I_{C_1C_2}} dI_{C_1C_2} = dI_{C_1C_2}, \tag{5.30}$$

$$dQ = \frac{\partial Q}{\partial V_{B_2E_1}} dV_{B_2E_1} + \frac{\partial Q}{\partial V_{B_2C_1}} dV_{B_2C_1} + \frac{\partial Q}{\partial I_{C_1C_2}} dI_{C_1C_2}. \tag{5.31}$$

Therefore, most of the parameters we extracted from output characteristics are optimized here. V_{dC} is also optimized here as we discussed in 4.4.5, for it can influence current gain. How these parameters influence the simulated results are shown in Figure 5.18 - Figure 5.25. The parameters, R_E, R_{th}, I_K, I_{hc}, SCR_{CV}, a_{Xi}, R_{CC}, R_{CV} and V_{dC} are simulated on output characteristics and cut-off frequency separately. Each time only one parameter is changed so

#	parameter	value	comment
1	R_E	14.81	
2	R_{th}	4.56k	
3	R_{CC}	31.89	
4	R_{CV}	99.13	
5	I_K	18.14m	
6	SCR_{CV}	1.025k	
7	I_{hc}	18.65m	
8	a_{Xi}	157.5m	
9	V_{dc}	884.0m	
10	mtau	1.182	
11	taue	519.9f	
12	taub	497.5f	
13	tepi	790.5f	
14	taur	64.66n	

Table 5.6: Parameters extracted from fitting cut-off frequency curves, high current output curves and h_{fe}, as shown in Figure 5.27.

we can observe the impact of parameters individually. Measured data are indicated by black markers, well-extracted values are represented by solid red lines and curves after changing one parameter are indicated by solid blue lines.

Thus, transit times are extracted along with output plots and h_{fe} curve. Transit times including τ_E, τ_B, τ_R, τ_{epi}, and non-ideality factor of emitter stored charge m_τ are used to describe charges. The maximum f_T at high bias is used to extract τ_E and τ_B. τ_{epi}, I_{hc} and SCR_{CV} are extracted from the degradation of f_T. We do the extraction at different V_{CB} to get meaningful parameters that can be used for various bias. f_T - V_{CB} at different bias are shown in Figure 5.27. Values of parameters used here are given in Table 5.6.

We also need to check Gummel plots since the value of R_E, R_{CC} and R_{CV} have been changed. Figure 5.28 shows that the Gummel curves barely changes, so we do not need to optimize these resistances again.

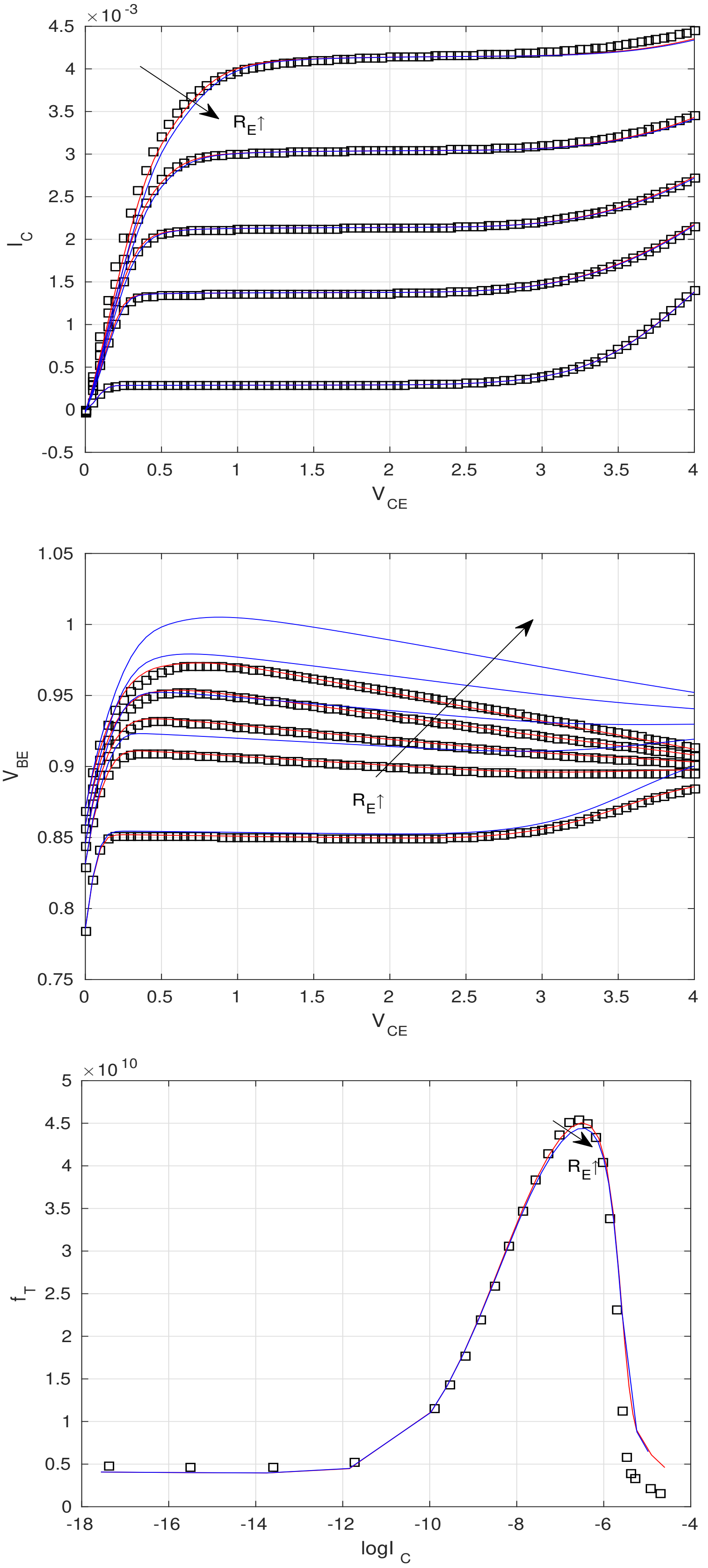

Figure 5.18: Impact of parameter R_E on output characteristics and f_T

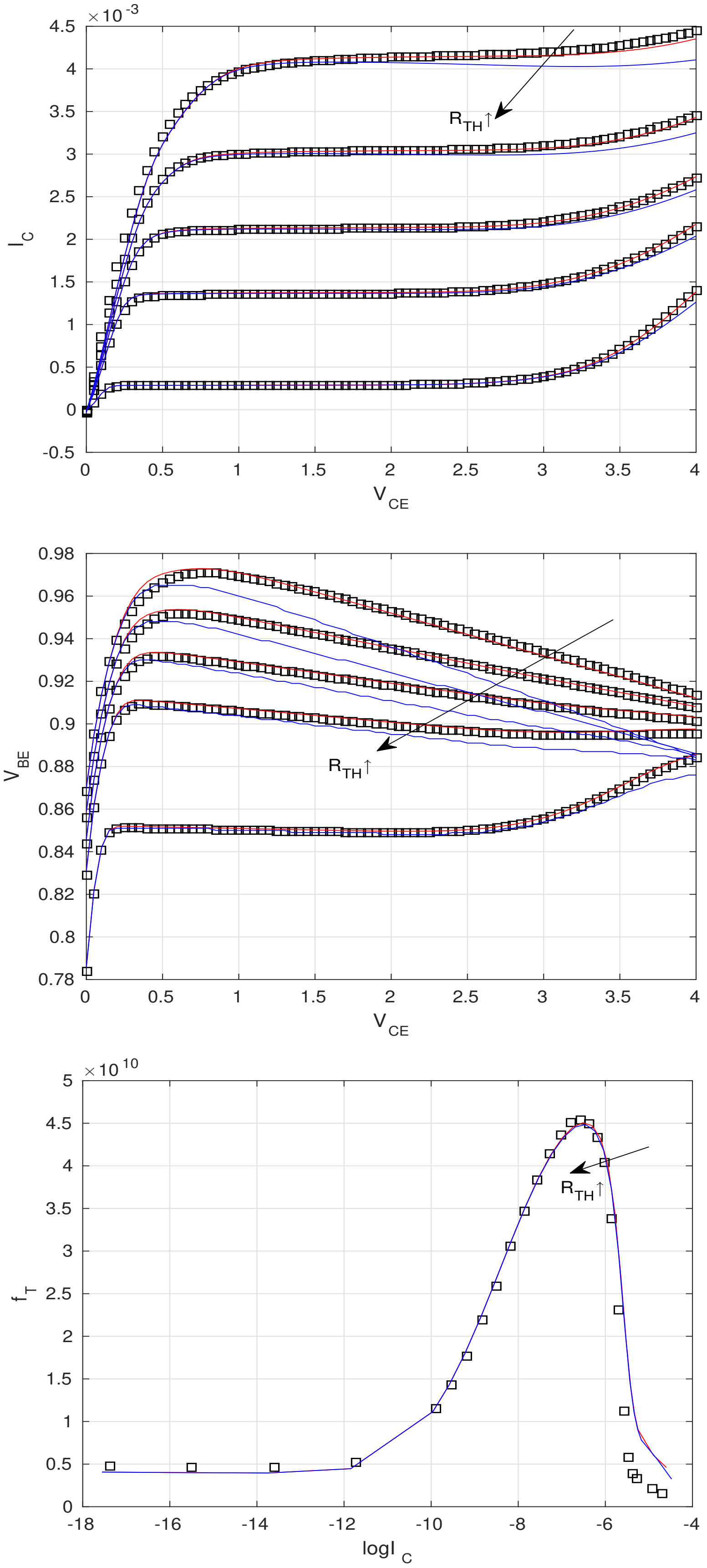

Figure 5.19: Impact of parameter R_{TH} on output characteristics and f_T

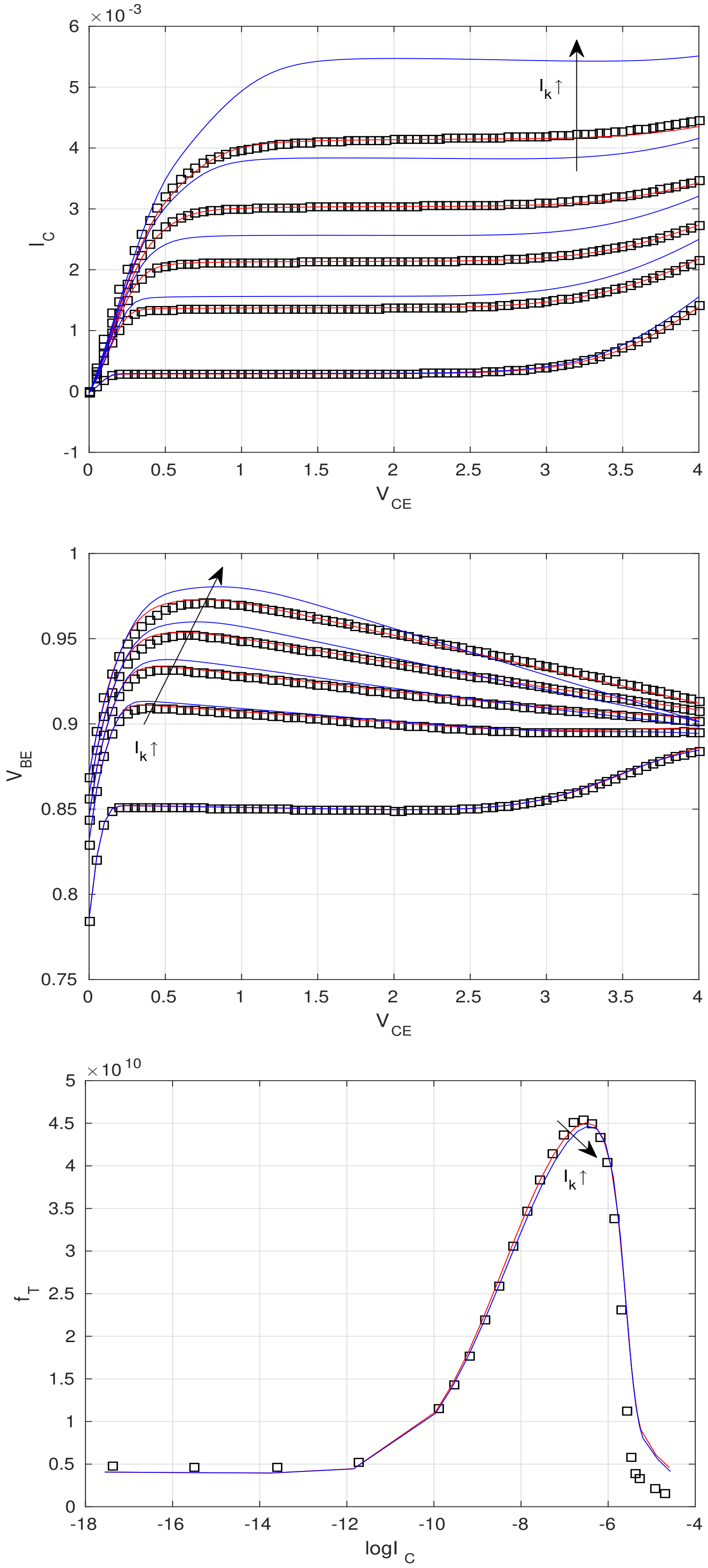

Figure 5.20: Impact of parameter I_K on output characteristics and f_T

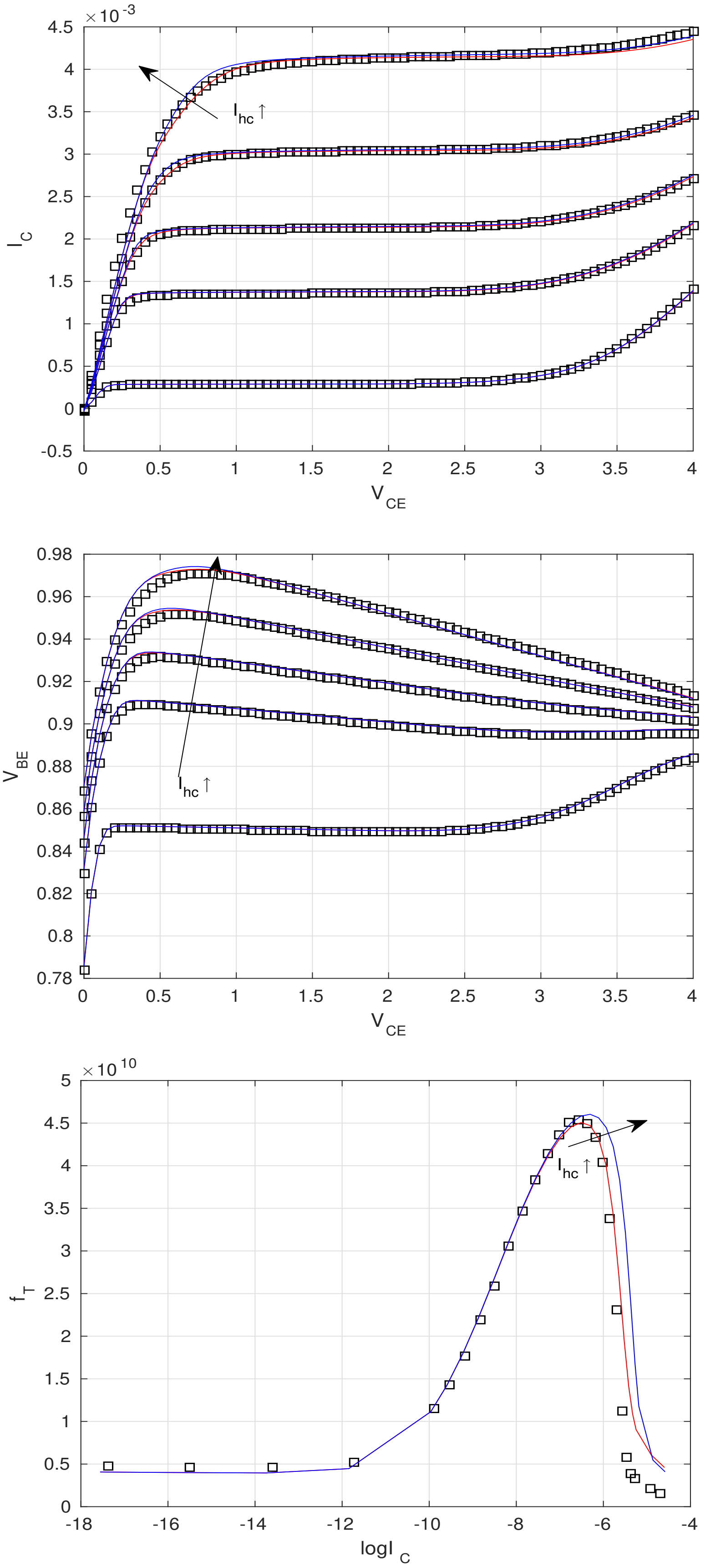

Figure 5.21: Impact of parameter I_{hc} on output characteristics and f_T

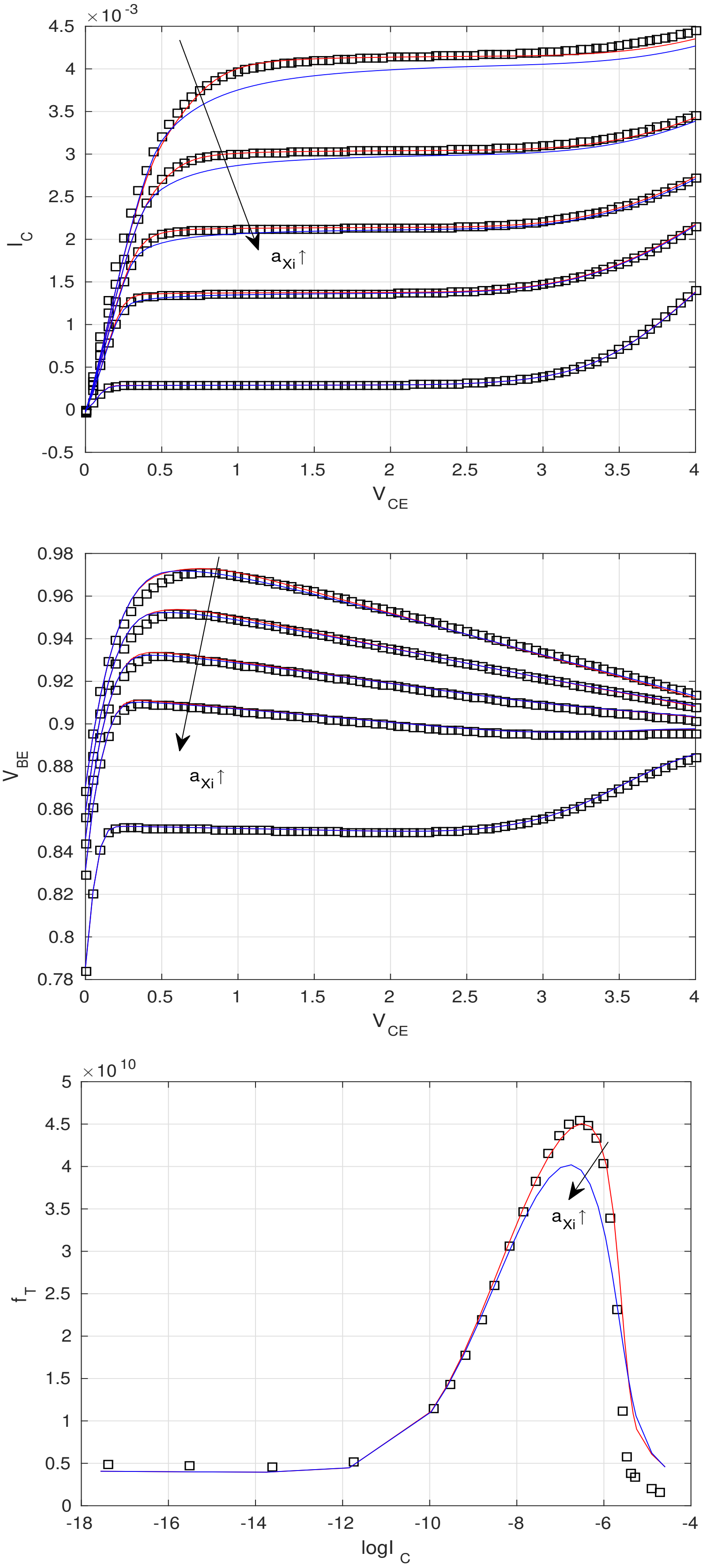

Figure 5.22: Impact of parameter a_{Xi} on output characteristics and f_T

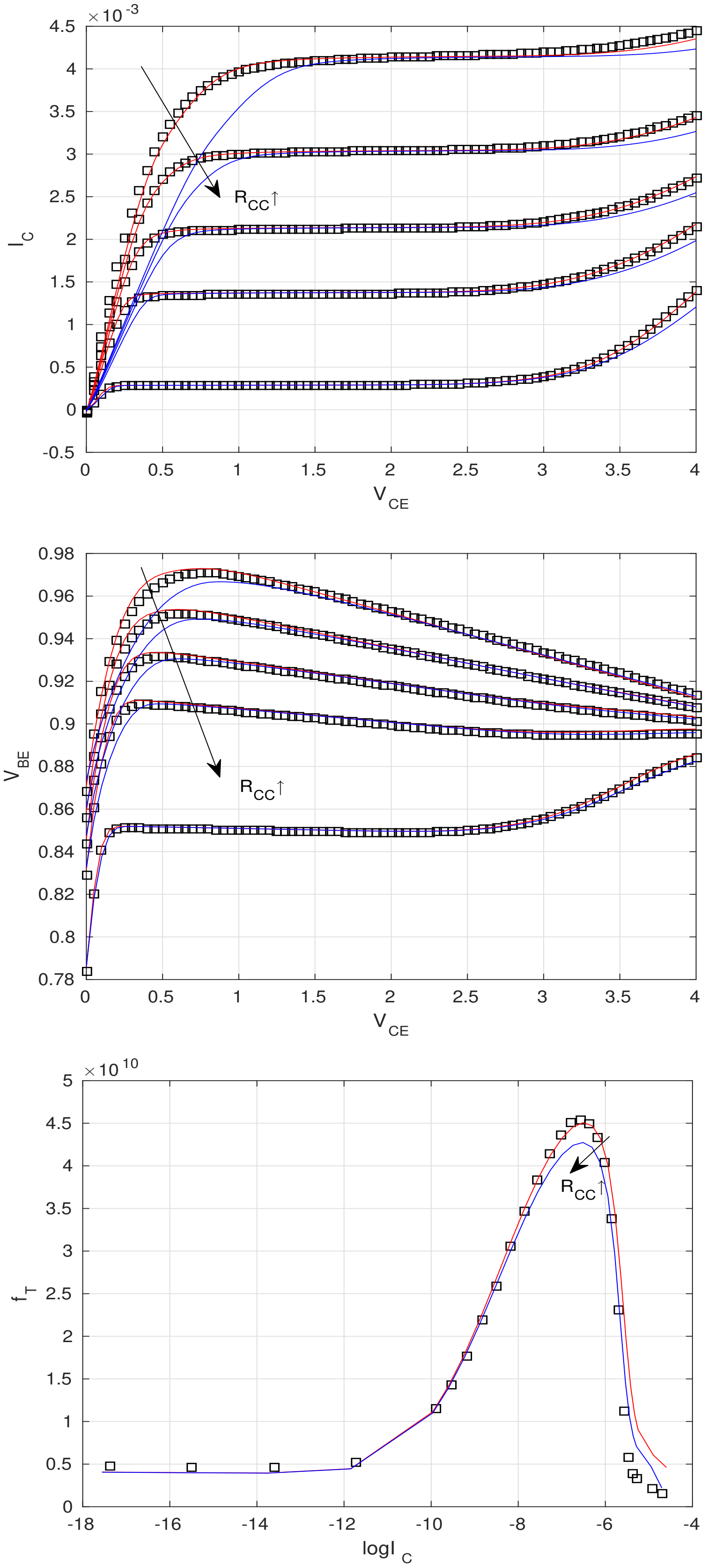

Figure 5.23: Impact of parameter R_{CC} on output characteristics and f_T

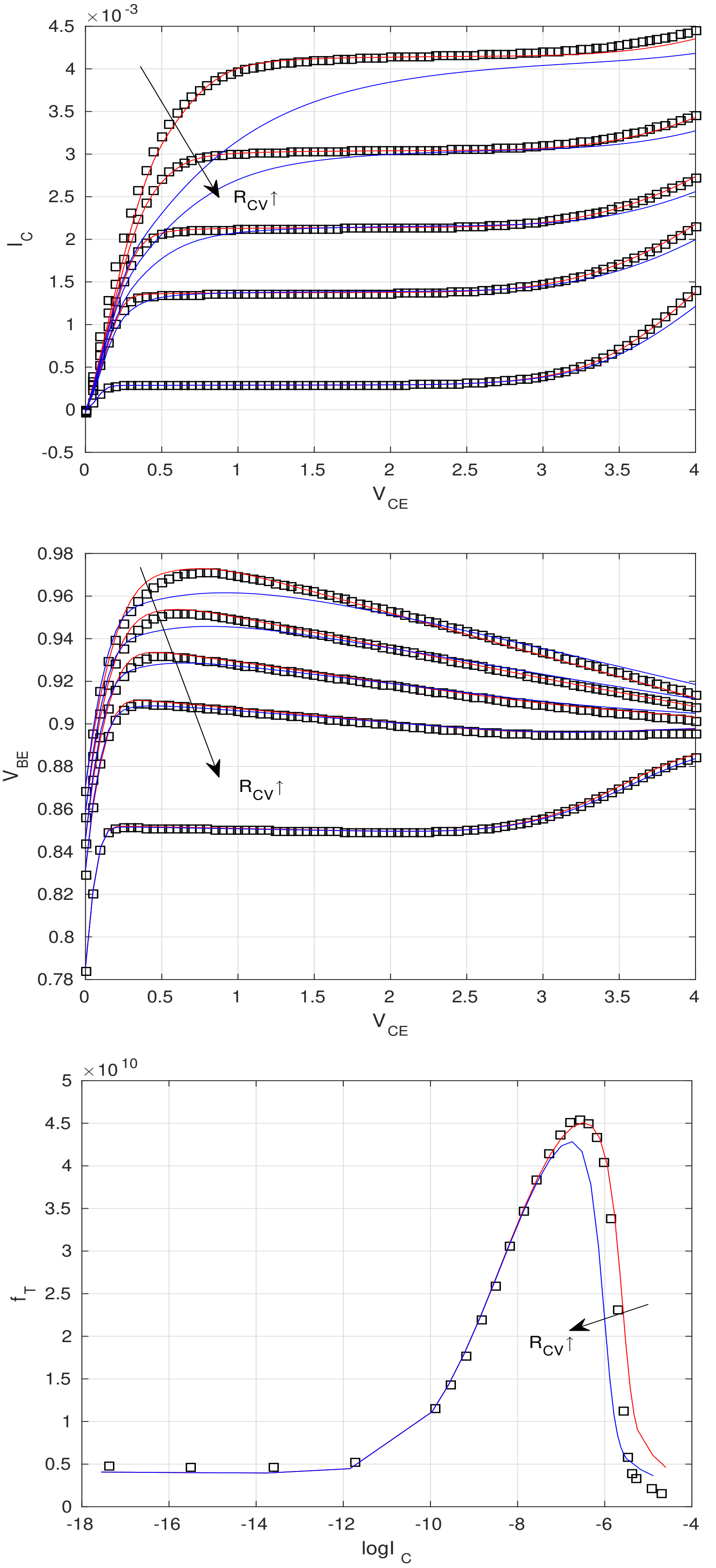

Figure 5.24: Impact of parameter R_{CV} on output characteristics and f_T

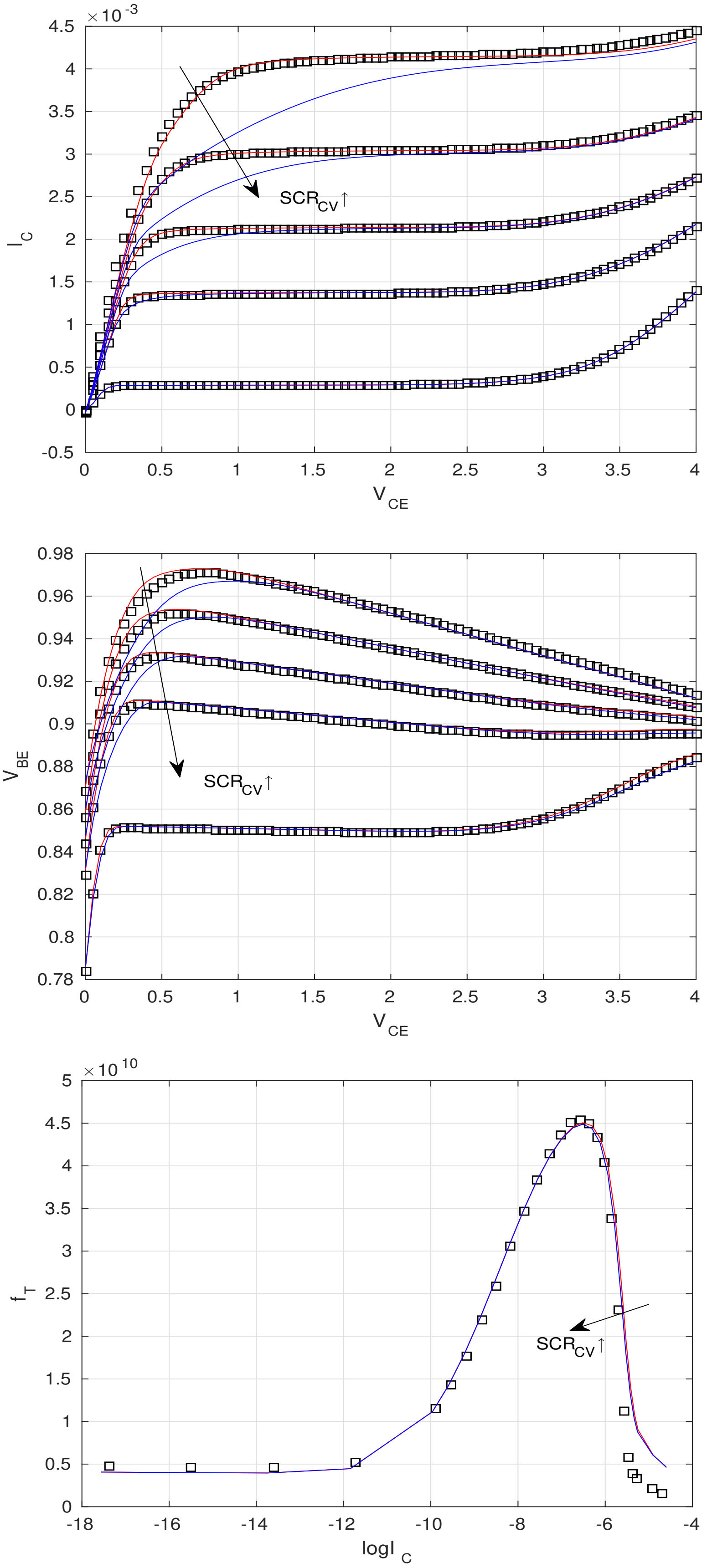

Figure 5.25: Impact of parameter SCR_{CV} on output characteristics and f_T

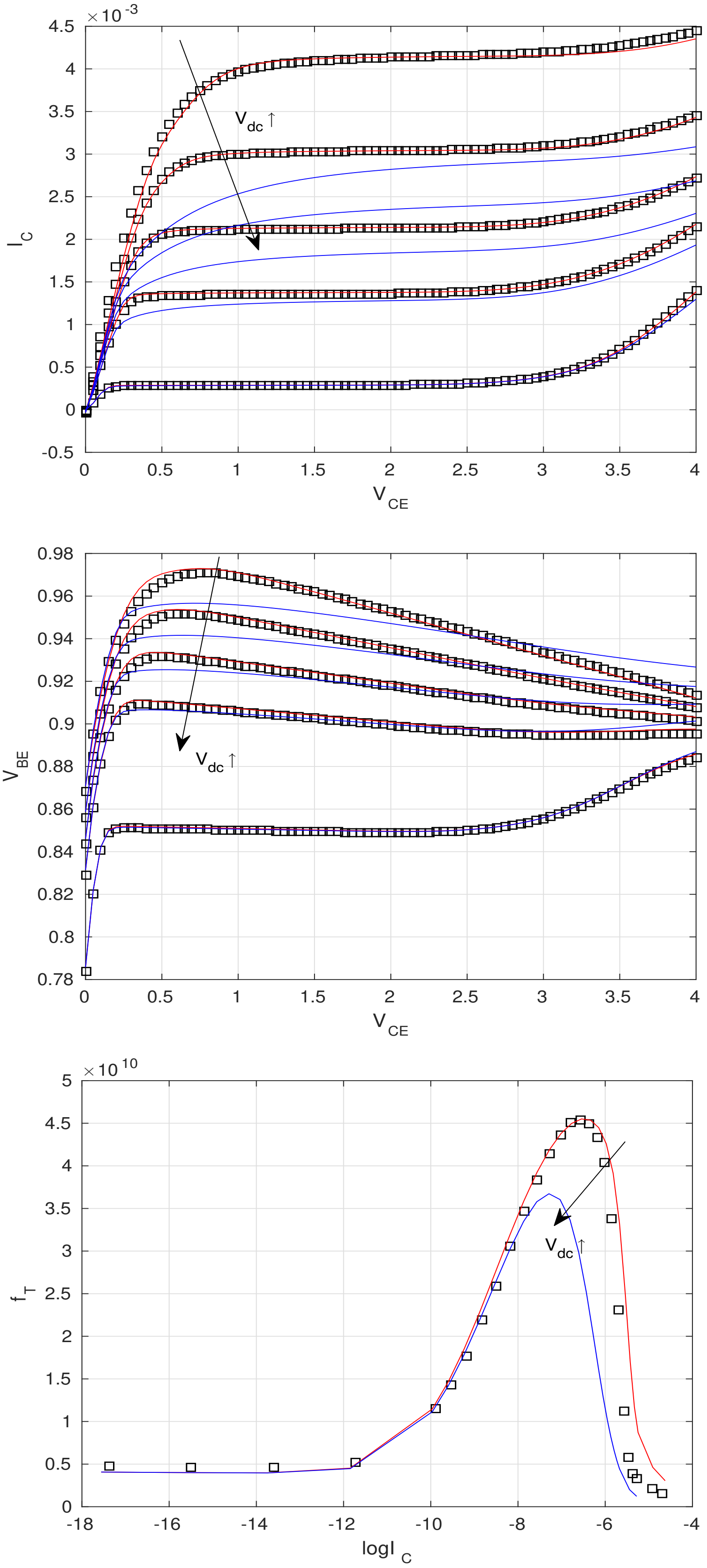

Figure 5.26: Impact of parameter V_{dC} on output characteristics and f_T

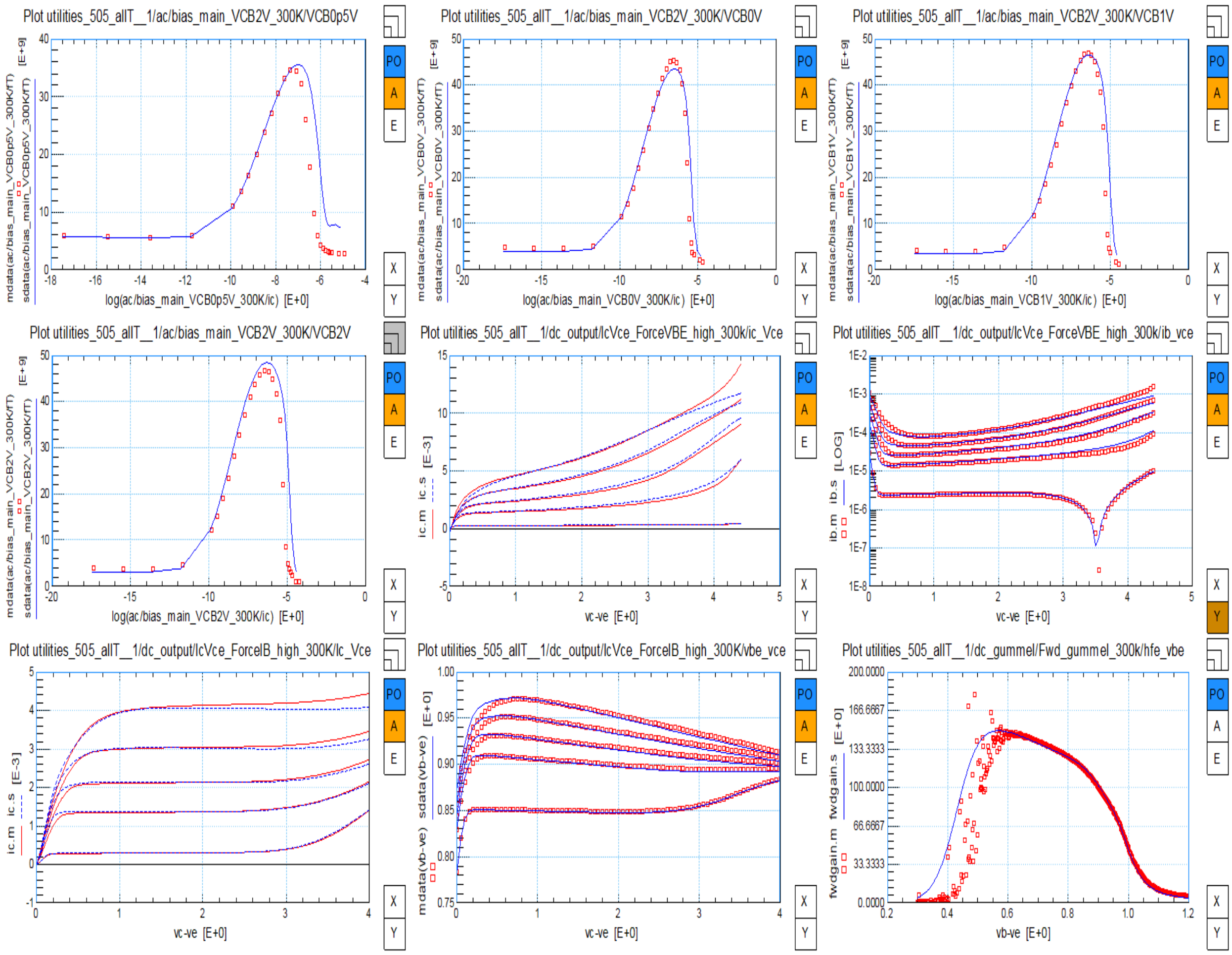

Figure 5.27: Extraction of f_T parameters at 300 K, generated by parameters in Table 5.6.

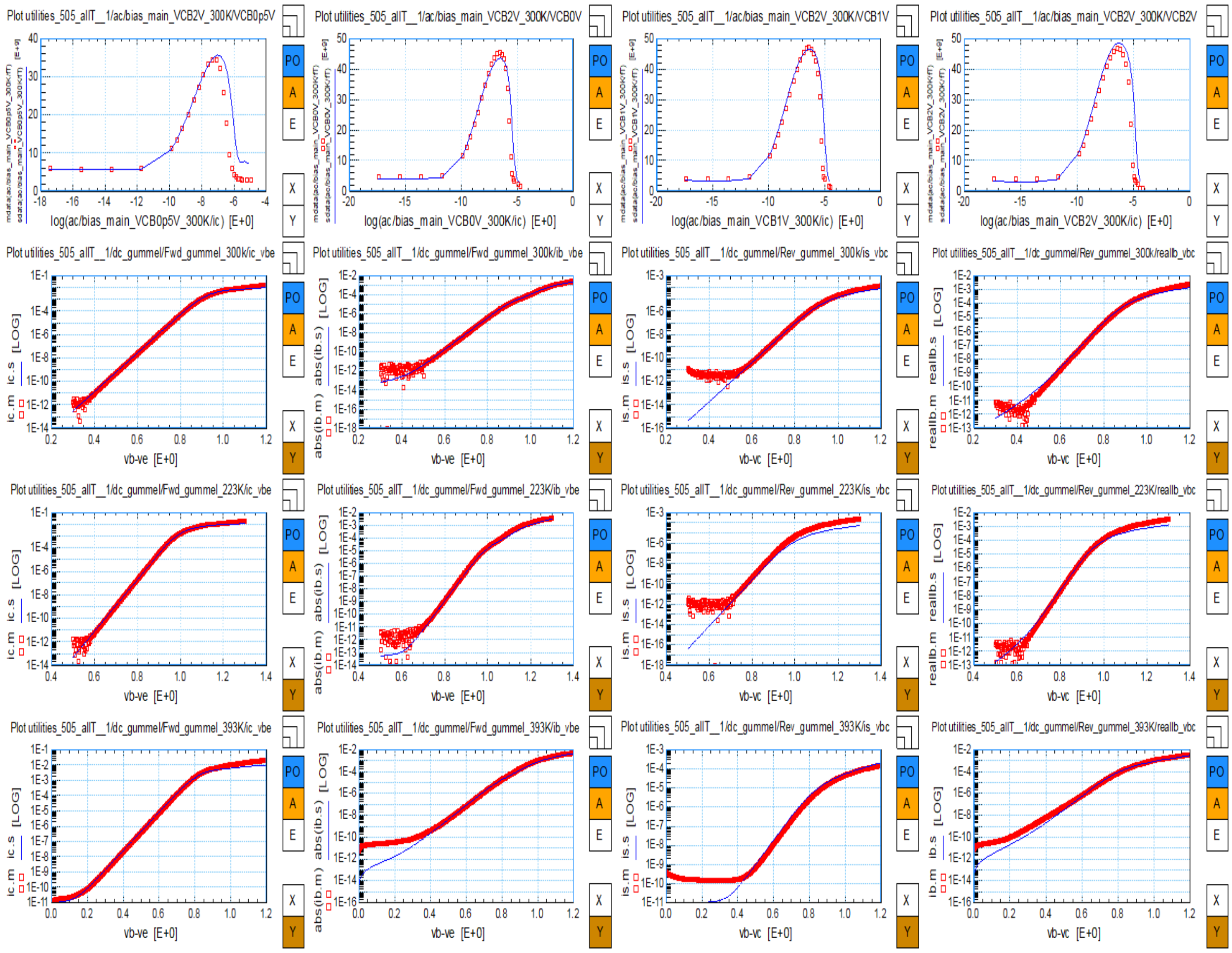

Figure 5.28: Check Gummel curves with f_T curves at 300 K, generated by parameters in Table 5.6.

#	parameter	value	comment
1	$\mathsf{A_B}$	1.169	
2	$\mathsf{A_{epi}}$	1.037	
3	$\mathsf{dV_{gTE}}$	109.2m	
4	$\mathsf{A_{QBO}}$	95.63m	

Table 5.7: Parameters used in temperature scaling of cut-off frequency, to generate Figure 5.29.

5.5 Temperature scaling of cut-off frequency

After doing extraction at 300 K, we need to extract the temperature scaling parameters of cut-off frequency. Transit times have temperature dependency as:

$$\tau_{ET} = \tau_E t_N^{(A_B-2)} exp[-\mathrm{dV}_{\mathrm{g}\tau_\mathrm{E}}/\mathrm{V}_{\Delta\mathrm{T}}], \tag{5.32}$$

$$\tau_{BT} = \tau_B t_N^{A_{QB0}+A_B-1} \tag{5.33}$$

$$\tau_{epiT} = \tau_{epi} t_N^{A_{epi}-1}, \tag{5.34}$$

$$\tau_{RT} = \tau_R \frac{\tau_{BT} + \tau_{epiT}}{\tau_B + \tau_{epi}}. \tag{5.35}$$

The bandgap voltage difference of emitter stored charge $dV_{g\tau_E}$ is extracted here. A_B, A_{epi} and A_{QB0} are used in previous extractions and they need to be optimized here. These temperature scaling parameters can be obtained by fitting f_T plots and output plots at 223 K, 300 K and 393 K together. Since A_B, A_{epi} and A_{QB0} also influence Gummel curves, Figure 5.29 is used to optimize these temperature scaling parameters by fitting f_T plots with high current output plots as well as related Gummel plots simultaneously. The parameters are given in Table 5.7.

As summerized in Table 4.11, we need to optimize $DAIS$ and V_{gB} due to the change of A_B and A_{QB0}. The change of $DAIS$ will also lead to the change of A_E, V_{gE}, A_{CX} and V_{gCX}. Therefore we optimize $DAIS$, V_{gB}, A_E and V_{gE} by fitting all output curves and forward Gummel curves together as shown in Figure 5.30. Then we optimize A_{CX} and V_{gCX} by fitting reverse Gummel plots as shown in Figure 5.31, high current output curves are also displayed

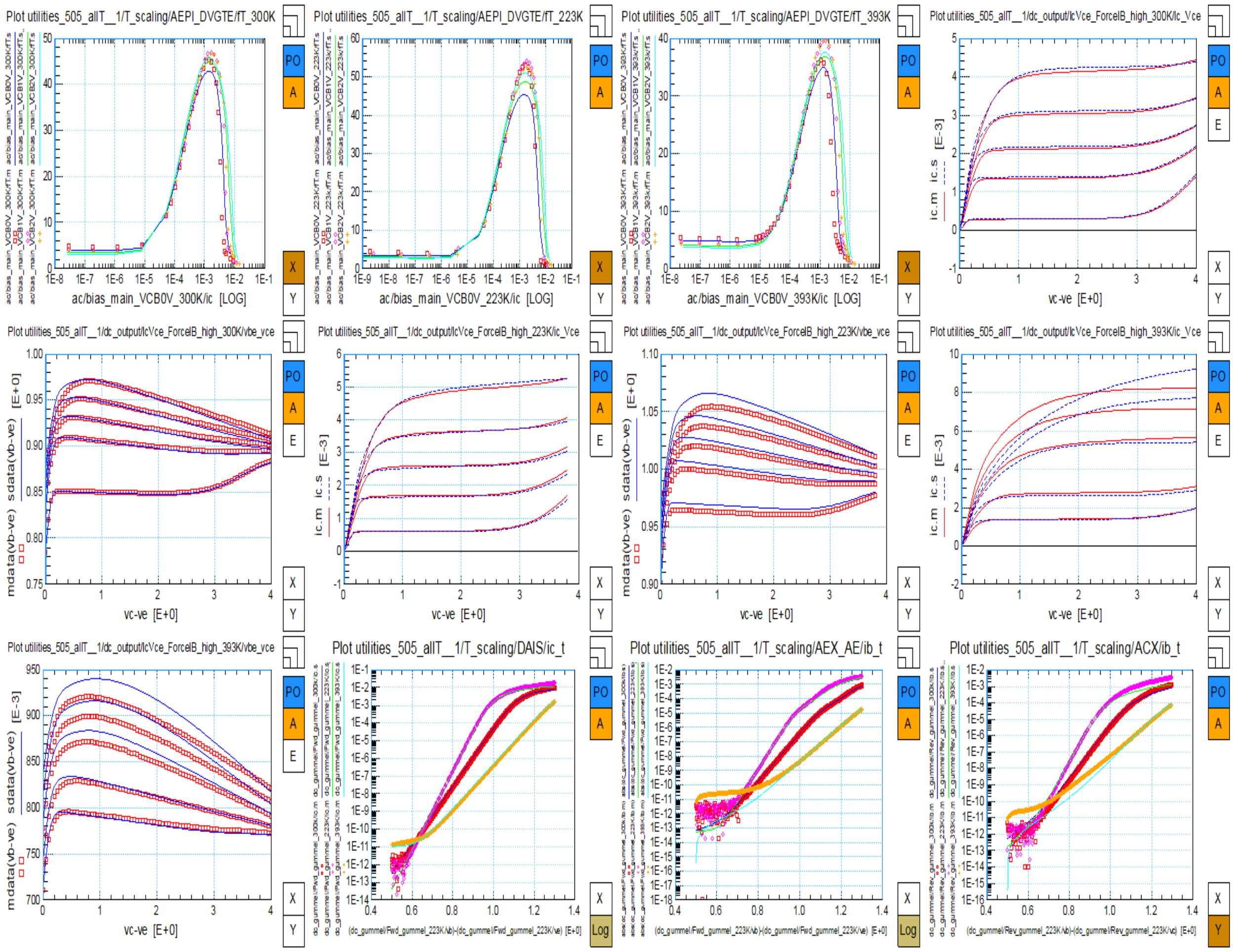

Figure 5.29: Temperature scaling of cut-off frequency, generated by parameters in Table 5.7.

to show that A_{CX} and V_{gCX} do not have much influence on output curves. The parameters optimized here are given in Table 5.8.

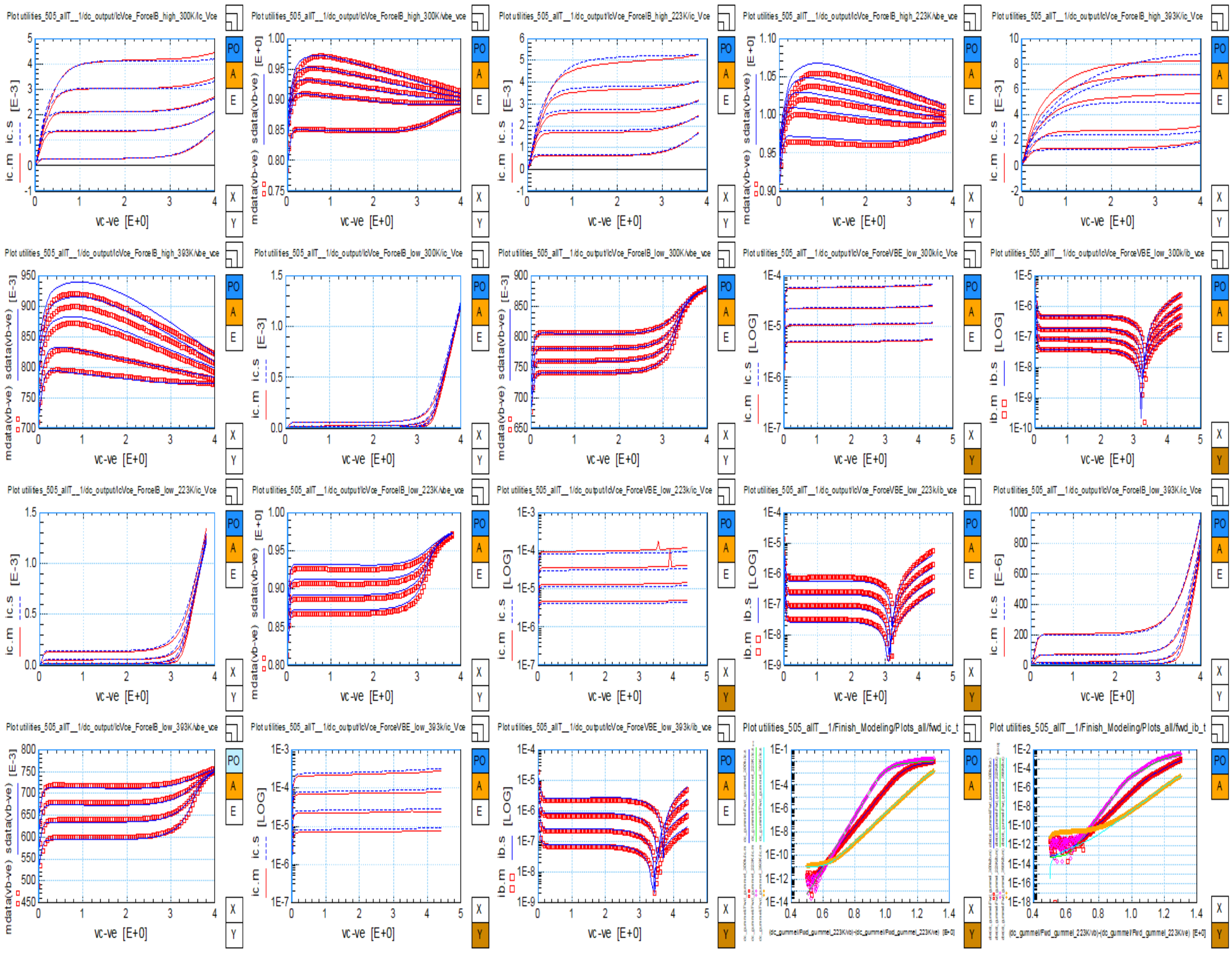

Figure 5.30: Optimizing forward Gummel curves with output curves at multiple temperature, generated by parameters in Table 5.8.

#	parameter	value	comment
1	DAIS	20.38m	
2	V_{gB}	1.133	
3	V_{gE}	1.149	
4	A_E	-534.2u	
5	V_{gCX}	1.122	
6	A_{CX}	1.099	

Table 5.8: Temperature scaling parameters optimized with high current output curves and Gummel curves, used to generate Figure 5.30 and Figure 5.31.

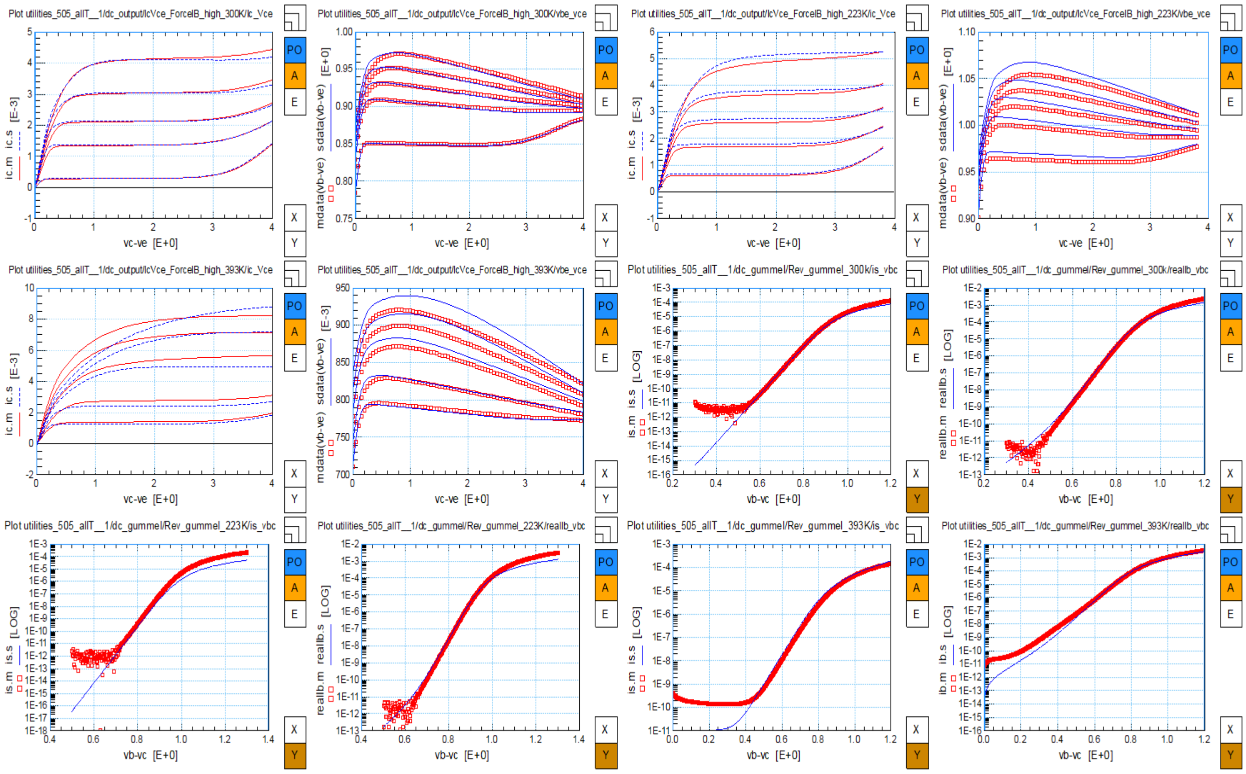

Figure 5.31: Optimizing reverse Gummel curves at multiple temperature, generated by parameters in Table 5.8.

Chapter 6

Extraction Results

This chapter shows important characteristics after extraction. Figure 6.1 shows curves of avalanche effect, forward and reverse currents, low current output characteristics and cut-off frequency at 300 K. Figure 6.2 presents forward and reverse currents in Gummel measurement after temperature scaling. Figure 6.3 shows high current output plots and f_T plots at different temperatures.

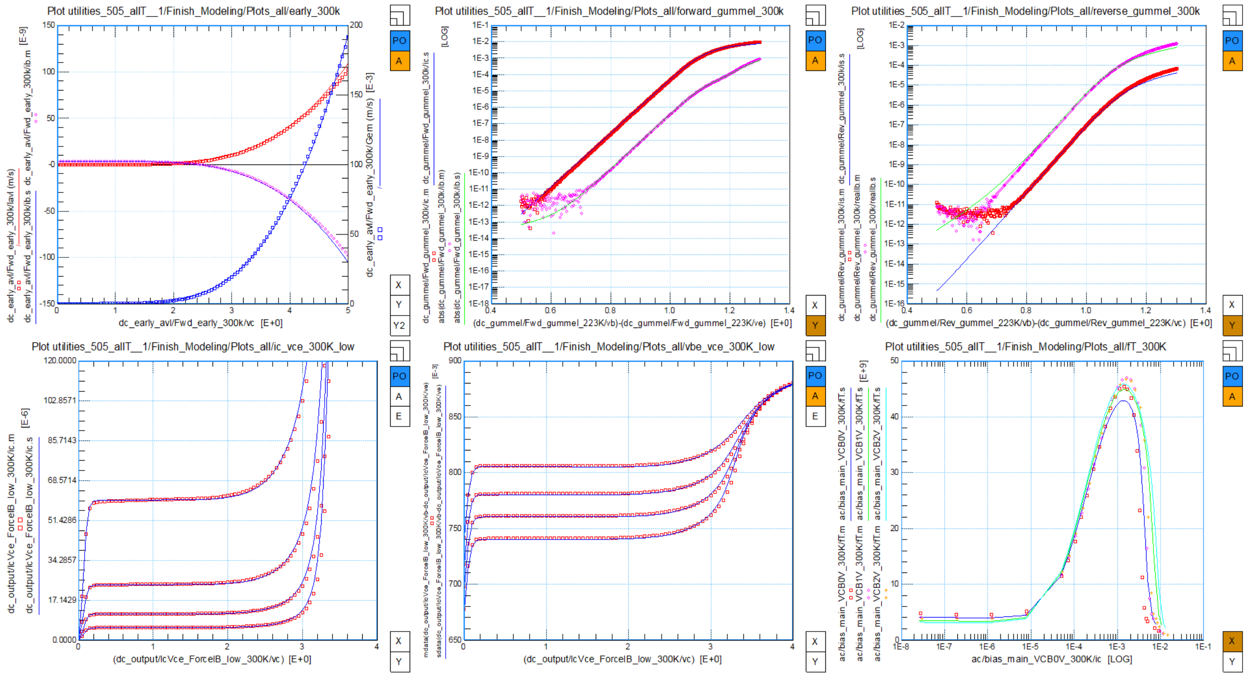

Figure 6.1: Important characteristics at 300 K.

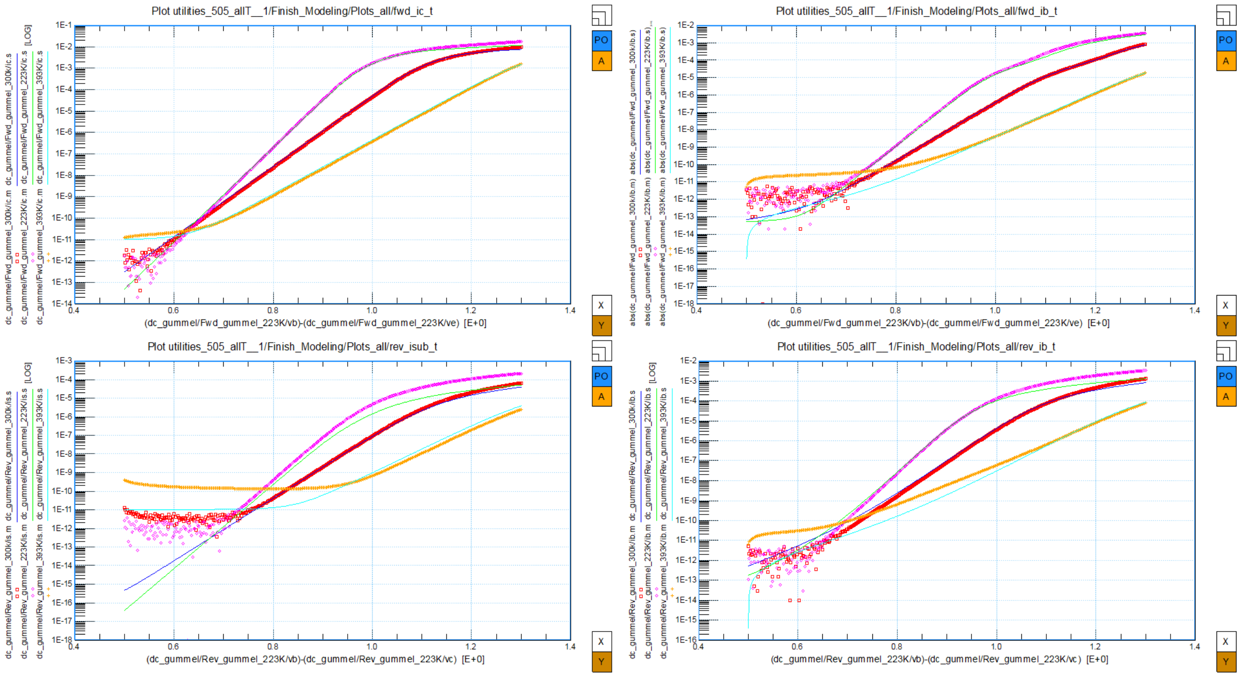

Figure 6.2: Currents of Gummel measurement at different temperatures.

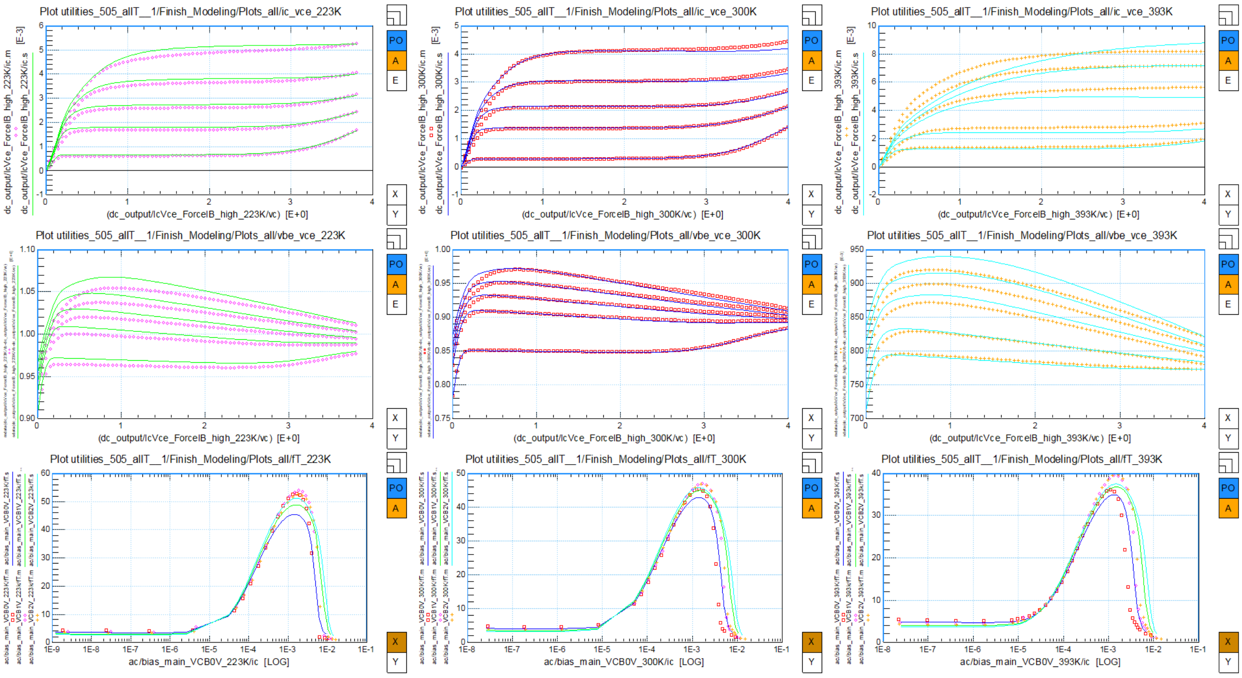

Figure 6.3: High current characteristics at different temperatures.

References

[1] B. O. Woods, “Device Characterization and Compact Modeling of the Silcon Germanium HBT in Extreme Temperature Environments,” Ph.D. dissertation, 2013.

[2] H.-C. Wu, “A scalable mextram model for advanced bipolar circuit design,” Ph.D. dissertation, TU Delft, Delft University of Technology, 2007.

[3] Z. Xu, “Physics, Modeling and Design Implications of RF Correlated Noise in SiGe HBTs,” Ph.D. dissertation, 2013.

[4] J. D. Cressler, “SiGe HBT technology: A new contender for Si-based RF and microwave circuit applications,” *IEEE Transactions on Microwave Theory and techniques*, vol. 46, no. 5, pp. 572–589, 1998.

[5] J. D. Cressler and G. Niu, *Silicon-Germanium heterojunction bipolar transistors*. Artech house, 2003.

[6] G. Gildenblat, *Compact modeling: principles, techniques and applications*. Springer Science & Business Media, 2010.

[7] J. Paasschens and R. Toorn, “Introduction to and usage of the bipolar transistor model Mextram,” 2002.

[8] G. Niu, R. van der Toorn, J. C. J. Paasschens, and W. Kloosterman, “The Mextram Bipolar Transistor Model Definition,” 2017.

[9] “Mextram Level 505.00 Code,” 2017, http://www.eng.auburn.edu/~niuguof/mextram/codes/index.html.

[10] S. Mijalkovic, “Compact modeling of SiGe HBTs: Mextram,” *Chapter 8.5 in Silicon Heterostructure Handbook: Materials, Fabrication, Devices, Circuits and Applications of SiGe and Si Strained-Layer Epitaxy*, 2005.

[11] J. Paasschens, R. H. Way, W. Kloosterman, and R. Havens, “Parameter Extraction for the Bipolar Transistor Model Mextram: Level 504,” in *level 504, Unclassified Report NL-UR 2001/801, Philips Nat. Lab., 2001.* Citeseer, 2001.

[12] Y. Wang, “Circuit Simulator Based Mextram Parameter Extraction of SiGe HBTs,” Master’s thesis, Auburn University, 2016.